The University Of Sheffield.

Synthesis of 5-Fluoruracil Dendritic Polymers and ^{19}F NMR Analysis of the Drug Release for MRI

Laila M Alhaidari

A Thesis submitted for the Degree of Doctor of Philosophy

Department of Chemistry, University of Sheffield

October 2018

Author's Declaration

The work described in thesis was carried out between January 2015 and 2018 in the department of chemistry at the University of Sheffield. It is the individual work of the Author. Any views expressed in this thesis are those of the author, and in no way represent those of University of Sheffield. This thesis has not previously been submitted, in part or whole, for any other degree in this University or any other institution.

Acknowledgments

First of all, none of the work in this thesis would have been possible without the funding. Saudi Arabia Cultural Bureau (SACB) is greatly acknowledged for the financial support.

I would like to express my deepest thanks to my supervisor Dr. Seb Spain for his patient guidance, fruitful discussions and encouragement throughout my PhD. It has been a great privilege to work with him and get to know him during the past four years.

I would like to express my sincere gratitude to the following individuals in the department of Chemistry for their assistance. Dr Sandra Van Meurs and Dr Craig Robertson are greatly acknowledged for their assistance with the NMR experiments and data analysis. I am very grateful to Rob Hanson for his help with chromatography, Keith Owens for his help with the Grubbs system, Simon Thorpe for the Mass spectroscopy analysis, Stephen Atkin for the elemental analysis. Thanks also goes to Dr Svet Tsokov in the EM Department for TEM training and his valuable advice.

I must also thank the former and present members of Spain group: Dr Laura Shallcross, Dr Kat Murray, Dom Gray, Jasmine Lord, Emma Owens, Tom Neal, Rheanna Perry, Marissa Morales, Anna Mroz, Ellen Moscrop, Josh Hayles and Sam Harrison for their friendly assistance in whatever I needed. It has been an absolute pleasure working with intelligent friendly people. One special thanks goes to Dom for GPC training and Marissa for proof-reading my thesis.

I would like to thank all my friends in the Graduate Research Centre (GRC): Dr Fatemah Aboshnaf, Hanadi Alshamlan, Hawazin Alnafeesah, Huda Imam Dasuki, Jabrah Alkorbi, Muneera Alrasheedi, Mariam Aldoghaim, Najwa Elfarsi, Nourah Alhusayni, Samira Hussein, Zainab Jaafar and Zainab Taher for the endless support, for the invaluable scientific discussions, and for all the fun we have had in the last few years. My sincere gratitude also goes to Asma Aljurani and her six stars for always being there.

I must express my gratitude to my husband, Sami Alabdulkarim, and my precious little boy, Ibrahim, who have nurtured, supported and motivated me without fail and in ways that nobody else could.

Finally, I would like to dedicate this thesis to my beloved parents, Mohammed and Salma, for their unconditional support, encouragement and love, and without which I would not have come this far.

Abstract

5-Fluorouracil (5-FU) is a chemotherapy drug used to treat a wide range of solid tumors. However, severe adverse side effects have been reported after its administration. Therefore, it is essential to directly image the release of 5-FU to help optimising biological efficacy and safety. Here, a new dendritic polymer that is covalently attached to the oligo-peptide bearing 5-FU in its α C-terminal glycine residue was developed for monitoring the release of 5-FU by ^{19}F MRI in an off/on mode. The NMR signal of this conjugate is quenched but in the presence of the enzyme, the release of 5-FU is triggered to produce a sharp NMR signal.

Initially, a library of dendritic polymers, with a large number of terminal groups for high loading capacity of 5-FU, was synthesised using reversible addition-fragmentation transfer mediated self-condensing vinyl polymerisation (RAFT-SCVP) of *N*,*N*-dimethylacrylamide (DMA) with 4-vinylbenzyl *N*-pyrrole carbodithioate (VBPC) as a chain transfer monomer. DMA and VBPC were found to polymerise with different reactivity suggesting that the final polymer was probably a hyper-star polymer.

The 5-FU polymer conjugate was then synthesised in a stepwise manner. The vinyl-modified tetrapeptide, Gly-Phe-Leu-Gly, was conjugated to the dendritic polymer surface via *in situ* aminolysis/Michael addition chemistry. The major challenge was the formation of disulfide coupled species either in the form of cross-linked material or high molecular weight contaminants which was eliminated by the use of phenyldimethylphosphine (Me_2PPh). This was followed by the attachment of 5-FU derivative dipeptide, Leu-Gly-α-(5-FU).

In the proof-of-principle experiment, enzymatic treatment using S9 from liver at pH 7.4 demonstrated a narrow ^{19}F NMR signal with a remarkable enhancement in T_2 relaxation time from 0.038 to 0.128 s as a result of 5-FU release. Since the MRI signal intensity is directly influenced by T_2 relaxation time, a switch ON signal is expected upon enzymatic cleavage. 5-FU displays very long T_2 relaxation time at pH 5.5. Therefore, more pronounced signal intensity switch would be expected in tumour This off/on response can be applicable for monitoring other fluorinated drugs and the oligo-peptide linkage can be replaced by any other degradable spacers.

Abbreviations

AB*-type	monomer with one vinyl functionality and one initiating group
AB_2-type	monomer with one A-functionality and 2 B functionalities
ACVA	4,4-azobis(4-cyanovaleric acid)
ATRP	atom transfer radical polymerisation
Boc	*tert*-butyloxycarbonyl
BPC	benzyl 1H-pyrrole-1-carbodithioate
Cbz	carboxybenzyl
CTA	chain transfer agent
CTM	chain transfer monomer
DB	degree of branching
DLS	dynamic light scattering
DIPEA	diisopropylethylamine
DMA	*N*,*N*-dimethylacrylamide
DMF	dimethyl formamide
5-FU	5-fluorouracil
Fmoc	9-fluorenylmethoxycarbonyl
GPC	gel permeation chromatography
HBPs	hyper-branched polymers
HBTU	*N,N,N′,N′*-tetramethyl-*O*-(1*H*-benzotriazol-1-yl)uronium hexafluorophosphate
HEA	*N*-hydroxyethylacrylamide
HPLC	high-performance liquid chromatography
HS-PDMA	hyper-star poly(*N*,*N*-dimethylacrylamide)
LAM	less activated monomers
L-PDMA	linear poly(*N*,*N*-dimethylacrylamide)
LPPS	liquid phase peptide synthesis
MAM	more activated monomers
Me_2PPh	phenyldimethylphosphine
M_n	number-average molecular weight
M_w	weight average molecular weight
MRI	magnetic resonance imaging
MS	mass spectroscopy
NMP	nitroxide-mediated polymerisation

RAFT	reversible addition-fragmentation chain transfer
Đ	dispersity
PMMA	poly(methyl methacrylate)
SCVP	self-condensing vinyl polymerisation
SHBPs	segmented hyper-branched polymers
SHB-PDMA	segmented hyperbranched poly(*N*,*N*-dimethylacrylamide)
SPPS	solid phase peptide synthesis
T_1	spin-lattice relaxation time
T_2	spin-spin relaxation time
TEM	transmission electron microscopy
TFA	trifluoroacetic acid
VBPC	4-vinylbenzyl *N*-pyrrole carbodithioate
γ	the feed ratio [DMA]:[VBPC]

Table of Contents

Chapter 1 Introduction **1**

1.1 Polymers 1

1.2 Polymer syntheses 2

1.3 Reversible Addition-Fragmentation Chain Transfer (RAFT) polymerisation 3

1.4 Monomer scope and selection of CTAs 4

1.5 Dendritic polymers 6

1.6 Self-Condensing Vinyl Polymerisation (SCVP) 7

1.7 SCVP mediated by RAFT 8

1.8 Scope of monomers and CTMs 10

1.9 Magnetic Resonance Imaging (MRI) 15

1.9.1 ^{19}F MRI 16

1.9.2 Polymeric ^{19}F MRI contrast agents 17

1.9.3 Smart contrast agents 22

1.9.4 pH-responsive probes 22

1.10 5-Fluorouracil prodrugs 25

1.11 Aims and outlines 27

Chapter 2 The Synthesis of dendritic poly(*N*,*N*-dimethylacrylamide) using SCVP-RAFT 30

2.1 Introduction 30

2.2 Results and discussion 31

2.2.1 Synthesis of segmented hyper-branched poly(*N*,*N*-dimethylacrylamide) (SHB-PDMA) 31

2.2.2 Preparation of segmented hyper-branched poly(*N*,*N*-dimethylacrylamide) (SHB-PDMA) of different degree of branching by varying the feed ratios 34

2.2.3 Preparation of hyper-branched poly(*N*,*N*-dimethylacrylamide) (HB-PDMA) of different sizes by varying the concentration 38

2.2.4 Investigating the relative reactivity of DMA and VBPC 43

2.2.5 Evolution of number average molecular weight, dispersity and degree of branching 47

2.3 Conclusion 49

2.4 Experimental 50

2.4.1 Analytical Techniques 50

2.4.2 Materials 52

2.4.3 Synthesis of 4-vinylbenzyl *N*–pyrrole carbodithioate (VBPC) (RAFT Agent) 52

2.4.4 Synthesis of segmented hyper-branched poly(*N*,*N*-dimethylacrylamide) (SHB-PDMA) by varying the concentration to dioxane 53
Chapter 3 Synthesis of peptide derivative of 5-FU 56
3.1 Introduction 56
3.2 Results and discussion 59
3.2.1 Synthesis and modification of the tetra-peptide Gly-Phe-Leu-Gly 59
3.2.2 Wang resin versus preloaded Wang resin 60
3.2.3 The synthesis of vinyl modified peptide 60
3.2.4 Synthesis of L-Leucyl-2-(5-fluorouracil-l-yl)-L,D-glycine (Leu-Gly(5-FU)): 64
3.2.5 Deprotection of Cbz blocking group 66
3.3 Conclusion 69
3.4 Experimental 69
3.4.1 Analytical technique 69
3.4.2 Materials 70
3.4.3 Synthesis of Gly-Leu-Phe-Leu using solid phase peptide synthesis (SPPS) 70
3.4.4 Synthesis of *N*-(Carbobenzyloxy)-L-leucyl-L,D-2-acetoxygly- cine Methyl Ester Cbz- Leu(α-OAc)-OMe (6) 72
3.4.5 Synthesis of *N*-(Carbobenzyloxy)-L-leucyl-2-(5-fluorouracil- 1- yl)-L,D-glycine Methyl Ester (7) 73
3.4.6 Synthesis of *N*-(Carbobenzyloxy)-L-leucyl-2-(5-fluorouracil- 1- y1)-L,D-glycine (8) 74
3.4.7 Synthesis of L-Leucyl-2-(5-fluoruracil-l-yl)-L,D-glycine (9) 74
3.4.8 Separation of L,L (9a) and L,D (9b) Diastereomers of L-Leucyl-2-(5-fluoruracil-l-yl)-L,D-glycine) 74
Chapter 4 Synthesis of the polymer peptide conjugate using aminolysis/Michael addition chemistry 76
4.1 Introduction 76
4.2 Results and discussion 78
4.2.1 The modification of SHB-PDMA via aminolysis/Michael addition reaction 78
4.2.2 Aminolysis in the presence of *N*-hydroxyethylacrylamide (HEA) as a Michael acceptor 79
4.2.3 Synthesis of polymer-peptide conjugates 84
4.3 Conclusion 92
4.4 Experimental 92
4.4.1 Instrumentation 92
4.4.2 Materials 92
4.4.3 Grafting the acrylamide to HS-PDMA 93

4.4.4 The synthesis of HS-PDMA-Gly-Leu-Phe-Gly 94
4.4.5 The activation of HS-PDMA-Gly-Leu-Phe-Gly carboxylic group 94
4.4.6 The synthesis of HS-PDMA-Gly-Leu-Phe-Gly-Leu-Gly(5-FU) 95
Chapter 5 Monitoring the release of 5-FU by ^{19}F NMR for MRI application 96
5.1 Introduction 96
5.2 Result and discussion 98
5.2.1 Proof-of-principle experiments 98
5.2.2 Enzyme catalysed release of the dipeptide derivatives of 5-FU 99
5.2.3 Enzyme catalysed release of 5-FU polymer conjugate 103
5.2.4 ^{19}F NMR of 5-FU derivatives at different pH 107
5.3 Conclusion 110
5.4 Experimental 111
5.4.1 Material 111
5.4.2 Release of 5-FU from 5-FU polymer conjugate and dipeptide derivatives of 5-FU 111
5.4.3 Instrumentations 111
Chapter 6 Conclusions and future work 113
6.1 Conclucions 113
6.2 Future work 115
References 117

Chapter 1 Introduction

1.1 Polymers

Since the discovery of the first synthetic polymer, Bakelite,[1] in the early 20th century there has been remarkable progress in polymer science. The word polymer means a large molecule, whose structure is composed of repeating units, monomers. One of the main advantages of polymers is their great versatility in terms of structure and composition.[2,3] Covalent bonding of monomers from the same type usually forms homopolymer while combining two or more monomers in different sequences results in block, alternating, or random copolymers. Furthermore, the polymer architecture can vary from simple linear chains to more complex dendritic or cross-linked polymers. Different polymer architectures and compositions are illustrated in Figure 1-1. Depending on the choice of monomers, their sequence, and the polymer architecture, chemical and/or physical properties can significantly be altered for specific application.[4,5]

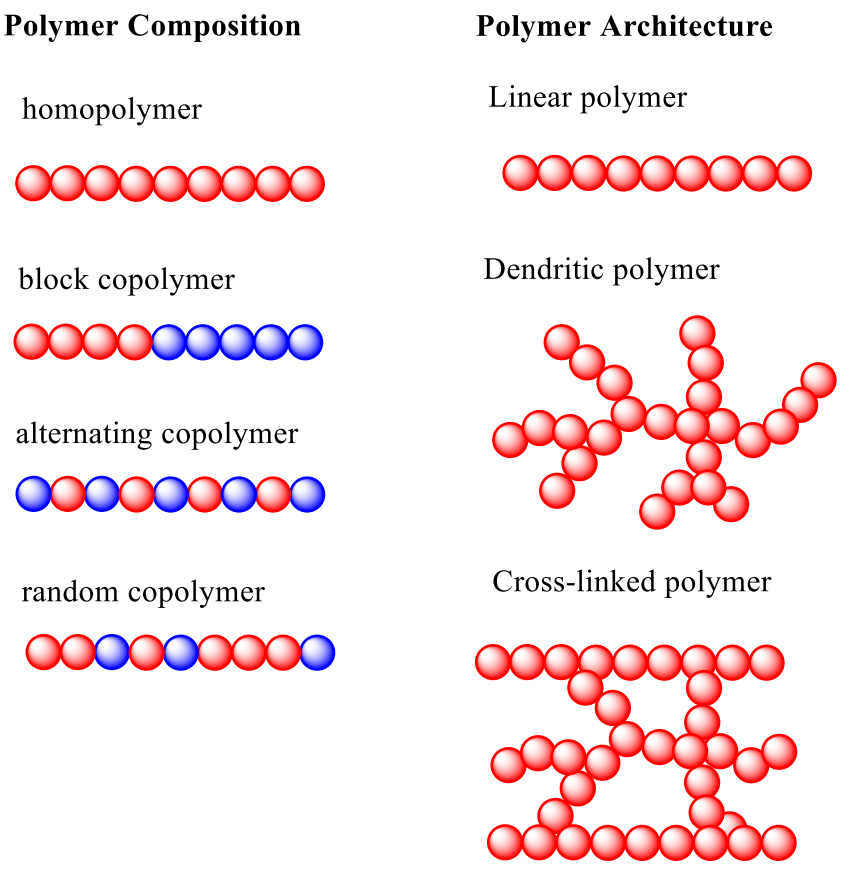

Figure 1-1. Possible polymer compositions and architectures

1.2 Polymer syntheses

Polymers can be mainly synthesised using two different types of polymerisations: step-growth polymerisation or chain-growth polymerisation.[6,7] Step-growth polymerisation often involves a series of condensation reactions, where a small molecule (e.g. H_2O or NH_3) is eliminated, and therefore it can be termed polycondensation.[6,8–10] The polymerisation typically employs bi-functional or multifunctional monomers which react to produce dimer, trimers, oligomers and eventually long chain polymers. Due to the nature of the polymerisation mechanism, molecular weight increases only slowly and high molecular weight can only be achieved at high monomer conversion (Figure 1-2).[11]

In contrast, chain growth polymerisation usually employs vinyl monomers that are capable of undergoing addition reactions.[5,12] The polymerisation consists of three distinct steps; initiation, propagation and termination. Depending on the nature of reactive centre, the polymerisation can be classified to free radical, anionic, or cationic. Among these, anionic polymerisation[13] might be considered as a "true living polymerisation"[14] as the process does not involve any intrinsic termination. Since all chains are initiated at the same time and propagate at roughly the same rate, molecular weight grows linearly with conversion (Figure 1-2) and hence well-defined polymers can be achieved with nearly mono-disperse molecular weight distribution and structural and compositional uniformity.[15–17] However, the polymerisation must be carried out under an inert atmosphere with rigorously dried reagents and glassware. Oxygen and carbon dioxide might react with the carbanion propagating centre to produce more stable peroxy or carboxyl anions that are not reactive enough to continue propagation.[5] Furthermore, the presence of a trace of water can cause termination.[12,16] Most importantly, the range of monomers that can be polymerised by anionic polymerisation is limited to monomers with electron withdrawing side groups to stabilise the delocalised negative charge.[16]

Free radical polymerisation is the most versatile chain growth polymerisation due its applicability to polymerise a broad variety of monomers, including those with functionality.[12,18] It is also synthetically much less demanding than anionic or cationic processes. However, due to the high reactivity and the high amount of radicals present in the system, unavoidable radical-radical termination usually results in poor control over molecular weight, dispersity and architecture (e.g. access to block copolymers).[11] In recent years, controlled radical polymerisation techniques have been developed. These include atom transfer radical polymerisation (ATRP),[19–21] nitroxide-mediated polymerisation (NMP),[22] and reversible addition-fragmentation chain transfer (RAFT) polymerisation.[23] Such techniques

ensure similar growth of propagating polymer chains by establishing a rapid dynamic equilibrium between active and dormant species. Shifting the equilibrium toward the dormant side ensures a low concentration of active radicals and thus minimises chain termination and chain transfer reactions. Due to the controlled process, all chains grow at roughly the same rate[24] allowing the synthesis of polymers with controlled molecular weight, dispersity, chemical composition, architecture, and well defined end group functionality.[25–29]

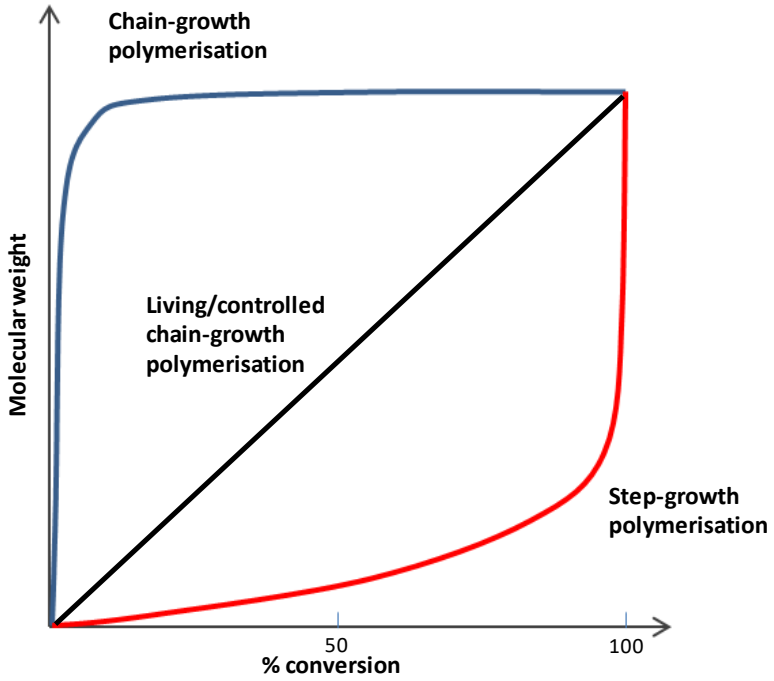

Figure 1-2. Molecular weight vs conversion in step-growth, chain-growth, and living/ controlled chain growth polymerisations

1.3 Reversible Addition-Fragmentation Chain Transfer (RAFT) polymerisation

RAFT polymerisation is arguably the most versatile method of controlled radical polymerisation because it is tolerant of a very wide range of functionalities in the monomer and solvent under a large number of experimental conditions.[30–33] The RAFT process was developed in 1998 by Rizzardo *et al.*[23] Unlike NMP and ATRP techniques, that rely upon reversible termination of propagating species,[34,35] RAFT is degenerative transfer-based system. To reach its deactivation−activation equilibrium, RAFT polymerisation typically employs a thiocarbonylthio chain transfer agent (CTA) with general structure illustrated in Figure 1-3.

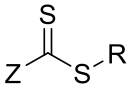

Figure 1-3. General structure of the chain transfer agent (CTA) employed in RAFT polymerisation

The accepted mechanism of RAFT polymerisation is illustrated in Scheme 1-1.[36] Owing to the nature of the RAFT process, the concentration of radicals during the activation−deactivation process remains unchanged.[31] An external source of initiator is utilised, typically those used in a conventional free radical polymerisation,[37] such as benzyl peroxide (BPO) and 4,4-azobis(4-cyanovaleric acid) (ACVA). After initiation, the propagating radical ($P_n^{\bullet}$) adds to the CTA (**1**) to form the radical adduct (**2**), which subsequently fragments to form a dormant macro CTA (**3**) and a new radical ($R^{\bullet}$) (**4**). The radical ($R^{\bullet}$) is capable of initiating further polymerisation to produce a new propagating radical ($P_m^{\bullet}$). After the consumption of the initially added CTA (i.e. completion of the "induction period"), the "main equilibrium" between propagating radicals (P_m or P_n) and dormant macro CTA (**3**/**6**) is established.

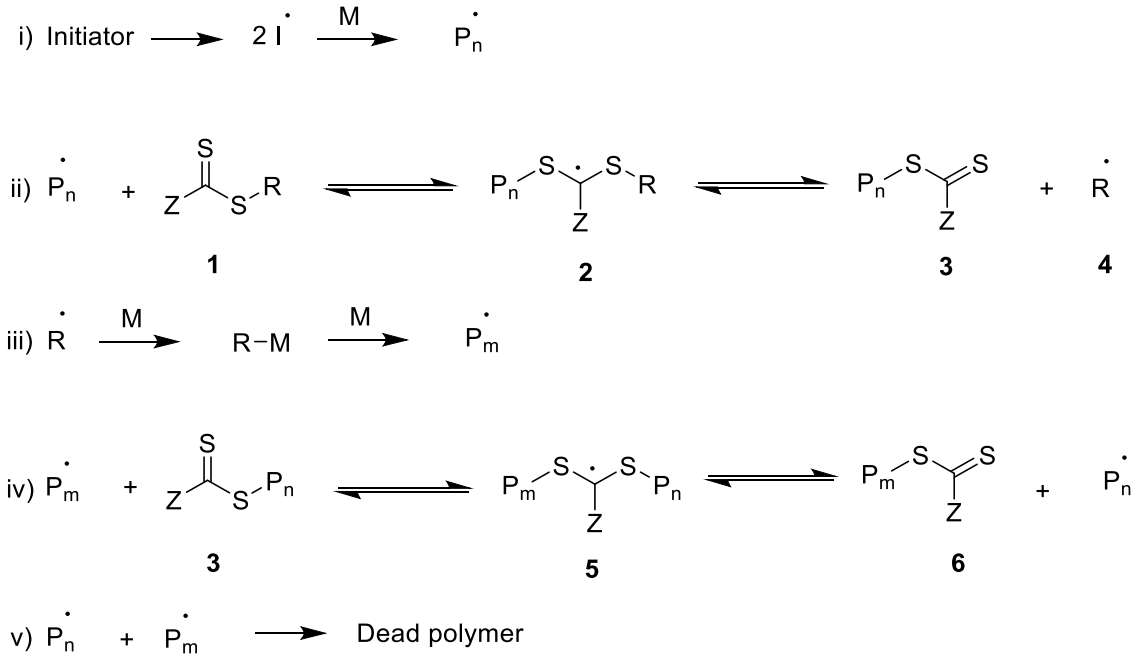

Scheme 1-1. Suggested mechanism for reversible-addition fragmentation chain transfer (RAFT) polymerisation[36]

1.4 Monomer scope and selection of CTAs

One of the key features of RAFT polymerisation is its ability to provide control over a wide range of monomers including those with functionalities (e.g. OH, NR_2, COOH, SO_3H).[30–32] RAFT polymerisation of monomers containing unprotected amines, that were thought to be a challenge owing to the expected aminolysis of the thiocarbonylthio moieties, has now become possible by tuning reaction conditions (i.e. protonating the amino group).[38] Generally, vinyl

monomers can be classified into more activated monomers (MAMs) and less activated monomers (LAMs). MAMs are those where the vinyl group is adjacent to an aromatic group, a carbonyl group or a nitrile, while LAMs are those where the vinyl group is adjacent to nitrogen, oxygen or halogen. Examples of MAMs include styrene, (meth)acrylates, (meth)acrylamides and acrylonitrile and for LAMs include vinyl acetate, *N*-vinylpyrrolidone and vinyl chloride.[30–32,39–41]

Careful selection of the CTA is needed before attempting RAFT polymerisation. As illustrated in Figure 1-3, the CTA typically consists of a thiocarbonylthio group with two substituents, R and Z that significantly influence the polymerisation kinetics and efficiency. The Z-group should effectively activate the C=S double bond towards radical addition whilst providing stability to the intermediate adduct formed when radicals add to the CTA.[23] As there are two classes of monomers, the CTA should be tailored to their different reactivity. Due to radical-stabilising substituent, MAM usually results in more stabilised propagating radical that must be matched with a more active CTA, such as dithioesters (Z = alkyl or aryl),[23] trithiocarbonates (Z = *S*-alkyl),[42] and aromatic dithiocarbamates (Z = pyrrole).[43] In contrast, propagating radicals with a terminal LAM are less stabilised. Therefore, a less active CTA, such as dithiocarbamate (Z = *N*-alkyl)[44] or xanthate (Z = *O*-alkyl)[45] are required. Recently, universal CTAs that control the polymerisation of both LAMs and MAMs and hence enabling access to poly(MAM)-*block*-poly(LAM) have been developed.[46–49] Benaglia *et al*.[49] reported an elegant example of pH-switchable *N*-(4-pyridinyl)-*N*-methyldithiocarbamate derivatives. Such CTAs offer a good control over the polymerisation of LAMs and when protonated also offer a control over the polymerisation of MAMs.

The Z-group needs to be an electron-withdrawing group to achieve a high transfer constant and to provide stability to the intermediate radicals **2** and **5** (Scheme 1-1).[30] However, the stability of the intermediate radicals should be finely tuned as the stability might increase the likelihood of inhibition or retardation. For example, aromatic dithioesters (dithiobenzoate where Z = Ph) might strongly stabilise the intermediate radical adduct causing retardation which arguably can be explained by two theories; slow fragmentation and cross termination.[36,50,51]

The R-group of the CTA should be a good homolytic leaving group to facilitate fragmentation of the CTA after addition of the propagating radical but at the same time be capable of reinitiating the polymerisation at a rate comparable to that of propagation, otherwise retardation is likely.[23] Therefore, a balance between radical stability and steric effects has to be met.[31]

Control over the polymerisation of monomers that form stable tertiary intermediate radicals (e.g. methacrylates and methacrylamides) requires the use of tertiary R-groups (e.g., cumyl, 2-

cyano-2-propyl)[52] or secondary aryl (e.g., α-cyanobenzyl).[53] In contrast, the use of primary or secondary R groups is required to control the polymerisation of monomers with high propagation rate constants (e.g. acrylamides, acrylates, styrene).[30]

Although the use of R-groups that mimic monomer radicals has been successful in the polymerisation of monomers with high propagation rate constants (e.g. acrylate, acrylamides),[54,55] the polymerisation of methyl methacrylate show inhibition as fragmentation of the polymethacrylate radicals is favoured in comparison with the single methacrylate.[52,56] Poor selection of Z- and R-group results in substantial retardation.[57] General guidelines for the selection of Z- and R-group are found in various reviews.[27,30,31,33,39,40]

1.5 Dendritic polymers

As illustrated earlier in Figure 1-1, polymer architecture can vary from linear chain to more complex dendritic polymers. The properties of the polymer are highly dependent on its structure. In recent years, significant attention has been paid to the synthesis of dendritic polymers due to their unique properties including good solubility, three-dimensional globular architecture, decreased chain entanglement, low viscosity, and the abundance of large number of terminal functional groups for post-polymerisation modification.[58] A wide range of possible dendritic polymer architectures can be formed,[59,60] some of which are presented in Figure 1-4.

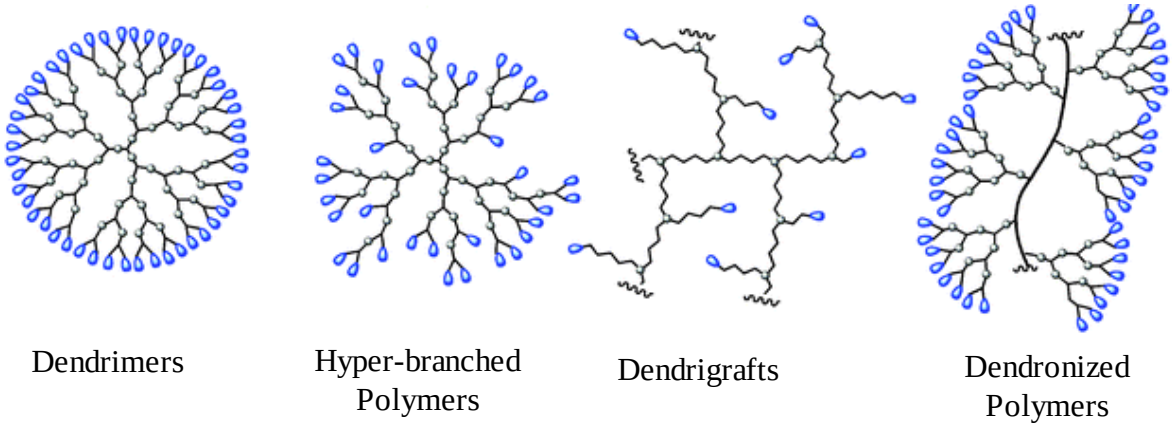

Figure 1-4. Different classes of dendritic polymers.[60] *Reprinted with permission from reference 60. Copyright (2009) American Chemical Society.*

Dendrimers are considered to be the best characterised class of dendritic polymers due to the high degrees of symmetry in their architecture.[58] Dendrimers are typically synthesised via the attachment of multifunctional repeating units to a central multifunctional 'core' by either a divergent[61] or a convergent[62] approach. The number of terminal groups on the dendrimers grows geometrically with the generation number. Although the monodisperse nature of

dendrimers yields interesting properties, the step-wise syntheses with time consuming purifications limit their availability. Furthermore, their growth at higher generations might be hindered by steric effects caused by the high degree of branching.[63,64]

Random hyper-branched polymers (HBPs)[65–67] are more attractive alternatives as they possess similar properties and are far easier to synthesise. The synthesis of HBPs can typically be accomplished in a one-pot reaction. Theoretical description of the synthesis of HBPs employing AB_x-type monomer ($x \geq 2$) was reported by Flory[68] in the early 1950s. However, it was not until 1988 when Gunatillake *et al.*[69] and Kim and Webster[70,71] independently reported the first examples of HBPs. This was then extended to include the copolymerisation of A_2 and B_3 monomers.[72] Although such technique has been used to synthesise soluble HBPs, the scope of monomer is limited to those polymerised using condensation polymerisation (AB_x or A_2+B_3). Recently, a number of synthetic methods have been developed. These include polymerisation of vinyl monomers in the presence of divinyl crosslinker,[73,74] self-condensing ring-opening polymerisation,[75,76] and self-condensing vinyl polymerisation (SCVP).[77]

1.6 Self-Condensing Vinyl Polymerisation (SCVP)

Self-condensing vinyl polymerisation (SCVP) is one of the most versatile approaches as it employs readily available vinyl monomers with less chance of gelation. SCVP process was first demonstrated by Fréchet *et al.*[77] in 1995, who described the polymerisation of [(1-chloroethyl)ethenyl]benzene using a ‘‘living’’ cationic polymerisation in the presence of $SnCl_4$. SCVP is a combination of vinyl chain-growth polymerisation and condensation polymerisation. The general mechanism of SCVP is illustrated in Scheme 1-2. The process typically employs an AB*-type monomer, where A stands for the vinyl group and B* stands for the initiating group. Activation of B to form B* moiety initiates the polymerisation of the vinyl monomer to form an AB_2-type monomer, that is usually used to synthesise HBPs, with one polymerisable vinyl group and two initiating/propagating sites. The condensation of such oligomers results in the formation of a HBP. Homopolymerisation of AB*-type monomers result in very condensed structure with high degree of branching (DB) of 0.466[78] (similar to those synthesised by conventional polycondensation method). Copolymerisation of AB*-type monomer with typical vinyl monomers produce HBPs with more linear character with DB lower than 0.466.[78,79] Those are typically termed segmented hyper-branched polymers (SHBPs).[79] Despite the low DB achieved, self-condensing vinyl copolymerisation has been

explored more thoroughly than homopolymerisation, as it offers more control over dispersity, degree of branching simply by tuning the stoichiometry of [M] to [AB*].[78,80]

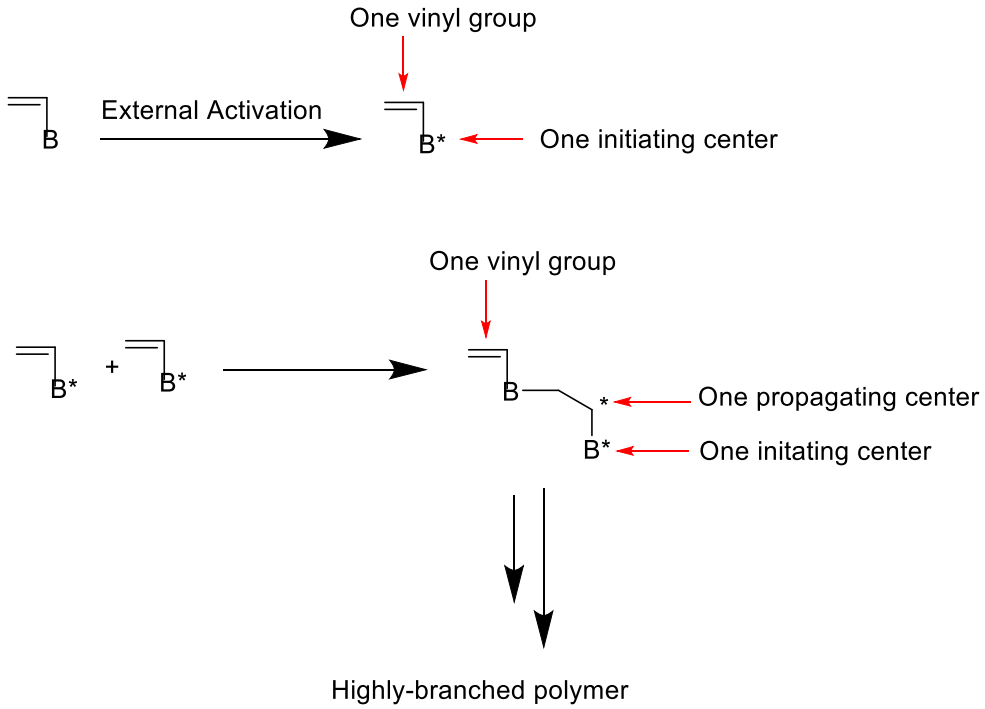

Scheme 1-2. Suggested mechanism for self-condensing vinyl polymerisation (SCVP)[77]

SCVP can be mediated by a number of techniques depending on the nature of the external stimulus that is applied. These include anionic,[81,82] cationic,[77] and controlled free radical polymerisations such as NMP,[83,84] ATRP,[85–88] and RAFT.[89]

1.7 SCVP mediated by RAFT

The first example of RAFT mediated SCVP was demonstrated in 2003 by Yang *et al.*[89] shortly after the introduction of both SCVP[77] and RAFT[23] in 1995 and 1998, respectively. The AB*-type monomer used in RAFT-SCVP is known as a chain transfer monomer (CTM) and is usually formed by introducing a polymerisable vinyl group into the CTA structure.[79] The vinyl group represents A while thiocarbonylthio represents the B* group. The vinyl group can be either on the Z-group (Z-approach) or the R-group (R-approach) of the CTM.[79,90] Such approaches can synthesise SHBPs with thiocarbonylthio moiety located at the branch points or the chain ends, respectively. In the first example of RAFT-SCVP, Yang *et al.*[89] used a styrenic dithioester (Figure 1-5), with polymerisable styryl unit as the Z-group, for the copolymerisation with styrene. Although this approach was able to synthesise SHBPs, the presence of hydrolytically unstable thiocarbonylthio group at every branch points and the steric hindrance

to access the CTA functionalities limit the use of this approach. Two years later, Rimmer *et al*.[91] modified the method by placing the polymerisable vinyl on the R-group of CTM (1, Table 1-1) for the copolymerisations of *N*-isopropyl acrylamide (NIPAM). This route avoids the introduction of thiocarbonylthio linkage into the branching point allowing further functionalisation. This was followed by several examples including Puskas *et al*.[92] work who synthesised segmented hyper-branched polystyrene using inverse structure compared with Yang *et al*.[89] CTM (2, Table 1-1).

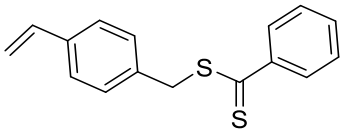

Figure 1-5. First CTM developed by Yang et al[89] *to synthesise segmented hyper-branched polystyrene*

Chain extension of SHBPs synthesised using either Z- or R-approaches results in polymers with totally different structures (Figure 1-6).[90] Despite the weak thiocarbonylthio linkages placed at every branch point for SHBPs synthesised by R-approach, chain extension of these results in polymers with interesting structures. For example, Patrickios *et al*.[93] produced novel segmented amphiphilic hyper-branched block copolymers of styrene (St) and vinylpyridine (VPy) in two step RAFT-SCVP employing Yang *et al*.[89] CTM (Figure 1-5). In this approach, one monomer is polymerised first, producing a segmented hyper-branched macro CTA. Due to the presence of reactive thiocarbonylthio at each branch point, the second block is inserted at the branch points (Figure 1-6). Such interesting structures could not be produced via SCVP mediated by NMP or ATRP.[90] In contrast, because of the presence of thiocarbonylthio at the periphery, chain extension of SHBPs synthesised by R-approach results in star-like block copolymers (Figure 1-6).[94–98]

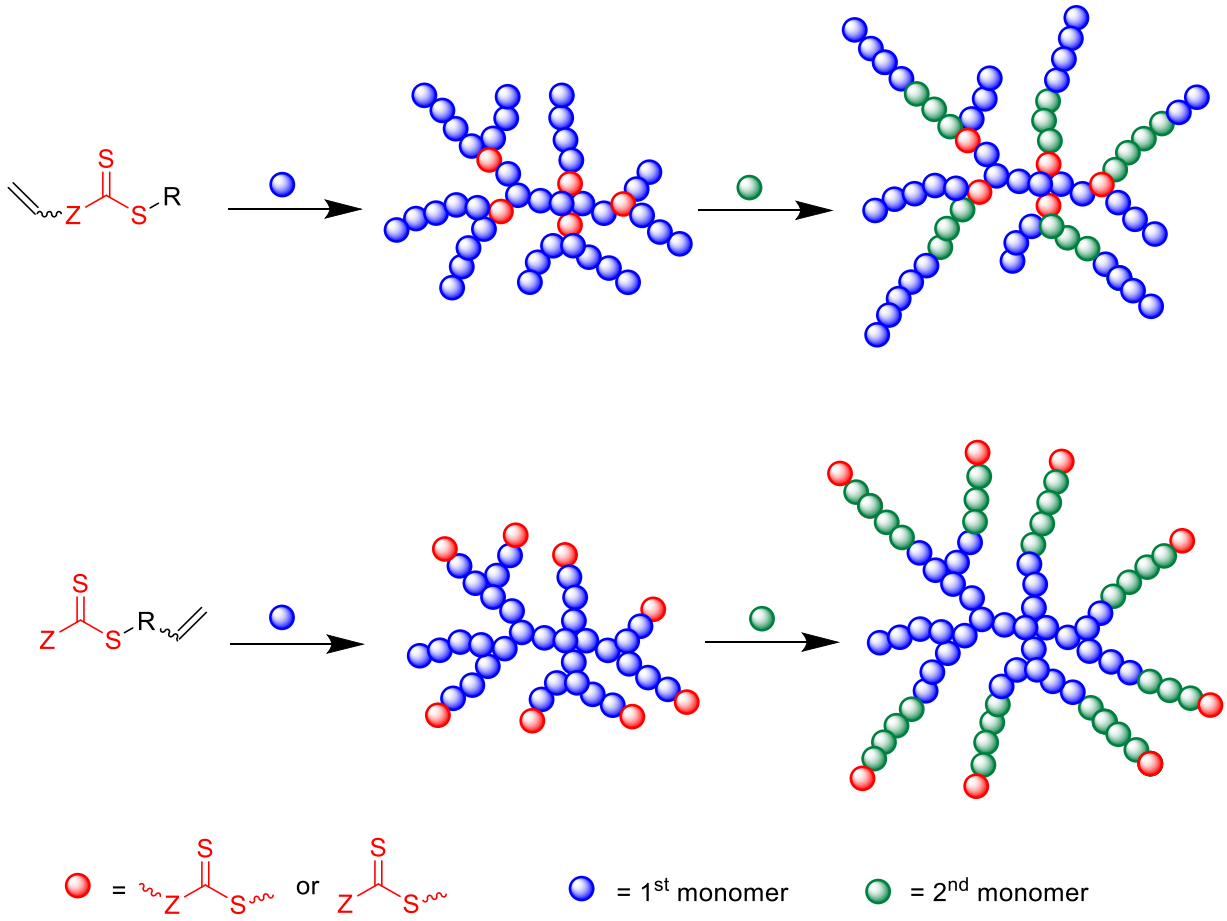

Figure 1-6. SHBPs synthesised using RAFT-SCVP using Z- or R- approach, chain extension of which resulted in polymers with different structures[90]

1.8 Scope of monomers and CTMs

In principle, monomers that undergo RAFT polymerisation can also be polymerised via RAFT-SCVP. Monomers that have been polymerised by RAFT-SCVP include styrenes, vinyl acetate, (meth)acrylates and (meth)acrylamides (Figure. A-1). Copolymerisation of CTM with protected amino acid-based monomers has also been reported.[98]

Selection of Z and R- group: Similar to conventional RAFT, selection of R- and Z-groups of the CTM is critical in RAFT-SCVP as it can significantly affect the polymerisation kinetics and efficiency.[79] Table 1-1 summarises the CTMs that have been developed to date. Dithioester,[89,91,92,95,99–101] trithiocarbonate[98,102–106] and aromatic carbamate[94,99,100,107] based CTMs (1-14, Table 1-1) have been developed for the copolymerisation with styrenes, acrylate, methacrylate and acrylamide monomers. Also, two xanthate-based CTMs[97,108] (15 and 16, Table 1-1) have been reported to offer control for the copolymerisation with vinyl acetate. Recently, a switchable dithiocarbamate-based CTM for the polymerisation of both MAMs and LAMs has been developed. Sudo *et al.*[109] has reported a universal CTM, namely (4-

vinyl)benzyl-*N*-methyl-*N*-(4-pyridyl) dithiocarbamate (Figure 1-7), for the facile synthesis of star-like block copolymers. Protonation of such CTM allows the polymerisation of St to form SHBP core which was chain extended by NIPAM. Deprotonation of the macro CTM allows the addition of vinyl acetate to form a star-like block copolymer.

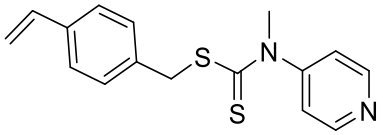

Figure 1-7. pH switchable CTM developed by Sudo et al.[109] *to synthesise star-shaped poly(MAM)-block-poly(LAM)*

To avoid retardation, consideration should be paid on the selection of R-group. CTMs with tertiary R-groups (3, 7, 9-14 in Table 1-1) have been selected to polymerise methacrylate and methacrylamide monomers whereas primary and secondary R-group (1, 2, 4, 5, 6, 15, 16 in Table 1-1) have been used to control the polymerisation of monomers with high propagation rate constants.

CTM polymerisable group: Careful consideration should be paid to the nature of the polymerisable vinyl group of the CTM. The reactivity ratio of the polymerisable group of CTM in comparison with that of the conventional monomer copolymerised greatly influences branch formation and hence the final structure of the polymer. Well-defined SHBPs with regular branching can only be formed if the reactivity of the polymerisable moiety is similar the monomer.[78,110] Formation of "hyperstars" is expected if vinyl group of CTM is much more reactive than the monomer, and "macroinimers" are formed in the opposite case.[110] When the vinyl group of CTM is much less reactive than the monomer, the CTM will act as an ordinary CTA and add monomer until the latter is completely consumed thus forming a "macroinimer". Linking reactions are not very pronounced and only become significant at high monomer conversion. Conversely, when the vinyl group of the CTM is much more reactive than the monomer, the CTM will first undergo SCVP to form a hyper-branched core, then start adding monomer to form star-like polymers or "hyperstars". The reactivity ratio will not only affect the final structure, but it will affect the molecular weight, dispersity and degree of branching. At any given [M]:[CTM], molecular weight, dispersity and degree of branching increase with increasing the reactivity of CTM.[110]

Generally, due to the nature of SCVP that combines the features of controlled chain growth and step-growth process (see Figure 1-2), high molecular weight polymers can only be achieved at very high conversion.[90] As illustrated at Figure 1-8, at very low conversions, the molecular weight increases linearly with conversion as it should in a conventional controlled

chain-growth polymerisation. At higher conversions the increase in the molecular weight becomes sharper caused by the linking step-growth reactions. However, this strongly depends on [M]:[CTM] and the reactivity ratio. At very small [M]:[CTM], the molecular weight increases with conversion similar to step-growth. When the reactivity of CTM vinyl group is much greater than the monomer, a strong increase in the molecular weight at low monomer conversion will be observed. This is because CTMs are consumed fast forming hyper-branched macro CTA. In contrast, when the reactivity of CTM vinyl group is much lower than the monomer, the molecular weight grows similar to conventional controlled chain-growth.

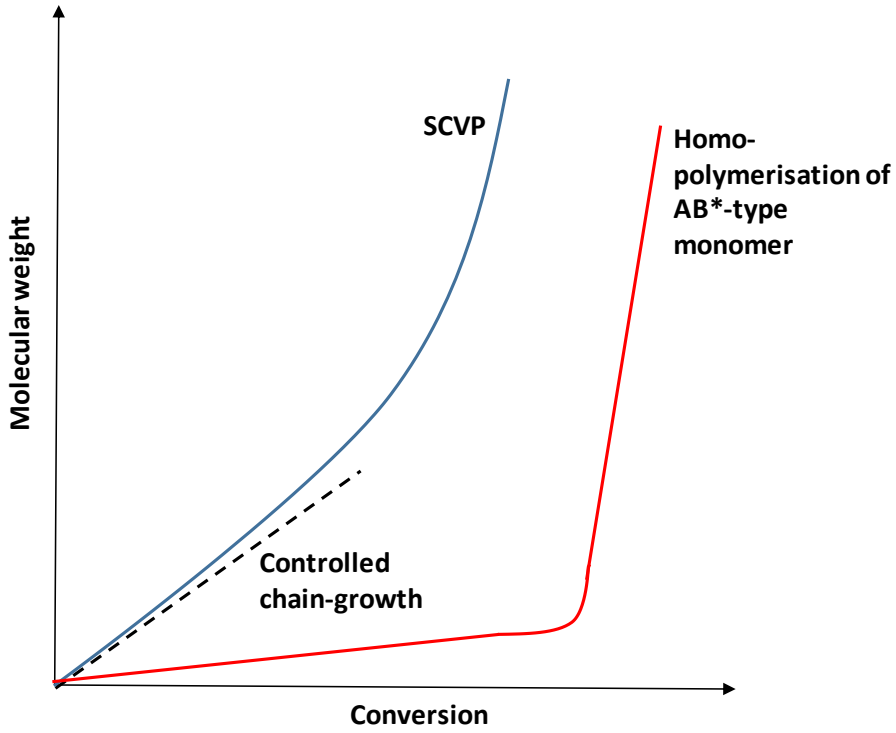

Figure 1-8. Dependence of molecular weight on conversion in SCVP

The dependence of degree of branching (DB) on conversion is shown in Figure 1-9. The revolution of DB strongly depends on [M]:[CTM]. In homo-SCVP and very small [M]:[CTM], the DB increases with conversion and the highest DB is reached at high monomer conversion. In contrast, at high [M]:[CTM], DB very quickly reaches its final value and then remains constant throughout the polymerisation. However, the DB is also affected by the reactivity ratio. A comprehensive explanation is found in reference 78 and 110.

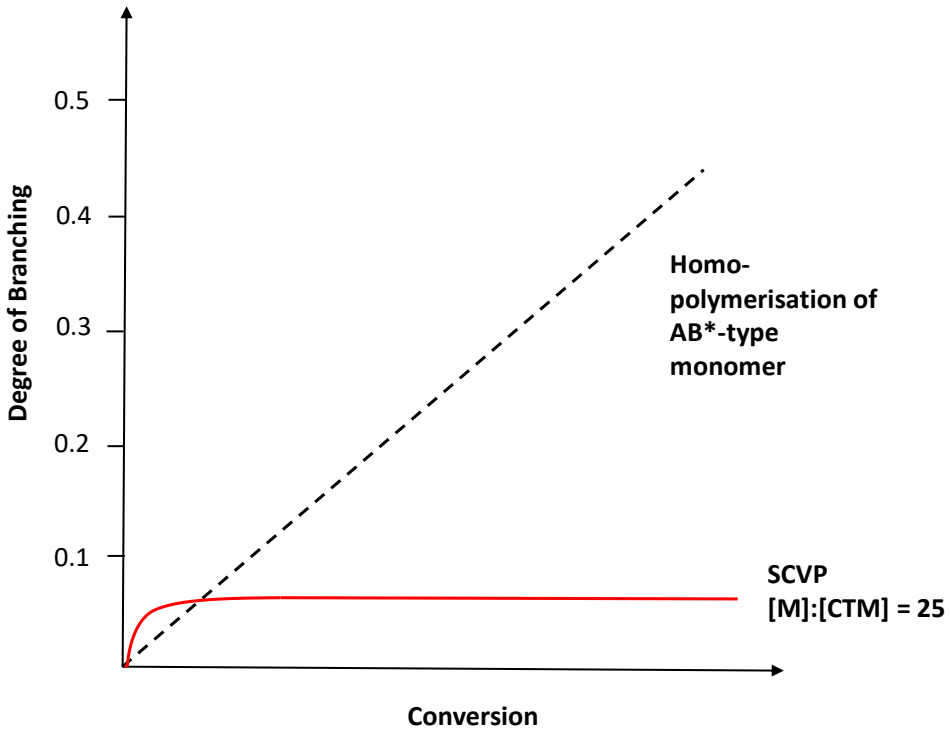

Figure 1-9. The dependence of degree of branching on conversion in SCVP. The final DB in homo-SCVP is 0.446 whereas the DB in SCVP at [M]:[CTM] =25 is 0.077

Table 1-1. CTMs that have been developed to date. The names and structures of monomers are shown in Figure. A-1.

	CTM	Monomer		CTM	Monomer
1	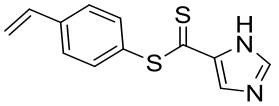	NIPAM[91,95]	9	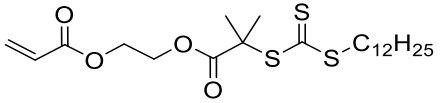	DMAEMA[101]
2	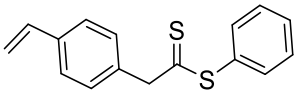	VPy and St,[93] AA[100]	10	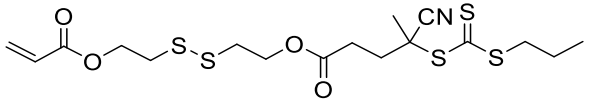	PEGMA[104]
3	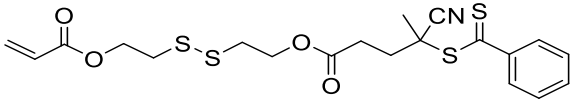	GMA[105]	11	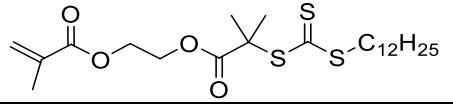	GMA[111]
4	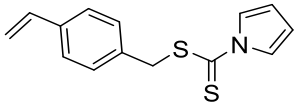	NIPAM,[99,107] AMPS,[94] AA[100]	12	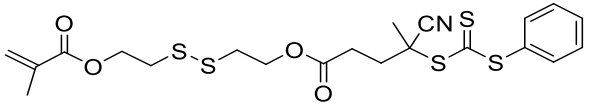	GMA[112]
5	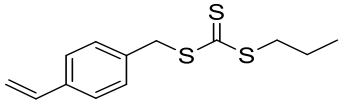	St[102]	13	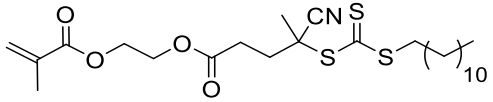	TFEMA co PEGMA[113]
6	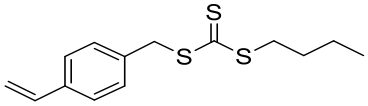	NIPAM[103] Boc-Val-HEA[98]	14	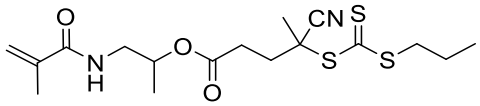	HPMA[106]
7	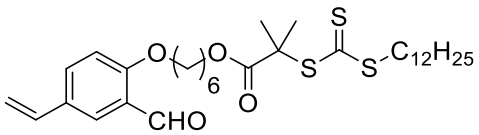	DMAEMA[114]	15	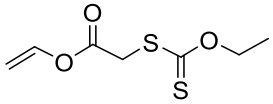	VA[108]
8	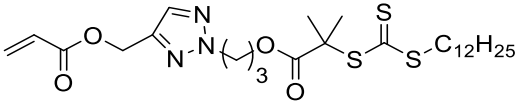	NIPAM[115]	16	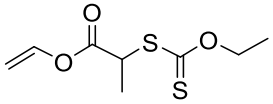	VA[97]

1.9 Magnetic Resonance Imaging (MRI)

Among the various imaging modalities that have been developed, magnetic resonance imaging (MRI)[116] is arguably the most versatile imaging technique owing to its advantages including relatively high temporal and spatial resolution. Unlike X-ray computed tomography imaging or radionuclide imaging (e.g. positron-emission tomography (PET) and single-photon emission computed tomography (SPECT)), MRI does not involve any ionizing radiation or radioactive tracers. It has no limitations due to sample penetration seen in optical imaging (e.g. fluorescence). Nevertheless, MRI is a relatively slow imaging modality and contrast agents are usually required to best highlight specific tissues or organs.[117–119]

The idea of imaging using NMR (i.e. MRI), developed by Lauterbur in 1973[116], depends on the ability of NMR active nuclei to align and precess around the direction of a static magnetic field. The application of orthogonal radiofrequency pulses alters the angle of rotation of precessing nuclei allowing the measurement of the resonance frequency. Once the radiofrequency is turned off, nuclei relax to their original alignment along the main static field. Relaxation can be defined by two time constants; the longitudinal relaxation (along the Z axis) and transverse relaxation (in X-Y plane). The longitudinal relaxation time, T_1, represents the loss of energy to the environment, and therefore is known as "spin–lattice relaxation time", while transverse relaxation time, T_2, represents the energy exchange between neighbouring spins and is called the "spin-spin relaxation time". The signal intensity in MRI is largely dependent on longitudinal and transverse relaxation times.[120–122]

Generally, MRI is employed directly for imaging the abundant hydrogen (mostly from water) inside the human body. The use of contrast agents, however, is commonly required to improve imaging contrast.[123–125] While such contrast agents are not directly visualised, they alter the relaxation times of surrounding water protons to best highlight the tissues of interest. Contrast agents can be classified into two types depending whether they cause change in T_1 or T_2 relaxation times generating positive or negative contrast, respectively. All contrast agents decrease both T_1 and T_2 relaxation times to varying degrees depending on the contrast agent nature.[126] Paramagnetic materials (e.g. gadolinium)[127,126] decrease both T_1 and T_2 but are considered as T_1 contrast agent (best imaged using T_1-weighted scans) as the change in magnitude in T_1 is much greater than that in T_2. On the contrary, superparamagnetic materials (e.g. iron oxide nanoparticles)[128–130] generally lead to a much larger decrease in T_2 than in T_1 and hence are considered as T_2 contrast agents (best visualized with T_2-weighted images).

Although such contrast agents have significantly improved the performance of MRI, the contrast is usually subtle due to large background signals arising from water protons in living tissues.

1.9.1 ^{19}F MRI

In recent years, ^{19}F MRI has been considered as a promising MRI technique owing to the lack of endogenous background signals. Only trace amounts ($<10^{-6}$ M) of fluorine are found in the body in the form of immobilised salts mainly in bones and teeth, resulting in a very short T_2 relaxation time that is not visible to conventional MRI technique.[131] ^{19}F has favourable NMR properties including 100% natural abundance, a large gyromagnetic ratio (40.08 compared with 42.58 MHz T^{-1} of ^{1}H), and high sensitivity (83% relative to ^{1}H). Moreover, ^{19}F resonance is very sensitive to subtle changes in the local environment due to 9 electrons surrounding ^{19}F nucleus rather than a single electron as in the case with ^{1}H, resulting in broad chemical shift range (>350 ppm compared with only 13 ppm for ^{1}H).[132]

^{19}F MR imaging was first demonstrated by Holland *et al*.[133] in 1977, only a few years after the discovery of ^{1}H MRI by Lauterbur.[116] However, the first in vivo ^{19}F MR images were only reported in 1985 when McFarland *et al*.[134] described images of rat abdomens. Since then, there has been tremendous progress in ^{19}F MR imaging for several quantitative applications, including real time monitoring of drug delivery,[135] tumour oxygenation studies,[136] and cell tracking.[137–141] A variety of small perfluorocarbon compounds (PFCs) with high number of equivalent fluorine atom (e.g. perfluorooctyl bromide (PFOB) and perfluoro-15-crown-5-ether (PFCE)) to maximise the signal to noise ratio and provide a single ^{19}F resonance have been developed.[142] Formulation of these PFCs into nanoemulsion particles with sizes in the range of several hundred nanometers has been the most commonly used approach to overcome their poor solubility for *in vivo* applications.[143–145] However, the large size (~200 nm) and instability of such emulsion droplets limit their use especially from imaging small features. The use of perfluorocarbons as ^{19}F MRI probes in biological applications is beyond the scope of this section and has been covered in many reviews.[143,146,147] The scope of this section is to cover the development of more sophisticated imaging probes particularly those polymeric-based and smart probes.

1.9.2 Polymeric ^{19}F MRI contrast agents

Within the past decade, extensive attention has been paid to the development of partially fluorinated polymers as a potential new generation of ^{19}F MRI contrast agents.[148,149] In order to achieve a good MR image intensity, ^{19}F-labelled polymers should meet specific criteria including high fluorine content, long T_2 relaxation times and short T_1 relaxation times as clearly stated in Equation 1-1.[150]

$$I = N(F)\left[1 - 2\exp\left(\frac{-(T_R - T_E)/2}{T_1}\right) + \exp\left(\frac{-T_R}{T_1}\right)\right]\exp\left(\frac{-T_E}{T_2}\right) \qquad \textit{Equation 1-1}$$

Where I is the imaging intensity, N(F) is ^{19}F content in the volume element of the image, and T_R and T_E are the pulse sequence repetition time and echo delay times, respectively. Furthermore, the contrast agent should preferentially have a single fluorine signal as multiple fluorine signals may result in lower signal intensity and imaging artifacts.[151]

Relative motion of nuclei is responsible for the fluctuations that cause relaxation. As illustrated in Figure 1-10, unlike small molecules or molecules with limited motion (solid state), polymers in solution tend to have efficient T_1 relaxation times (i. e. short T_1). Short T_1 relaxation time is favourable as it determines the relaxation delay between pulses.[152,153] The relaxation delay between scans must be at least five times the longest T_1 relaxation time to ensure that the nuclear spin system relaxes back to equilibrium before the next pulse is applied. A short T_1 relaxation time allows more scans within certain time-frame and hence a better signal-to-noise ratio can be obtained. However, due to the slow molecular motion, polymers tend also to have short T_2 relaxation times. As the signal line-width is inversely proportional to T_2 relaxation time, a short T_2 leads to signal line-broadening and in some cases, it can lead to loss of signal intensity.[152] The relative motion of ^{19}F nuclei and hence T_2 of relaxation times are greatly influenced by polymer structure and composition.

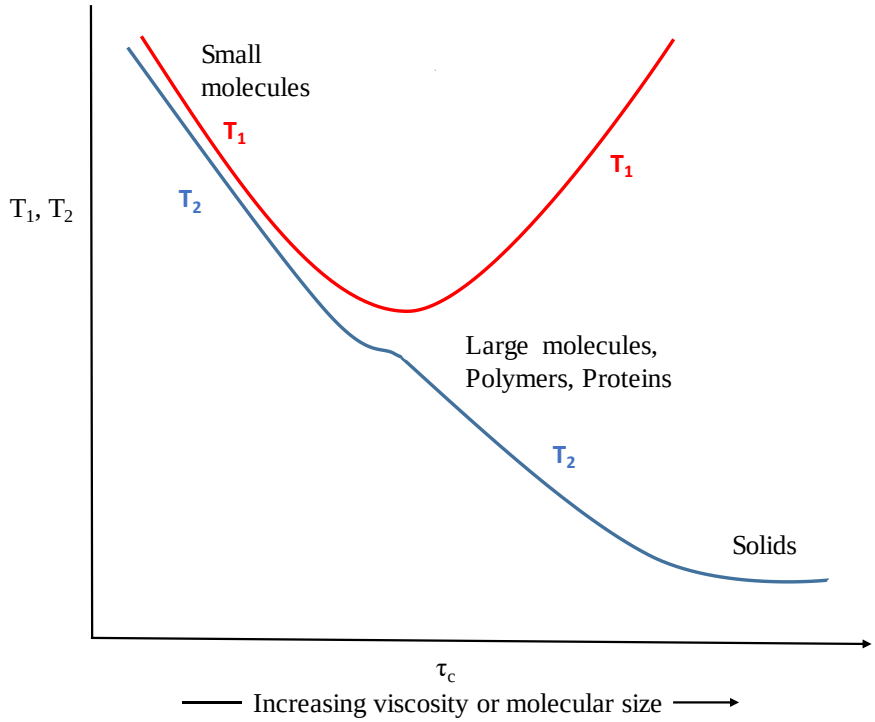

Figure 1-10. Dependence of T_1 and T_2 relaxation times on the correlation time τ_c.[153] *τ_c is defined as the time it takes the average molecule to rotate one radian.*

There are several mechanisms by which molecular motions can influence nuclear relaxation polymeric systems: the most important are dipole-dipole interactions and chemical shift anisotropy. [152,154] As in the case with other active NMR nuclei, dipole-dipole interactions are the most common mechanism for relaxation of ^{19}F nuclei in polymeric systems. The strength of dipolar coupling depends on nuclei involved. Nuclei with a large gyromagnetic ratio (proton and fluorine) will be the most effective in causing relaxation. Due to the low natural abundance of ^{13}C, ^{19}F is less likely affected by ^{13}C nuclei.[140] Dipole-dipole relaxation for ^{19}F nuclei shows a strong distance dependence between dipoles. On the other hand, chemical shift anisotropy is the second important mechanism for fluorine relaxation. Nuclei with a large chemical shift range are more likely to be affected by chemical shift anisotropy.[152] Unlike ^{1}H, ^{19}F is surrounded by 9 electrons and therefore its chemical shift is much more sensitive to the orientation of the molecule relative to the magnetic field.

The T_2 of ^{19}F nuclei is greatly influenced by localized segmental motions, and at least for high molecular weight polymers (over 10,000 Da), the overall reorientation of the entire chains makes only a small contribution to relaxation.[152] For example, it is sometimes observed that the line for side chain signals is sharper than the main chain signals suggesting that the side chains experience additional motion relative to the main chain atoms.[152] Generally, fluorine nuclei within chain segments undergoing restricted motion exhibit short T_2 relaxation

times,[155,156] whereas fluorine nuclei within chain segments experiencing large amplitude molecular motion show reasonably long T_2 relaxation times.[157,158] For example, a number of micelles with poorly solvated core and water soluble corona as ^{19}F MRI contrast agents have been developed.[155–157,159] The incorporation of fluorine nuclei within the poorly solvated hydrophobic core results in large dipolar coupling and hence shortening T_2 relaxation times. Nystrom *et al.*[155] synthesised linear poly(acrylic acid)-b-poly(styrene-co-pentafluorostyrene) block copolymers that self-assembled into micelles in aqueous solution. In this study, ^{19}F nuclei were buried within the poorly solvated hydrophobic core resulting in non-detectable ^{19}F signal from the aqueous solution. Similarly, Peng *et al.*[156] developed a range of amphiphilic block copolymers in which poly(acrylic acid) represents hydrophilic region and n-butyl acrylate copolymerised with a fluorinated acrylate represents hydrophobic region as illustrated in Figure 1-11. Such block copolymers again self-assembled into micelles in aqueous solution with the ^{19}F nuclei incorporated within the hydrophobic cores. However, in this case due to the low T_g of the core components, the ^{19}F signal was detectable but a low T_2 value of 1.75 ms was obtained from the aqueous nanoparticle solutions.

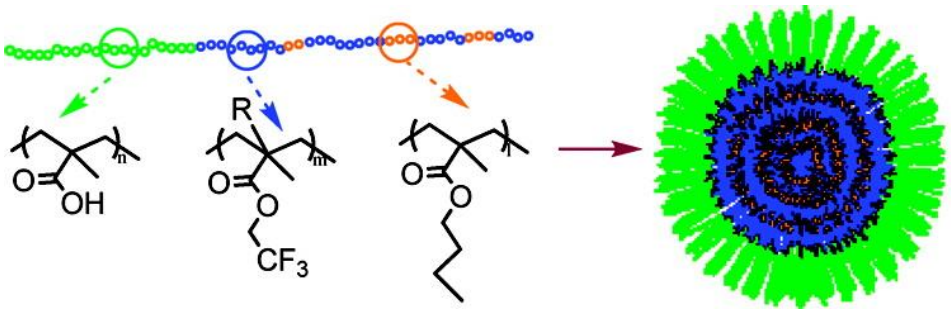

Figure 1-11. A simplified representation of a micelle developed by Peng et al.[156] with fluorinated segmented located in the poorly solvated core. ^{19}F signal, but low T_2 of 1.75 ms, was obtained thanks to low T_g of the core components. Reprinted with permission from reference 156. Copyright (2009) American Chemical Society.

In contrast, the incorporation of fluorine nuclei within the corona will enhance their motion leading to elongation in T_2 relaxation times and good image intensity. Wooley *et al.*[157] reported a range of amphiphilic star fluoropolymers prepared by grafting poly(acrylic acid-co-trifluoroethyl methacrylate) copolymer coronas from a hydrophobic hyperbranched core previously synthesised via SCVP mediated by ATRP. Such amphiphilic block copolymers were successfully self-assembled into stable micelles in aqueous solution as shown in Figure 1-12. In this study, fluorine nuclei were incorporated within the flexible corona resulting in a narrow ^{19}F resonance signal, short T_1, and reasonably long T_2 (50–56 ms). Although such micelles successfully produced adequate MRI images, due to the limited fluorine

concentrations, a long scan time was required and therefore they were not suitable for *in vivo* application.

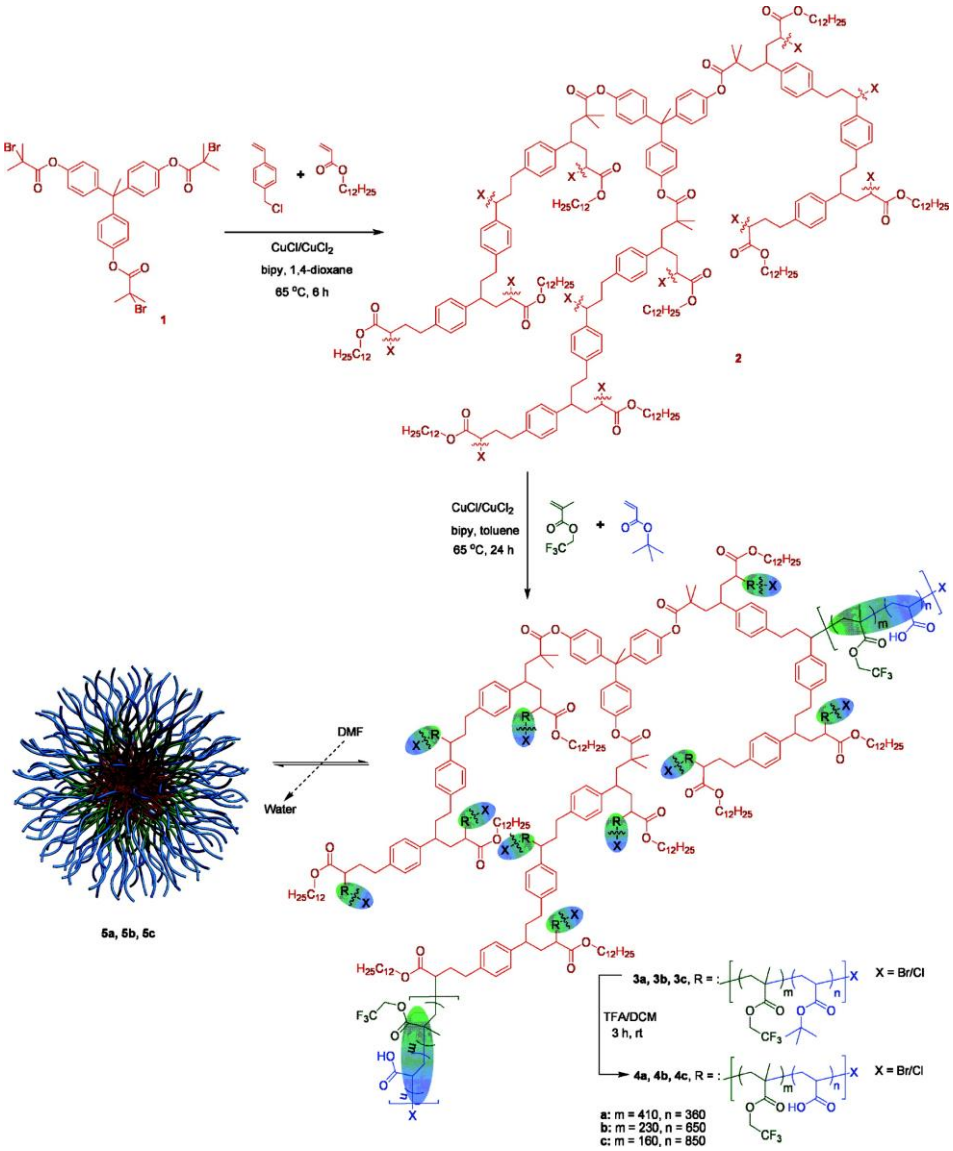

Figure 1-12. A representation of the micelle developed by Wooley et al.[157] *with fluorinated segments located in the soluble corona. Reprinted from reference 157.*

High ^{19}F content is required to achieve a good signal-to-noise ratio as ^{19}F MRI intensity is directly related to the fluorine content (Equation 1-1). For example, Zhao *et al.*[158] reported the synthesis of a range of fluorinated diblock copolymer of poly(oligo(ethylene glycol) methyl ether methacrylate-co-2,2,2-trifluoroethyl acrylate-b-poly(styrene-co-3-vinylbenzaldehyde) (poly(OEGA-co-TFEA)-b-poly(St-co-VBA)) nanoparticles, including spheres, worm-like particles and vesicles, through RAFT mediated polymerisation-induced self-assembly (PISA). To maintain high flexibility, fluorine nuclei were incorporated within the corona. T_1 and T_2 relaxation times were independent of the morphology of the nanoparticles, suggesting similar dynamics of the corona for the different morphologies. However, ^{19}F MRI signal intensity was

strongly dependent on the morphology as the surface area, and hence the fluorine content, changes. The intensity of ^{19}F MRI signal increased with increasing fluorine content from spherical particles to vesicles.

Although high ^{19}F concentration is required to achieve a good signal-to-noise ratio, high fluorine concentration might lead to aggregation and, in turn, to shortening T_2 relaxation times.[160] It is important to tailor the structure to load high concentration of ^{19}F while maintaining segment motion. Among various polymeric architectures, dendritic polymers are especially promising due to their constrained shape that minimises fluorine dipole-dipole interactions by maximising the distance between the spins (fluorine and protons).[161–163] Furthermore, high ^{19}F content can be achieved (up to 20 mol % fluorinated monomer) while maintaining high segmental mobility. Thurecht *et al.*[164] reported the synthesis of a range of fluorinated (trifluoroethylacrylate) hyperbranched polymers with acid, alkyne and mannose functionalities through RAFT polymerisation in the presence of ethyleneglycol dimethacrylate as a branching agent which was chain extended with polyethyleneglycol monomethylether methacrylate. Polymers with acid functionalities that formed the basis of the study exhibited a short T_1 of about 500 ms and relatively long T_2 of 88 ms. These were successfully imaged *in vivo* using ^{19}F MRI 2h after the injection into mice in under 10 min (Figure 1-13).

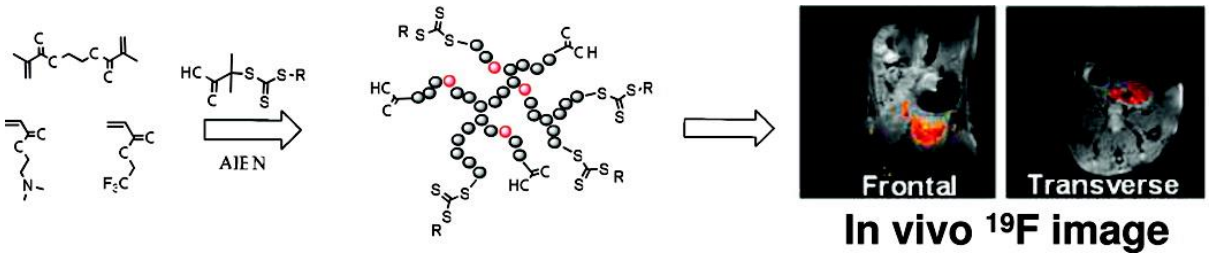

Figure 1-13. A representation of the hyper-branched fluorinated polymer developed by Thurecht et al.[164] MRI images of mouse abdominal region 2 h following injection of the polymer into mouse tail vein. The greyscale ^{1}H MR images are overlaid with ^{19}F MR images. Reprinted with permission from reference 164. Copyright (2010) American Chemical Society.

The presence of side chains increases the steric interference between the groups leading to slow chain dynamics.[152] It is clear, for example, from the comparison of segmented hyper-branched poly(2,2,2-trifluoroethyl acrylate-co-poly(ethylene glycol) methyl ether acrylate) SHBP-(TFEA-co-PEGA) and segmented hyper-branched poly(2,2,2-trifluoroethyl methacrylate-co-poly(ethylene glycol) methyl ether methacrylate) SHBP-(TFEMA-co-PEGMA) that the presence of methyl side chain affects the local motion of the ^{19}F nuclei as witnessed by T_2 relaxation times and ^{19}F NMR signal intensity.[113] SHBP-(TFEA-co-PEGA) and SHBP-(TFEMA-co-PEGMA) with similar fluorine contents of about ~3.0 wt % have T_2 relaxation times of 11 and 87 ms respectively.

1.9.3 Smart contrast agents

More recently, there has been a keen interest in the development of ^{19}F MRI smart contrast agents.[148,149] These contrast agents are switched on upon being activated by a certain stimulus such as pH, oxygen or enzymes. Such smart agents usually remain invisible until the particular stimuli is encountered. The switch can be reversible or irreversible based on the ability of the contrast agent to return to their original state or not. The scope of this section is mainly to cover smart polymeric-based probes.

1.9.4 pH-responsive probes

In the last few years, a number of pH-responsive fluorinated polymers have been developed. Such contrast agents are particularly useful for probing solid tumours due to the well-known acidic extracellular pH compared with normal tissues.[165] Such pH responsive probes can be achieved by either incorporation of a pH-responsive ionisable moiety in the polymer structure or chemical conjugation of a pH-responsive linkage between the polymer and the drug.[166–169] An example of pH-responsive probes achieved by incorporation of a pH-responsive moiety was reported by Wang *et al.*[167,168] who synthesised star polymers with either a cross-linked[168] or branched[167] core consisting of 2,2,2-trifluoroethyl acrylate (TFEA, offering detectable ^{19}F MRI signal) and 2-(dimethylamino)ethyl methacrylate (DMAEMA, providing pH responsiveness) as shown in Figure 1-14. The T_2 relaxation time was strongly dependant on the pH of the solution. A strong ^{19}F signal with reasonably extended T_2 relaxation time were only obtained at low pH, owing to the protonation of PDMAEMA tertiary amino group and hence increasing the hydrophilicity of the core, enhancing the mobility of fluorinated segments.

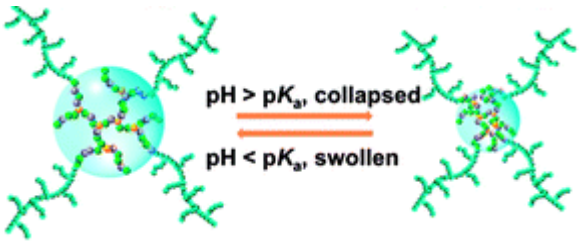

Figure 1-14. A representation of the fluorinated star polymer with hyper-branched core developed by Wang et al.[167] *Reprinted with permission from reference 167. Copyright (2013) American Chemical Society.*

A pH-responsive probe can also be achieved by introducing a pH-responsive linkage between the drug and the fluorinated agent. Fuchs *et al.*[169] reported a switchable ^{19}F probe induced by the release of hydrophobic drug (Figure 1-15). The hydrophobic drugs were attached to the

partially fluorinated hyper-branched polymers through an acidic cleavable hydrazine or self-immolative disulfide- linkage (oxidation responsive linkage). The attachment of the hydrophobic drug resulted in restricted mobility, hence short T_2 relaxation times and attenuated ^{19}F MRI signal. Upon drug release, the mobility of the fluorinated moieties improved resulting in an increase in ^{19}F T_2 relaxation times and increase in ^{19}F MRI signal intensity. This example has given the basis for ^{19}F MRI contrast agent capable of monitoring and quantifying drug release.

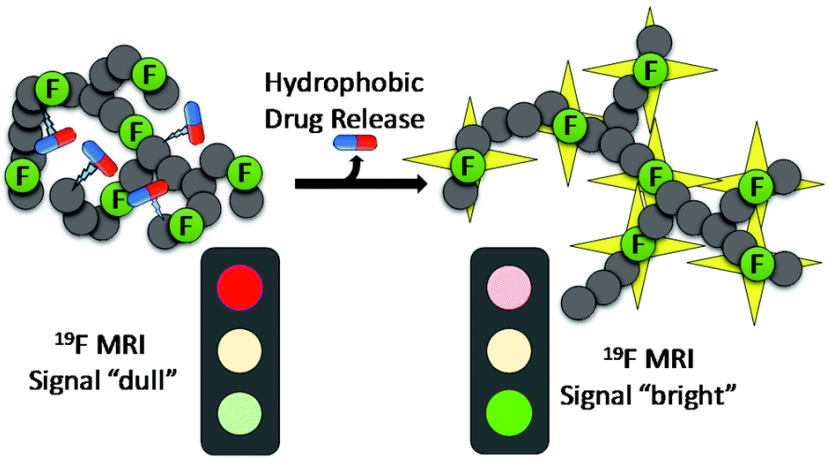

Figure 1-15 Schematic representation of the contrast agent developed Fuchs et al.[169] ^{19}F MRI signal intensity switch as a result of increase the motion is induced by release of hydrophobic drug. Reprinted with permission from reference 169. Copyright (2017) American Chemical Society.

1.9.4.1 Oxidation responsive probes

Although reactive oxygen species (ROS) such as the superoxide anion and hydrogen peroxide are found in low levels in all cells, high concentrations are found in cancer, inflammations and other chronic diseases.[170–172] Probing ROS by ^{19}F MRI is very useful in detecting and following-up treatment of such diseases.

Fu *et al.*[159] reported novel ^{19}F polymeric probes that can be activated by ROS. The probes consisted of thioether- and fluorine-containing methacrylate monomers were produced by ATRP technique using a hydrophilic poly(ethylene glycol)-based initiator. Schematic representation of the probe is shown in Figure 1-16. Such probes self-assembled in aqueous solution to form core-shell micelles with ^{19}F nuclei incorporated within the poorly solvated hydrophobic cores. Consequently, the mobility of the ^{19}F nuclei was significantly restricted resulting in attenuating the ^{19}F NMR and MRI signals. Treatment using ROS resulted in oxidation of the hydrophobic thioether groups to the hydrophilic sulfoxide groups, leading to the disassembly of the micelles. The disassembly of the micelles enhanced the mobility of

fluorinated segments and therefore elongated the T_2 relaxation times with a noticeable improvement of ^{19}F NMR and MRI signals.

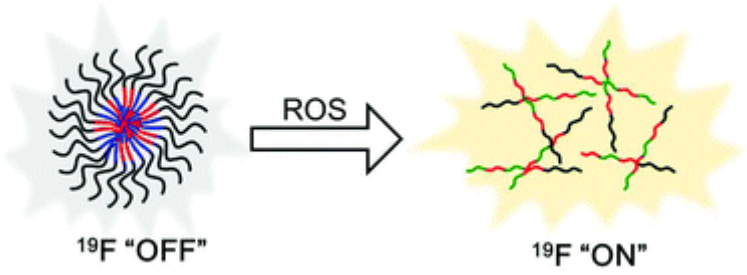

Figure 1-16. Schematic illustration of contrast agent developed by Fu et al.[159] *^{19}F MRI signal intensity switch as a result of disassembly of the aggregated nanoparticles upon treatment with reactive oxygen species (ROS). Reprinted with permission from reference 159. Copyright (2017) American Chemical Society.*

1.9.4.2 Enzyme responsive probes

To date, no polymeric enzyme responsive contrast agents have been developed. Two classes of switchable ^{19}F MRI contrast agents have been developed for probing enzymatic activities: one shows chemical shift changes and the other displays a signal intensity switch dependent on paramagnetic relaxation enhancement upon enzymatic treatment. Although, chemical shift imaging has been successfully used to detect the activity of β-galactosidase either *in vitro* and *in vivo*, [173–175] the approach is limited to the magnitude of the chemical shift change. In contrast, switchable contrast agents dependent on paramagnetic relaxation enhancement upon enzymatic cleavages seem very promising. It is well-known that paramagnetic metal (e.g. Gd) tend to shorten both T_1 and T_2 relaxation times of ^{19}F nuclei and the degree of which significantly depends on the distance between the metal and ^{19}F nuclei. In 2008, Mizukami *et al.*[176] reported a new ^{19}F MRI contrast agent for determining the activity of the protease caspase-3, where a Gd-based chelate has been linked to a trifluoromethoxy benzyl group via a caspase-3-cleavable peptide sequence (Figure 1-17). Initially, the intramolecular paramagnetic effect of Gd^{3+} resulted in a very short T_2 relaxation time and quenched ^{19}F MRI signal. Upon cleavage by caspase-3, the ^{19}F-labeled ligand dissociates from the Gd-based chelate, resulting in an enhancement in the ^{19}F T_2 relaxation time and a detectable ^{19}F MRI signal. In the following year, the same group developed a similar but multimodal imaging contrast agent in which trifluoromethoxy benzyl group was replaced by a fluorescent group, 7-amino-4-trifluoromethylcoumarin. A similar mechanism was exploited by coupling a fluorinated ligand to a Gd-based chelate using either lactam or galactose moiety linkers allowing for the detection β-lactamase or β-galactosidase activity.[177,178]

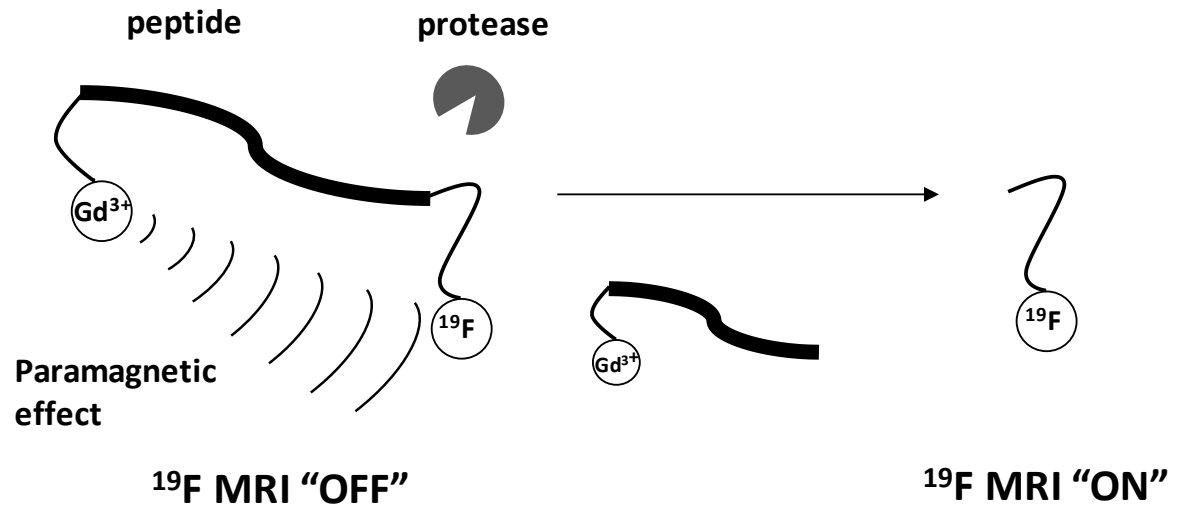

Figure 1-17. Schematic representation of ^{19}F MRI Probe developed by Mizukami et al[176] for detecting the activity of the protease caspase-3

1.10 5-Fluorouracil prodrugs

5-Fluorouracil (5-FU) is an analogue of uracil used as chemotherapeutic agent for the treatment of a wide range of solid tumours including colorectal cancers, breast cancer, head and neck cancer and pancreatic cancer.[179–183] 5-FU requires cellular uptake and metabolic activation to exert cytotoxicity.[184–186] Due to its structure, 5-FU rapidly enters the cell using the same facilitated transport mechanism as uracil. It is subsequently converted intracellularly to a number of active metabolites with the main cytotoxic activity being via inhibition of thymidylate synthase, hence blocking the thymidine formation required for DNA replication. Furthermore, its metabolites are incorporated into DNA and RNA, leading to other cytotoxic actions including DNA strand breakage and a decrease in protein synthesis. However, more than 80 % of 5-FU are converted into inactive metabolites requiring continues administration of high doses. Moreover, like other chemotherapeutic agents, 5-FU has high nonspecific toxicity toward cells. As a result, cancer treatment with 5-FU is typically accompanied with a high incidence of severe toxic side effects. In order to reduce the toxic side effects and minimise the delivery problems, a number of 5-FU polymer conjugates have been developed. The type of linkage used to conjugate the drug to the polymer substrate greatly influences site-specific release of 5-FU. Approaches used to deliver 5-FU using a single bond to link the drug to the polymer carrier have resulted in non-specific chemical hydrolysis within the blood stream.[183,187–189] A more effective approach is to use specific oligo-peptides bearing 5-FU in its α C-terminal glycine residue.[179–182,190] These oligo-peptide sequences are designed to be stable in the blood stream but biodegradable by lysosomal enzymes to produce free 5-FU in a

stepwise process as shown in Scheme 1-3-B.[191] The cleaved dipeptide derivative of 5-FU (pro-prodrug) is chemically stable but produce chemically unstable α-5-FU glycine (prodrug). The inherent chemical instability of α-substituted glycine, where α-substituent is a good leaving group (e.g. Cl, Br, OAc, SR, NR_2), is well known.[191] This unstable glycine derivative undergoes rapid decomposition to produce 5-FU.

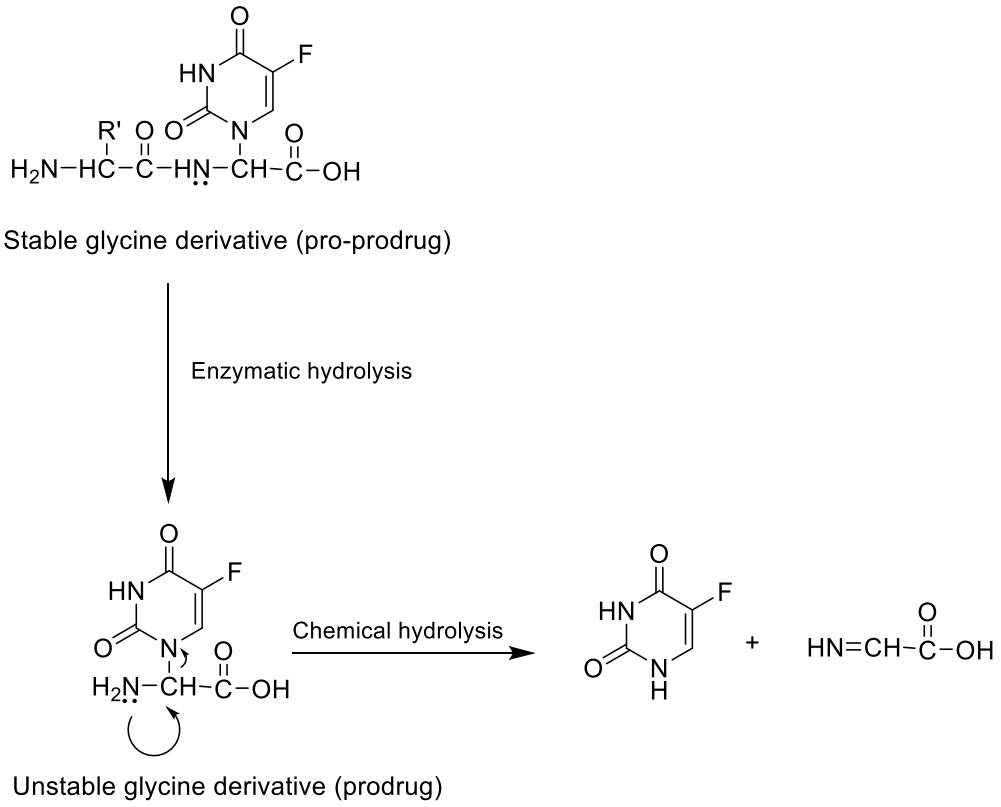

Scheme 1-3 The degradation mechanism of dipeptide derivative of 5-fluorouracil[191]

Recently, Putnam and Kopecek[179] have developed a number of 5-FU polymer conjugates with oligo-peptide side chains, having a (5-FU) glycine carboxyl residue at the C-terminus (Figure 1-18). The conjugates were stable in buffer solutions but hydrolysed in the presence of the enzyme. The enzymatic hydrolysis depended on the composition of the amino acid adjacent to the C-terminal substituted glycine, configuration at the C-atom carrying 5-FU as (levorotatory vs dextrorotatory) and the total length of the oligo-peptide sequence spacer (tetra-peptide vs hexa-peptide). Among various oligo-peptide chains used only hexa-peptides released 5-FU and 5-FU derivatives. The composition of the amino acid (R`) adjacent to the C-terminal substituted glycine greatly influenced the enzymatically catalysed release of free 5-FU. By comparing the release products from conjugates containing Leu and Ala adjacent to the C-terminal substituted glycine, conjugate with Ala resulted in 60 % release of only 5-FU derivatives, while polymer with Leu resulted in quantitative release of 5-FU derivatives and free 5-FU (50.6 %). Although there have been many examples of controlled 5-FU release from polymeric carrier,[179–182,190]

there still exist enormous challenges regarding in vivo, real-time monitoring to precisely determine not only when and where but crucially how much of the drug is released.

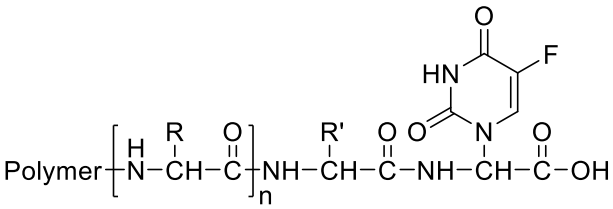

Figure 1-18. General structure of 5-fluouracil polymer conjugate with oligopeptide spacer developed by Putnam and Kopecek. Where n = 2 or 4, R' = $CH_2CH(CH_3)_2$ or CH_2Ph.

1.11 Aims and outlines

The overall aim of the project is to design and synthesise a new switchable polymeric-based ^{19}F MRI contrast agent triggered by enzymatic cleavage for monitoring the release of fluorinated drug. The approach relies upon the transformation of the fluorinated drug polymer conjugate prodrug with short T_2 relaxation time to the free fluorinated drug with enhanced T_2 relaxation time and hence good image intensity upon treatment with enzyme. based on the hypothesis shown in Figure 1-19. 5-FU is an anticancer drug with detectable ^{19}F NMR signal and used as a model fluorinated drug in this study.

It is hypothesized that the contrast agent will circulate with accumulation at target-site via enhanced permeability and retention (EPR) effect and the oligo-peptide linkers will be selectively hydrolysed by lysosomal enzymes. 5-FU release will change T_2 ^{19}F MRI sufficiently to enable differentiation between attached and released drug. In the absence of the enzyme, 5-FU polymer conjugate is expected to have short T_2 relaxation time and quenched ^{19}F MRI signal. It is well-known that ^{19}F moieties within the polymer probe experience slow tumbling rates leading to significantly reduced T_2 relaxation time. As ^{19}F MRI signal intensity is directly proportional to T_2 relaxation time, T_2 shortening leads to poor signal intensity. Incubation of the polymeric probe with the enzyme should induce the release of free 5-FU accompanied with an extension of T_2 relaxation times and an enhancement in the^{19}F MRI signal.

To this end, a dendritic polymer that is covalently attached to the oligo-peptide bearing 5-FU in its α C-terminal glycine residue will be synthesised. The choice of using dendritic polymer was based on its shape-persistence to prevent ^{19}F dipole-dipole interactions for relatively a highly-sensitive image along with its high density of terminal groups for high 5-FU loading capacity. The choice of Gly-Leu-Phe-Gly-Leu-Gly-5-FU from other oligo-peptides have been

used to deliver 5-FU,[179–182] was based on its known degradation ability by lysosomal enzymes that the prodrug would encounter in the tumour.

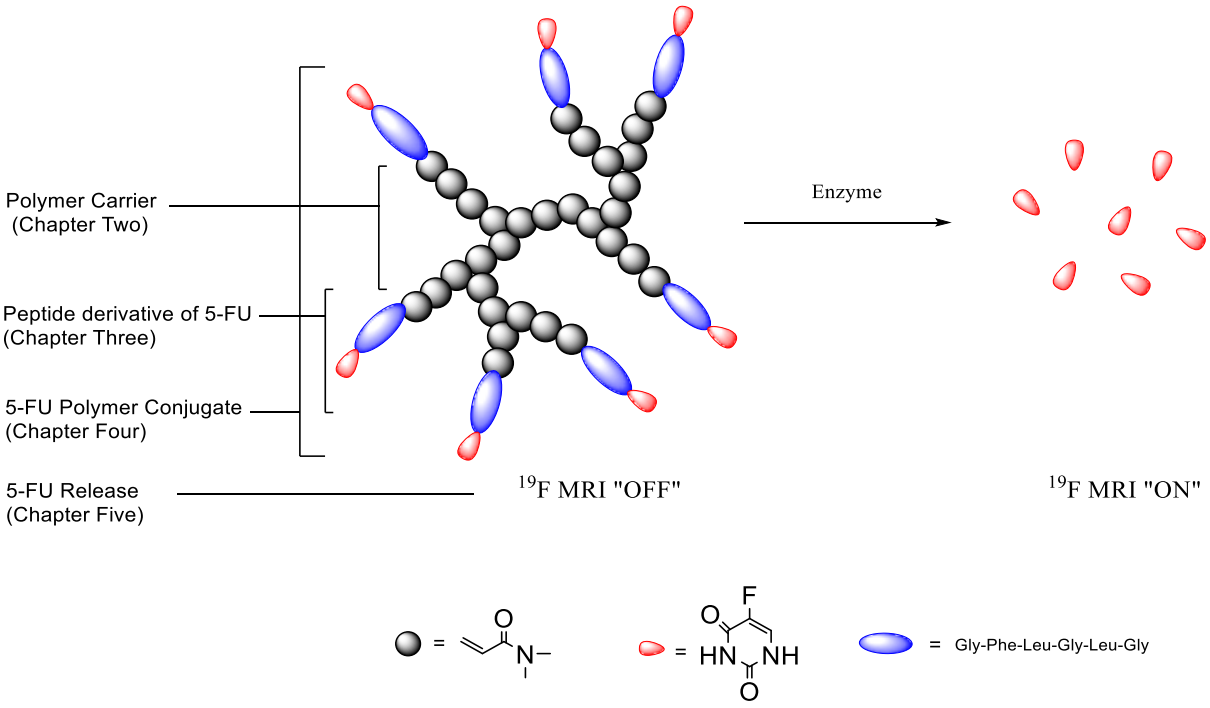

Figure 1-19 ^{19}F MRI switch induced by fluorinated drug release

The overall structure of the study takes the form of six chapters, including this introduction.

Chapter 2 will discuss the synthesis of dendritic poly(*N*,*N*-dimethylacrylamide)s. The polymers were synthesised by RAFT mediated SCVP of *N*,*N*-dimethylacrylamide (DMA) with 4-vinylbenzyl-pyrrole carbodithioate (VBPC) as a polymerisable CTM. The high density of thiocarbonylthio end groups of the resultant polymers will allow the installation of peptide. The polymers were characterised using gel permeation chromatography (GPC), dynamic light scattering (DLS) and transmission electron microscopy (TEM). Towards a better understanding of the structure and the properties of the polymers, kinetic of the polymerisation was studied.

Chapter 3 will concern the synthesis of the dipeptide, Leu-Gly-α-(5-FU), and the tetra-peptide, Gly-Phe-Leu-Gly for the synthesis of oligopeptide carrying 5-FU as α-substituent of terminal glycine moiety, Gly-Phe-Leu-Gly-Leu-Gly-α-(5-FU). The dipeptide, Leu-Gly-α-(5-FU), was synthesised according to a method described in the literature,[179] while the tetra-peptide, Gly-Phe-Leu-Gly, was synthesised by standard Fmoc solid phase peptide synthesis process.[192] The modification of the tetra-peptide with acrylic acid resulted in a peptide with vinyl terminal that can be attached to the polymer via aminolysis/Michael addition chemistry. An attempt of

coupling reaction commonly used in peptide chemistry to form the desired hexa-peptide was unsuccessful. Therefore, these peptides were conjugated directly into the polymer.

Chapter 4 will discuss the synthesis of the polymer-peptide conjugate. Growing the peptides on the polymer surface is a good method to avoid undesired side products as the polymer can be purified after each step by simple dialysis. To optimise the reaction conditions, the conjugation of a commercially available substance, *N*-hydroxyethyl acrylamide (HEA), was firstly examined. The polymer-peptide conjugate was synthesised mainly by a couple of steps; the attachment of the tetrapeptide via aminolysis/Michael addition chemistry and the attachment of the dipeptide after the activation with pentafluorophenol.

Chapter 5 will examine the principle "the ability of monitoring 5-FU release from polymer carrier using ^{19}F MRI". For optimisation purpose, the release of 5-FU from the dipeptide was firstly studied. Then, the release of 5-FU from the polymer-peptide conjugate was examined. 5-FU release was monitored by ^{19}F NMR along with T_1 and T_2 ^{19}F NMR.

Chapter 6 will present general conclusions from the work and future work.

Chapter 2 The Synthesis of dendritic poly(*N*,*N*-dimethylacrylamide) using SCVP-RAFT

2.1 Introduction

In recent years, significant attention has been paid to the synthesis of dendritic polymers due to their unique properties including enhanced solubility, decrease chain entanglement (constrained structure), low solution viscosity, and the presence of a large number of end groups at the periphery for post-polymerisation modification.[66] Dendrimers are considered to be the best characterised class of dendritic polymers due to the high degrees of symmetry in their architecture.[58,59] However, multistep dendrimer syntheses,[61,62] with time consuming purifications, limit their availability. Less regular hyper-branched polymers[65–67,193,194] are a more attractive structure as synthesis is easier. Conventional hyper-branched polymers synthesised by AB_2, and A_2+B_3 condensation polymerisation,[69–71] however, possess compact structures making full post-polymerisation functionalisation extremely difficult. Segmented hyper-branched polymers (SHBPs)[195–200] with long linear chains minimize the steric hindrance between the branched backbone increasing the conversion of the post-modification functionalisation. The synthesis of SHBPs can be typically accomplished in a one-pot reaction. Self-condensing vinyl polymerisation[77] is one of the most versatile techniques to create SHBPs, as it can be applied to readily available vinyl monomers subject to radical polymerisation. In SCVP a conventional monomer is copolymerised with a polymerisable AB* type monomer, where A is a vinyl group and B* is an initiating group. SCVP can be mediated by a number of polymerisation techniques, depending on the choice initiating group. These include cationic polymerisation,[77] anionic polymerisation,[81,82] atom-transfer radical polymerisation (ATRP),[85,87,88,201] nitroxide-mediated polymerisation (NMP),[83,84] and reversible addition–fragmentation chain transfer (RAFT) polymerisation.[89,91,95,106,115,202] Of these, RAFT is one of the most versatile methods because of its tolerance to a very wide range of functionality in the monomer and the solvent, and its non-demanding experimental conditions.[30,31] The AB* type monomer employed in RAFT-SCVP is known as a chain transfer monomer (CTM). Like other controlled radical polymerisations, RAFT-SCVP offers a number of advantages.[79] The formation of a macroscopic gel is minimised due to the low concentration of active radicals present in the system. Furthermore, a polymer with predetermined degree of branching and controlled branch length can be readily prepared by altering the stoichiometry of [M] to [CTM].

However, these well-defined statistical segmented hyper-branched copolymers can only be made when the reactivity ratio of the vinyl group of CTM and other monomers are well matched.[97,101,106]

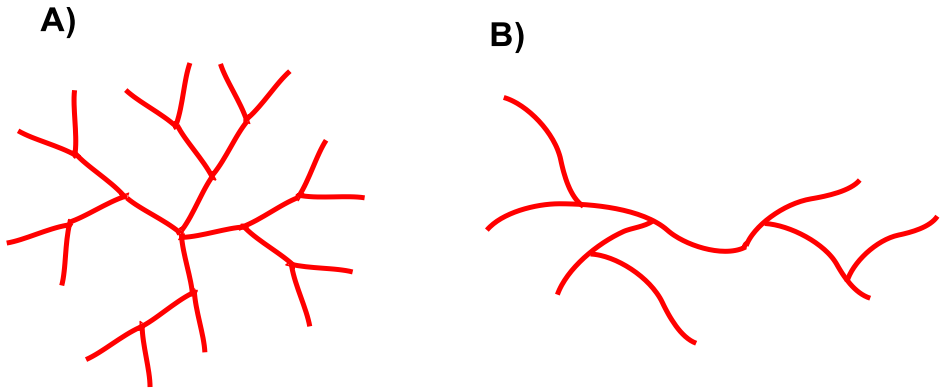

Figure 2-1 Schematic representation of A) hyper-branched polymer B) segmented hyperbranched polymer

This chapter details the synthesis of segmented hyper-branched poly(*N*,*N*-dimethylacrylamide) (SHB-PDMA) via RAFT-SCVP. The synthesis involved the polymerisation of *N*,*N*-dimethylacrylamide (DMA) with 4-vinylbenzyl *N*-pyrrole carbodithioate (VBPC) as CTM. The effect of: a) the feed ratio [DMA]:[VBPC], γ, b) monomer concentration on the degree of branching (DB), number average molecular weight (M_n), and particle size will be studied. Additionally, a kinetic study of the polymerisation is included to get better understanding of the polymer architecture and properties.

2.2 Results and discussion

2.2.1 Synthesis of segmented hyper-branched poly(*N*,*N*-dimethylacrylamide) (SHB-PDMA)

4-vinylbenzyl *N*-pyrrole carbodithioate (VBPC) was prepared in three steps, according to a previously reported procedure (Scheme 2-1).[107] The first two steps involve the abstraction of pyrrole NH proton with the help of sodium hydride and subsequent nucleophilic attack to carbon disulfide. The final step involves another nucleophilic attack to 4-vinylbenzyl chloride to yield VBPC. The chemical structure was confirmed by ^{1}H and ^{13}C NMR spectroscopy as shown in Figure 2-2. The ^{1}H NMR spectrum exhibits the characteristic resonance signals due to the vinyl protons at 5.30, 5.79 and 6.70 ppm together with other resonance signals assigned to the benzyl and pyrrole moieties. ^{13}C NMR displays carbon resonance signal due to C=S at 199.0 ppm along with other carbon signals due to vinyl, benzyl and pyrrole units.

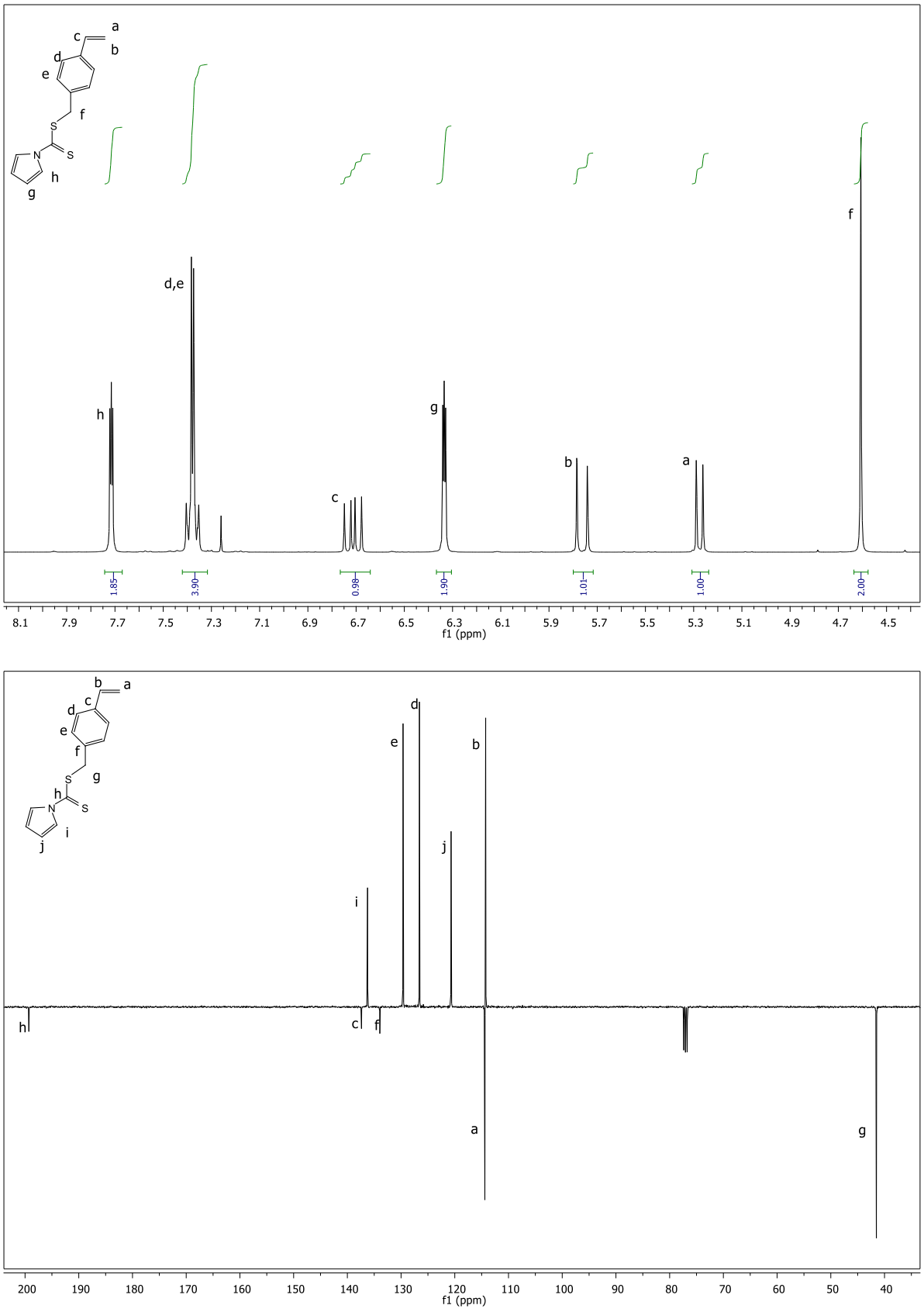

Figure 2-2. ^{1}H and ^{13}C NMR spectra of 4-vinylbenzyl N-pyrrole carbodithioate (VBPC) in $CDCl_3$

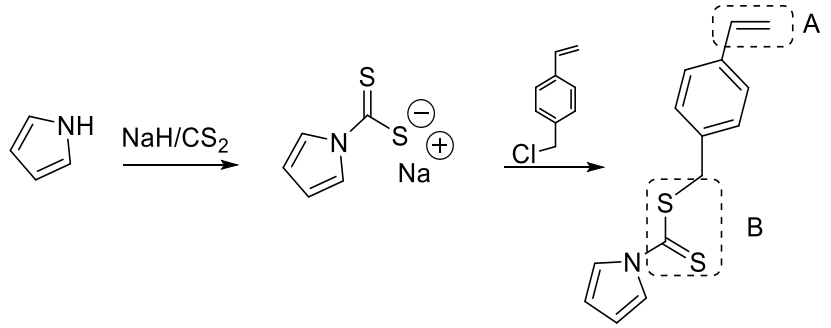

Scheme 2-1. Synthesis of 4-vinylbenzyl N-pyrrole carbodithioate (VBPC)

Dithiocarbamate, where the nitrogen lone pair is a part of an aromatic ring system, pyrrole, has been used as an effective mediator to control radical polymerisation of both acrylamides and styrenic monomers.[30] VBPC is a typical CTM for RAFT mediated SCVP, in which B* is the thiocarbonylthio moiety for the polymerisation of a styryl polymerisable double bond (A in Scheme 2-1) along with DMA. Also, it was reported that VBPC was used as CTM in RAFT-SCVP of acrylamide monomers such as *N*-isopropylacrylamide (NIPAM)[99,107] and 2-acrylamido-2-methyl-1-propanesulfonic acid (AMPS)[94] to yield soluble segmented hyper-branched polymers at high monomer conversions. RAFT copolymerisations of DMA and VBPC were conducted in 1,4-dioxane as the solvent in the presence of 4,4′-azobis(4-cyanovaleric acid) (ACVA) as the radical source at 60 °C under a N_2 atmosphere. The reaction scheme for the preparation of SHBPs with pyrrole end groups and the styryl moiety as a branching point is shown in Scheme 2-2.

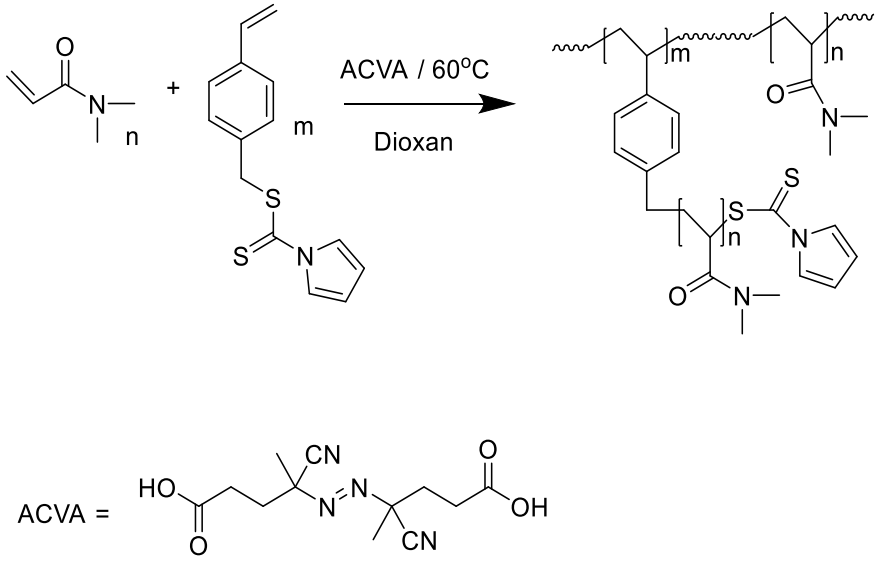

Scheme 2-2. Synthesis of segmented hyper-branched poly(N,N-dimethylacrylamide) (SHB-PDMA) via RAFT-SCVP

2.2.2 Preparation of segmented hyper-branched poly(*N*,*N*-dimethylacrylamide) (SHB-PDMA) of different degree of branching by varying the feed ratios

First, various feed ratios of [DMA]:[VBPC], γ, were used while the [VBPC]:[ACVA] ratio were kept constant 1:1. The polymers were characterised by ^{1}H NMR spectroscopy and gel permeation chromatography (GPC) to find out monomer conversion, DB and M_n as summarised in Table 2-1. Despite the high conversion of DMA (99%) achieved for all feed compositions, polymers remained soluble and no gelation was observed.

^{1}H NMR spectroscopy analysis confirms the formation of branched structure for PDMA with the main peaks being the peak at 2.70 ppm representing the -CH_3 derived from DMA, broad singlet between 6.83 and 7.17 ppm representing the phenyl protons and the terminal pyrrole's hydrogen singlets at 6.33 and 7.71 ppm. For a comparison, a linear PDMA (L-PDMA) sample was synthesised using the equivalent non-polymerisable CTA, benzyl 1H-pyrrole-1-carbodithioate (BPC). As shown in Figure 2-3, the phenyl moiety was observed as a very broad-line signal in SHB-PDMA compared with its linear analogue (i.e. L-PDMA), indicating the incorporation of the styryl unit in the main chain and hence the successful formation of the desired branched structure. In L-PDMA, phenyl protons experience additional motion, as it represents the chain ends, and hence sharper peaks were observed. Furthermore, the disappearance of vinyl resonance signals between 6.72 to 5.26 ppm confirms the complete elimination of unreacted DMA and VBPC monomers after dialysis against deionised water. The typical resonance signals of the protons for the SHB-PDMA are assigned in Figure 2-3.

Table 2-1. Result of RAFT-SCVP copolymerisation of DMA with VBPC in dioxane at 60 °C at different feed ratios

γ	Time / h	Conv / % [a]	$M_{n(exp)}$ / kDa[b]	$M_{n(th)}$ / kDa[c]	Đ[b]	$DB_{(exp)}$[d]	$DB_{(th)}$[e]
20	24	99	7.4	2.2	1.75	0.088	0.095
30	24	99	10.2	3.2	2.06	0.062	0.064
40	24	99	14.2	4.2	2.37	0.052	0.048

[a] Determined by ^{1}H NMR spectroscopy of crude reaction mixture, [b] Measured by GPC in DMF calibrated with linear PMMA homopolymer standards, [c] Theoretical M_n calculated considering RAFT linear Equation 2-4, [d] Calculated degree of branching from NMR using Equation 2-2, [e] Theoretical degree of branching calculated using Equation 2-3

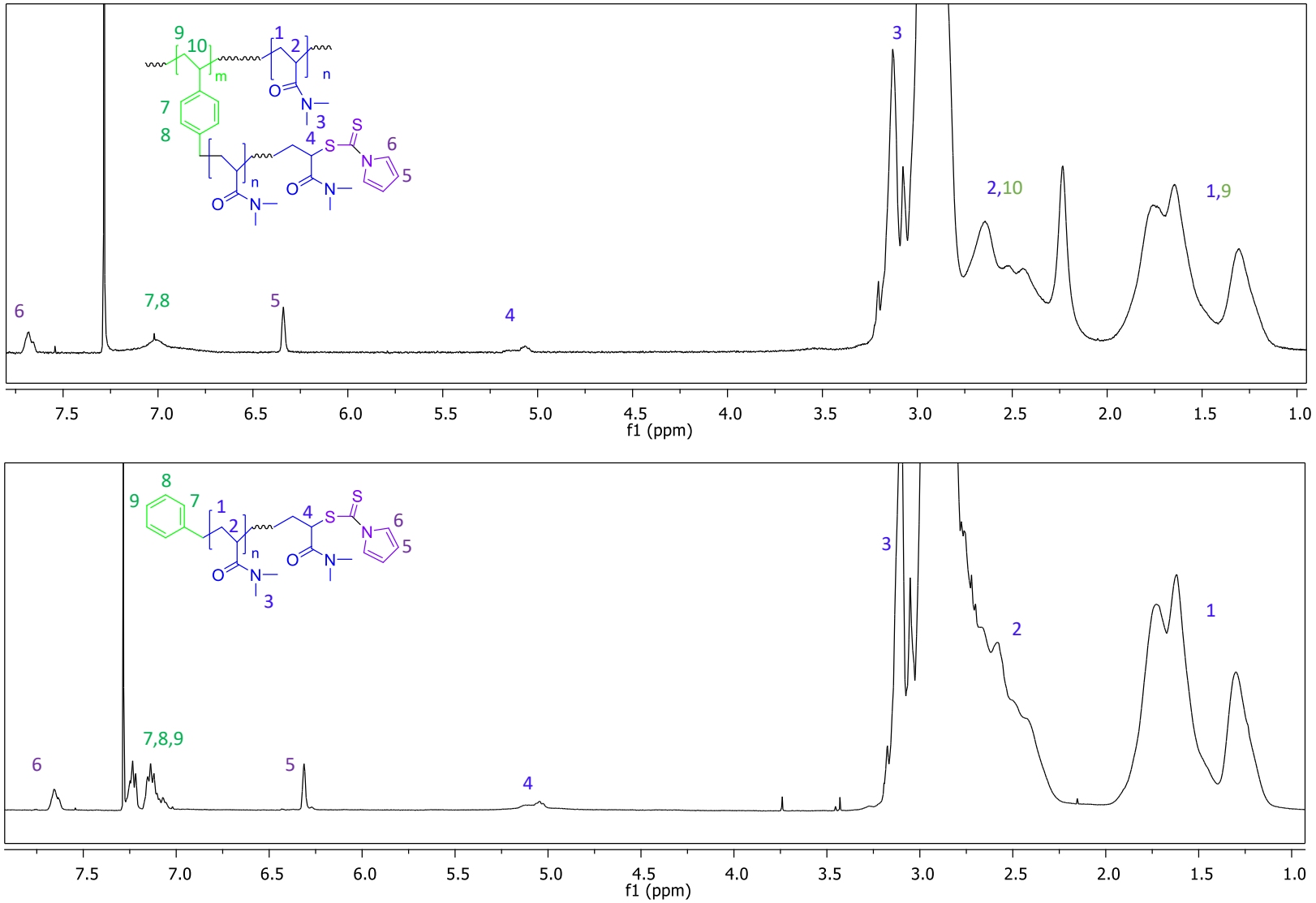

Figure 2-3. ^{1}H NMR of segmented hyper-branched poly(N,N-dimethylacrylamide) (SHBP-DMA) and linear poly(N,N-dimethylacrylamide) (L-PDMA) in $CDCl_3$

DB is a crucial parameter in describing the structure of branched polymers. The degree of branching of the linear polymers is equal to 0, whereas perfect dendrimers have a DB of 1.[78] The homo-SCVP of the inimer (in the absence of conventional vinyl monomer) results in a hyper-branched polymer with a maximum DB of 0.466.[80]

The DB can be calculated according to the definition given by Hawker *et al*.[203](Equation 2-1).

$$DB = \frac{D + T}{D + T + L} \qquad \textit{Equation 2-1}$$

Where D, T, and L represent the mole fraction of dendritic unit, terminal unit and linear unit respectively. However, according to this equation all linear species would have DB > 0 (e.g. the linear dimer would have DB of 1). This error arises because of the presence of terminal units in both the numerator and the denominator. Therefore, a modified equation was introduced for the calculation of DB.[204,205] Since each new branch always adds one branchpoint and one terminal group, terminal units can be excluded.

$$DB = \frac{2D}{2D + L} \qquad \textit{Equation 2-2}$$

In SHB-PDDMAs, the value of D was determined by integrating the proton at 6.83-7.17 ppm corresponnding to the phenyl group of VBPC (7,8 in Figure 2-3). L was calculated by integrating the DMA methyl proton at 3.28-2.75 ppm (3 in Figure 2-3).

The DB of SHBPs synthesised via RAFT-SCVP process mainly depends on the feed ratio, γ.[80] Therefore, a targeted DB can be obtained by simply tuning γ. As expected, the increase of γ resulted in polymers with lower degree of branching (i.e a low concentration of CTM resulted in a low degree of branching). If less CTM is present, there will be less branching in the polymer and therefore the longer the chain. This gives more repeating units per branch and hence gives a lower degree of branching. As illustrated in Table 2-1, these DB values calculated are close to the theoretical values calculated using Equation 2-3.[78]

$$DB_{theo} = \frac{2\left(1 - e^{-(\gamma+1)x_m}\right)\left[x_m - \left[\frac{1 - e^{-(\gamma+1)x_m}}{\gamma + 1}\right]\right]}{\gamma x_M + 1 - (1 - x_M)(2 - e^{-(\gamma+1)x_M})} \qquad \textit{Equation 2-3}$$

Where γ and x_m refer to [DMA]:[VBPC] ratio and monomer conversion, respectively. As the DB values were calculated based on the assumption of equal rate constants for copolymerisation, they represent a rough estimate and the actual DBs might differ. It should be emphasised that the DB only deals with numbers but not with the location (i.e. distribution)

of the branch points and hence this parameter does not reflect the final structure of the polymer. Two polymers with the same DB value might differ in their structures.[206,207]

M_n, M_w, and Đ values were determined by gel permeation chromatography (GPC) using an RI detector and using DMF as eluent. Molecular weights were calculated relative to linear homo-poly(methyl methacrylate) (PMMA) standards. With the variation of the feed ratio, γ, from 20 to 40, the M_n of SHBPs varied from 7,400 Da to 14,200 Da with a relatively high Đ in the range of 1.75–2.37 (Table 2-1). As expected, the $M_{n(exp)}$ values determined by GPC are greater than the theoretical molecular weight ($M_{n(th)}$), calculated using the equation of the linear RAFT polymerisation (Equation 2-4), due to more propagating centres typically observed in RAFT-SCVP reactions.

$$M_n = \frac{[DMA]}{[VBPC]} \times M_w of\ DMA \times conversion + M_w of\ VBPC \qquad \textit{Equation 2-4}$$

However, GPC gave underestimated M_n values and the actual M_n values of SHB-PDMAs are expected to be higher due to the nature of branched polymers. Because of their compact structure, branched polymers of a certain molecular weight usually exhibit lower hydrodynamic volumes compared to their linear analogues.[208] More accurate molecular weight values[209] can be obtained using mass-online sensitive detectors such as a multiangle light scattering detectors (MALLS)[210,211] and/or a viscosity detector, using the universal calibration (UNICAL),[212] in corporation with conventional RI concentration detector.

The molecular weight distributions derived from DMF GPC were broad as expected for polymers synthesised by RAFT-SCVP approach (Figure 2-4). These distributions have slight shoulders, suggesting the presence of lower molecular weight fractions. Furthermore, it was also found that increasing the feed ratio resulted in polymer with higher molecular weight indicating increasing the chain length between the branch points.

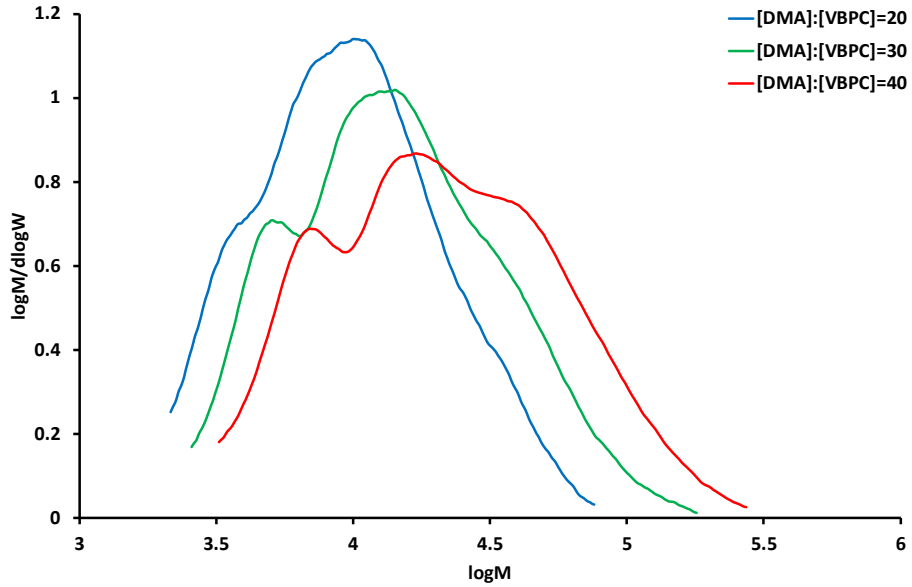

Figure 2-4. Molar mass distributions of SHBPs prepared by varying the feed ratios derived from DMF GPC

2.2.3 Preparation of hyper-branched poly(*N,N*-dimethylacrylamide) (HB-PDMA) of different sizes by varying the concentration

In the previous polymerisations the molar ratio of VBPC to ACVA was very high (1:1) as has been previously reported[213] an excess amount of initiator will result in a large fraction of carboxylic groups at the chain ends as a result of the bimolecular termination of the polymer radicals and ACVA radicals. This will remove the thiocarbonylthio moiety while this work aims to keep the thiocarbonylthio moiety and conjugate the peptide via aminolysis/Michael addition chemistry. Therefore, the ratio of VBPC to ACVA was reduced to 1:0.2. Also, the feed ratio of DMA to VBPC, γ, was kept constant and the concentrations were varied to form polymers with different molecular weights and sizes.

The feed ratio of [DMA]:[VBPC]:[ACVA] used was 50:1:0.2, while DMA concentration to dioxane was varied from 10 to 50 wt%. SHB-PDMA was first synthesised by deoxygenating the reaction mixture via nitrogen bubbling for 30 minutes prior to running the copolymerisation. All the copolymerisations were made in triplicate and characterised using NMR spectroscopy, GPC, and dynamic light scattering (DLS). Although this method was able to synthesise soluble SHBPs at very high conversion, the results were inconsistent. This is probably due to the inconsistency of nitrogen quality and limited control over the flow rate. To overcome this problem, the reaction mixture was degassed by three freeze-pump-thaw cycles and backfilled with N_2. This part will focus on the results from copolymerisation reactions using three freeze-pump-thaw cycles as it is more consistent. The results are summarised in Table 2-2. The segmented hyper-branched polymers were named accordingly: SHB-PDMA

stands for segmented hyper-branched poly(*N*,*N*-dimethylacrylamide) and the number 10 to 50 wt% represents the concentration of the synthesis. For example, SHB-PDMA-30wt% is SHB-PDMA synthesised by SCVP-RAFT and the monomer concentration relative to dioxane was 30 wt%.

Table 2-2. Result of RAFT-SCVP copolymerisation of DMA with VBPC in dioxane at 60 °C at γ =50

polymer	γ	Time / h	Conv / % [a]	$M_{n(exp)}$ / kDa[b]	$M_{n(th)}$ / kDa[c]	Đ[b]	$DB_{(exp)}$[d]	$DB_{(th)}$[e]	RB[f]
SHB-PDMA-10 wt%	50	24	91	13.5	4.8	1.78	0.038	0.039	26
SHB-PDMA-20 wt%	50	24	96	19.9	5.0	2.70	0.038	0.039	26
SHB-PDMA-30 wt%	50	7	93	25.5	4.9	3.77	0.038	0.039	26
SHB-PDMA-40 wt%	50	6	91	32.0	4.8	8.11	0.038	0.039	26
SHB-PDMA-50 wt%	50	4	92	33.0	4.9	11.92	0.038	0.039	26

[a] Determined by ^{1}H NMR spectroscopy of crude reaction mixture, [b] Measured by GPC in DMF calibrated with linear PMMA homopolymer standards, [c] Theoretical M_n calculated considering RAFT linear Equation 2-4, [d] calculated degree of branching using Equation 2-2, [e] Theoretical degree of branching (Equation 2-3), [f] RB=DB^{-1}

The polymers were analysed by ^{1}H NMR spectroscopy to find percentage conversion and degree of branching. Soluble SHBPs were achieved at high conversion (more than 90%) for all concentrations as shown in Table 2-2. However, the risk of gel formation increased with concentration as the reaction progressed. SHB-PDMA-50wt%, for instance, turned completely to insoluble gel materials at 4 h (above 90% conversion), possibly caused by cross-links via unwanted bimolecular termination of polymeric radicals. Shorter reaction times were required for high concentration systems to form soluble SHBP with about 90% conversion.

Compared with lower feed ratios (Table 2-1), γ=50 resulted in polymers with lower degree of branching of about 0.038 for all concentrations. This was expected. A lower amount of CTM results in the formation of fewer branch points and therefore a lower degree of branching. The DB value calculated has an excellent agreement with the theoretically predicted value of about 0.039. The average branch length, the average number of repeat unit by branch (RB), was calculated to be almost 26 according to RB=DB^{-1}.

The molar ratio of DMA to VBPC in the SHBPs can be calculated from the peak intensity ratio of methyl protons to styryl protons. The value is 40, which is lower than the aimed feed ratio

(γ = 50) probably due to the incomplete conversion of DMA (90–96%) as well as the high reactivity of vinyl group of the styryl monomer compared with the reactivity of DMA, as will be explained later. It is worth mentioning that the calculation was made in deuterated chloroform. The low ratio could also be due to the different solvation behaviour of DMA and styryl units in $CDCl_3$.

M_n, M_w, and Đ values were determined by DMF GPC. Despite the equivalent formulation of the reaction mixtures, GPC showed that the M_n of resultant polymers increased with concentration. With the variation of the reaction concentrations from 10 to 50 wt%, the M_n of SHBPs increased from 13,500 Da to 33,000 Da with a relatively broad Đ in the range of 1.8–11.9 (Table 2-2). Figure 2-5 shows molecular weight distributions derived from DMF GPC. The broad multicomponent distributions are expected from SHBPs synthesised by hybrid condensation/chain growth SCVP copolymerisation. These distributions have slight shoulders, suggesting the presence of lower molecular weight fractions. These low molecular weight fractions appear to be less prominent in the higher concentration samples where linking reaction is more likely compared with lower concentration systems.

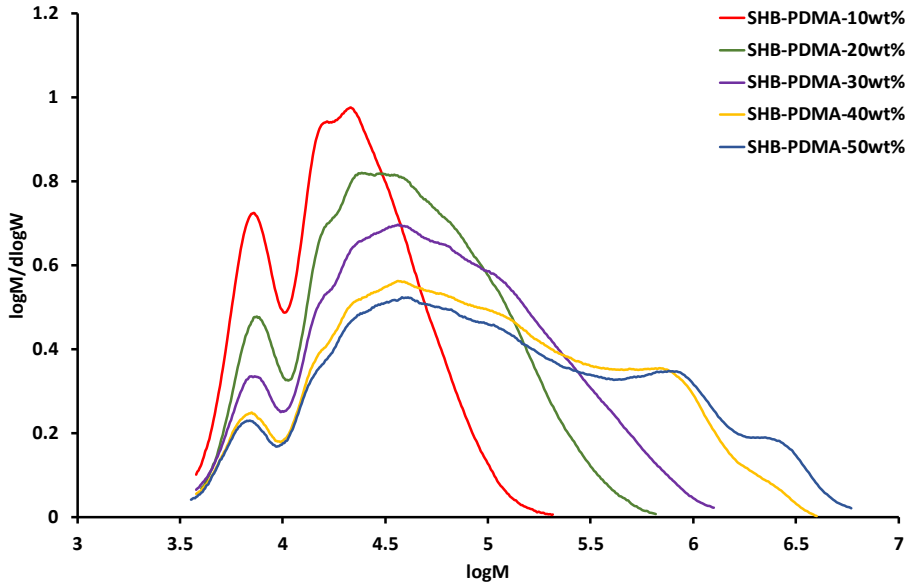

Figure 2-5. Molar mass distributions of SHBPs prepared by varying concentrations derived from DMF GPC

The particle size of polymers in water was measured using DLS operated at 25 °C (Figure 2-6). The hydrodynamic size varied from 7.5 nm to 24.1 nm with increasing concentration. SHB-PDMA-10 wt%, SHB-PDMA-20 wt% SHB-PDMA-50 wt% show bimodal distribution. The first distribution may represent individual particles while the other one represents the aggregation.

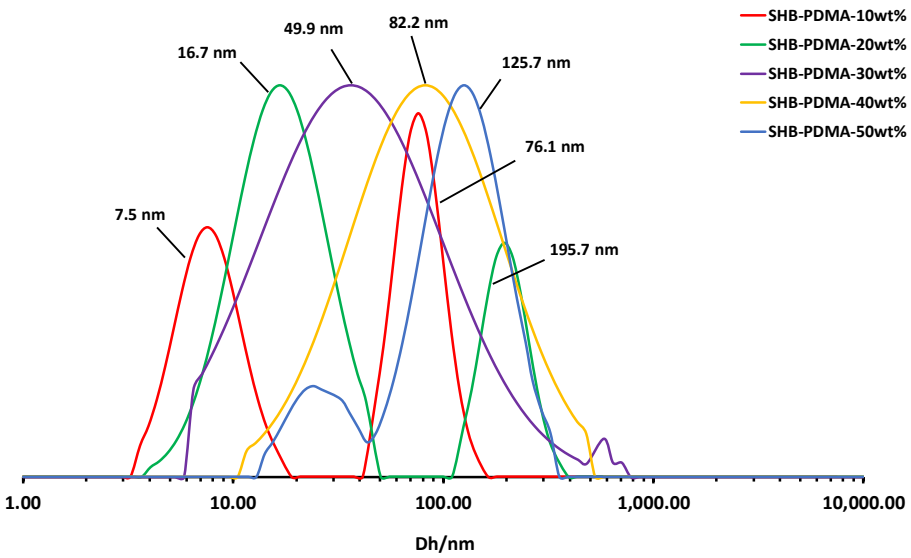

Figure 2-6. Particle size distributions of SHB-PDMAs in water from DLS operated at 25°C

The particle size was also measured by transmission electron microscopy (TEM) and the results were compared with DLS results (Table 2-3). Staining with uranyl formate allowed for developing electron contrast. Figure 2-7 shows TEM images of the particles produced with 10, 20 and 50wt%. Particle diameters assessed from TEM confirmed the trend obtained from DLS, however, are generally much smaller. This is somewhat expected since DLS is an intensity based technique and show more emphasis on the larger objects of the distribution, while TEM is a number based technique and shows stronger emphasis on the smallest components of the size distribution. The images show large particle with diameter of 17, 25, and 120 nm for SHB-PDMA-10 wt%, SHB-PDMA-20 wt%, and SHB-PDMA-50 wt% respectively. Because of their small population compared with small particles, they could not be noticed in the histogram distributions.

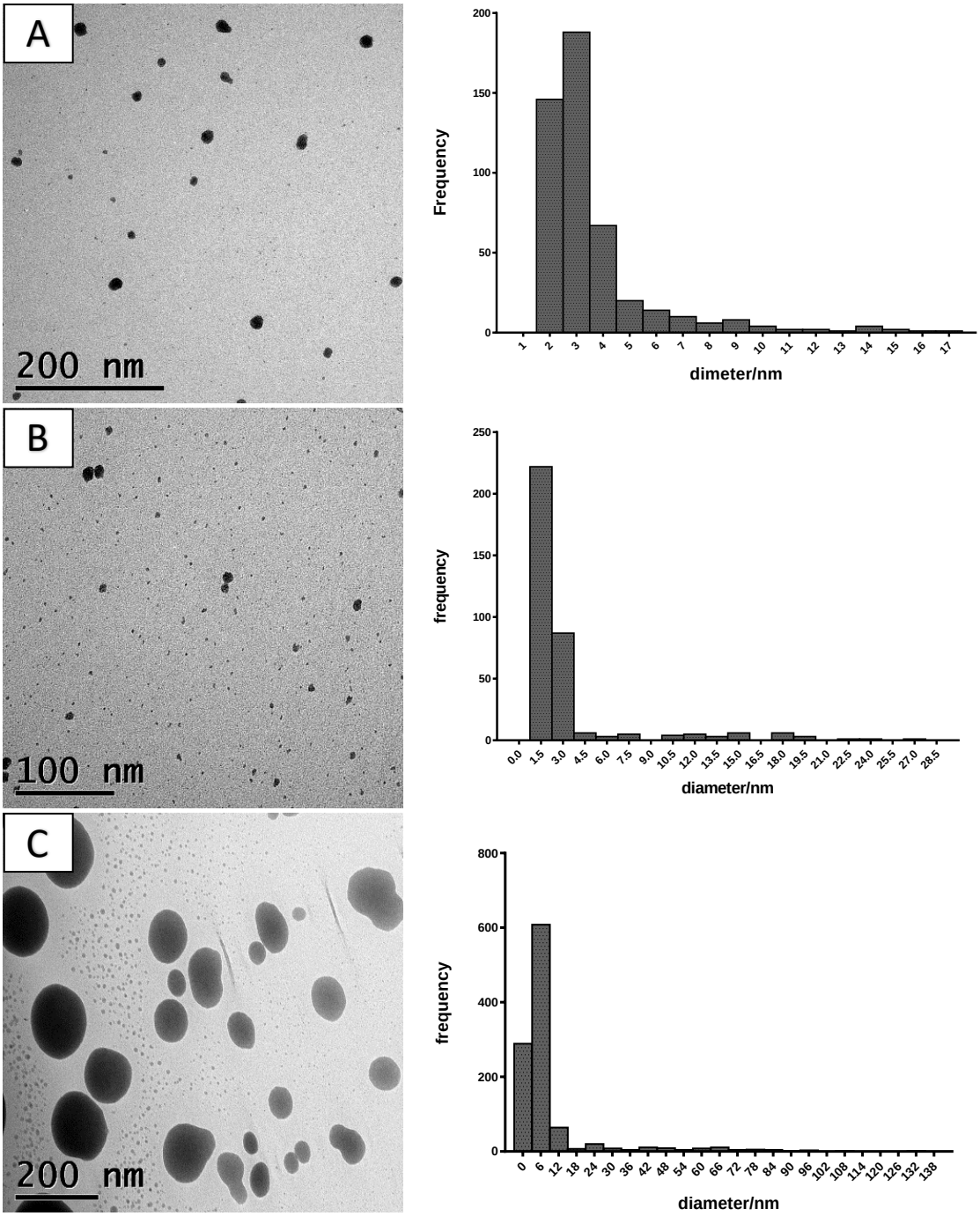

Figure 2-7. TEM images of A) SHB-PDMA-10wt%, B) SHB-PDMA-20wt% and C) SHB-PDMA-50wt% stained with uranyl formate

Table 2-3. A comparison between DLS and TEM data for SHB-PDMAs

polymer	DLS		TEM	
	1st distribution/ nm	2nd distribution/ nm	1st distribution/ nm	2nd distribution/ nm
SHB-PDMA-10 wt%	7.5	76.1	3.5	15.0
SHB-PDMA-20 wt%	16.7	195.7	3.0	24.0
SHB-PDMA-30 wt%	49.9	-	-	
SHB-PDMA-40 wt%	82.2	-	-	
SHB-PDMA-50 wt%	24.1	125.7	6.1	96.6

2.2.4 Investigating the relative reactivity of DMA and VBPC

Like conventional RAFT polymerisation, both R- and Z-substituents of the CTM can have a significant influence on RAFT-SCVP polymerisation kinetics and efficiency. However, the polymerisable functionality (i.e. the vinyl group) of the CTM in RAFT-SCVP should be carefully selected.[79] The relative reactivity of the vinyl group of the CTM and the monomer greatly influences the distribution of the branch points and hence the formation of SHBP.[78,80,110] Statistical SHBP with well distributed branch points can only be formed when the reactivity of CTM and co-monomers are similar. When the CTM is highly reactive in comparison with the co-monomers, the branch points will be formed in early stage of the copolymerisation, and "hyperstars" might be formed. However, very low reactivity CTMs might result in a "macroCTMs" and branch point will be formed at the end. Here, the relative reactivity of DMA and VBPC was investigated simply by sampling a moderate amount of the reaction mixture at $\gamma = 50$ and 50wt% of DMA in dioxane for ^{1}H NMR analysis without any precipitation (Figure 2-8). The intensity change of the vinyl resonance signals for both monomers was used to calculate the monomer conversion. As expected, both vinyl signals became weaker as the reaction proceeded. The vinyl signals of the styryl monomer derived from VBPC had completely disappeared in the early stages of the polymerisation with almost a complete conversion within 80 min. This was accompanied with little polymerisation of DMA (i.e. a long induction period). This suggests that styryl monomer is much more reactive than DMA under these conditions. This different reactivity indicates that a homogeneous distribution of the branch points was not achieved. The polymer formed is possibly a hyperstar block copolymer. Representation of hyperstar vs segmented hyperbranched structure is shown in Figure 2-9.

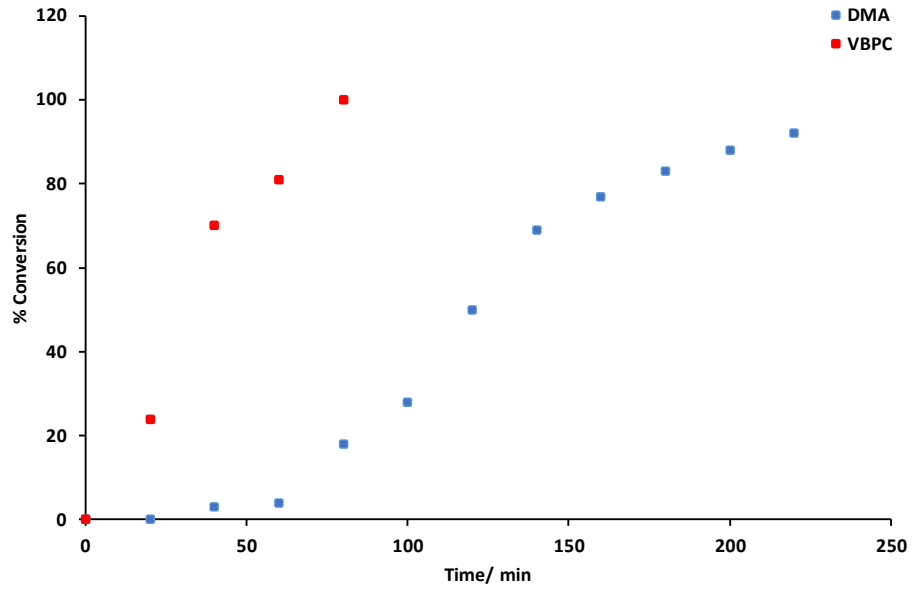

Figure 2-8. Conversion vs time plot of SCVP copolymerisation at [DMA]:[VBPC] = 50 and 50wt% of DMA in dioxane

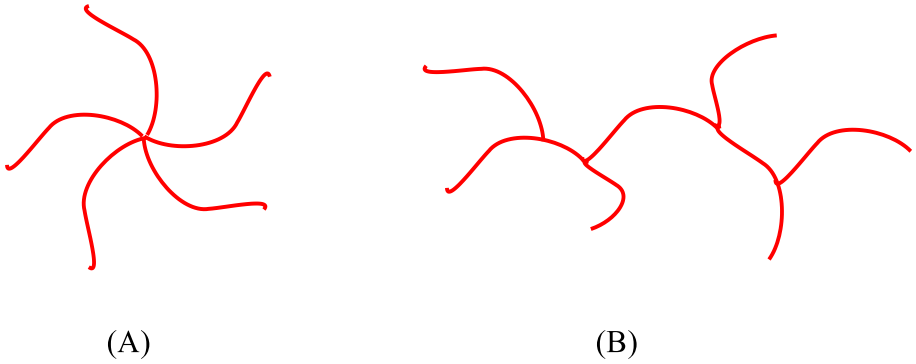

(A) (B)

Figure 2-9. Representation of A) hyperstar and B) segmented hyperbranched structures

Figure 2-10 shows $Ln[M]_0/[M]$ vs time plot of SCVP for at γ = 50 and 50wt% of DMA in dioxane. The plot displays an extended induction period with virtually no polymerisation activity of DMA within the first 80 min, suggesting that the equilibrium of reversible addition-fragmentation was slow. With decreasing the concentration of the polymerisations from 50 wt% to 10 wt%, the induction period increases accompanied with a decrease in overall polymerisation rate (Figure 2-11). It is noteworthy mentioning that the polymerisation of DMA using equivalent non-polymerisable RAFT agent, BPC, also shows a long induction period (Figure 2-12). After the induction period, the pseudo-first-order rate plot shows fairly linear relationship (Figure 2-10).

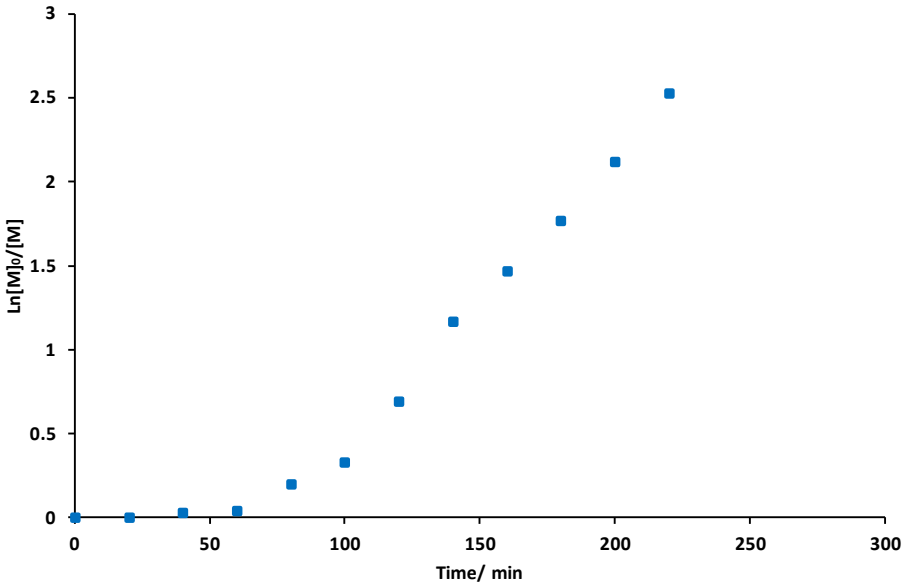

Figure 2-10. Ln[M]$_0$/[M] vs time plot of SCVP copolymerisation at [DMA]:[VBPC] = 50 and 50wt% of DMA in dioxane

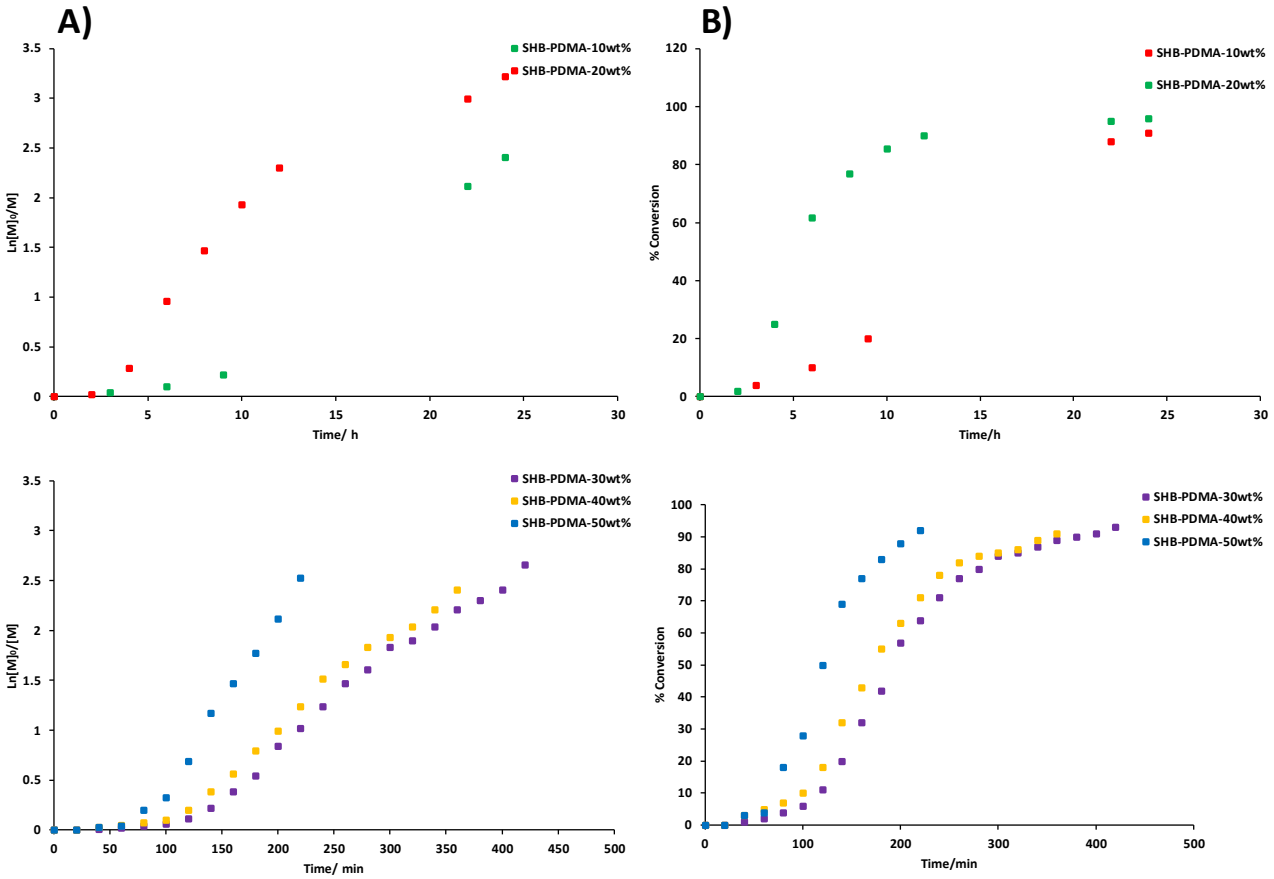

Figure 2-11. A) Ln[[M]$_0$/[M] vs time plots B) conversion vs time plots of VBPC mediated the polymerisations of DMA at different concentrations

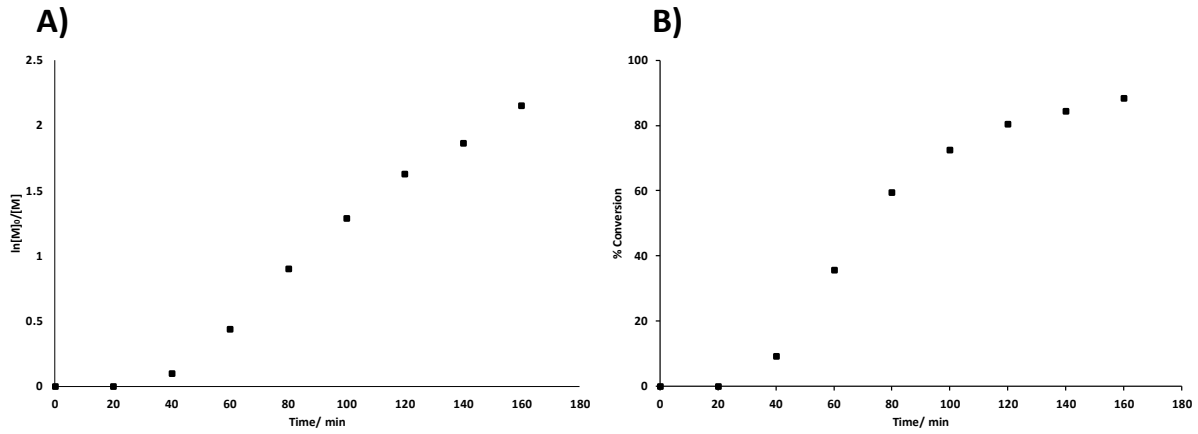

Figure 2-12. A) Ln[[M]0/[M] vs time plot B) conversion vs time plot for RAFT of DMA using non-polymerisable RAFT agent, benzyl-1-pyrrolecarbodithioate (BPC)

The induction period and retardation seen in some RAFT polymerisations are not clearly understood, however several explanations have been proposed. These include avoidable causes (e.g. ineffective degassing) as well as poor selection of the Z- and R-group for the monomer polymerised. As the polymerisation mixture was degassed by 3 freeze-pump-thaw cycles, ineffective degassing as a cause of retardation is not likely to be the case. Therefore, the inhibition observed in the DMA polymerisation can be attributed to the choice of R- and/or Z-group of the RAFT agent.

The main two theories explained the retardation are linked with the stability (slow fragmentation) of the intermediate RAFT/polymeric radicals. On one hand, slow fragmentation of the intermediate radicals induces rate retardation by itself.[36] On the other hand, increasing the stability of these radicals will increase their concentration enhancing the probability of terminating side reaction.[50] Monteiro *et al*.[51] ascribed the rate retardation in dithiobenzoate-mediated polymerisation (where Z = Ph) to the stabilisation of intermediate radical by phenyl group, which allows for delocalisation of the radical into the aromatic system. In the polymerisation of DMA using VBPC, the rate retardation can also be ascribed to the resonance structures of the intermediate radicals (Scheme 2-3).

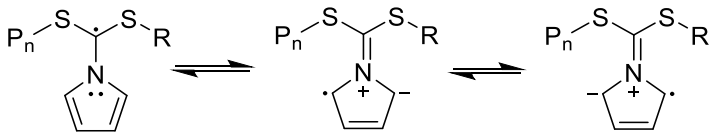

Scheme 2-3. Resonance structures of the intermediate radical occurring in the aromatic dithiocarbamates mediated RAFT polymerisation

Poor selection of R group (i.e. R ability to reinitiate the polymerisation) has also been reported as a cause of inhibition. Furthermore, Barner-Kowollik group[214] ascribed the induction period

in the polymerisation mediated by cumyl dithiobenzoate to the formation of dicumyl radicals, Ph-C(S-cumyl)$_2$. In the polymerisation of DMA using VBPC, the induction period can also be attributed to the formation of diphenyl radicals via the reaction of excess VBPC with benzyl radicals which might decrease the extent of reinitiation occurring until the main equilibrium is achieved, leading to a long induction period.

2.2.5 Evolution of number average molecular weight, dispersity and degree of branching

To further investigate the evolution of the structure during RAFT-SCVP, the dependence of M_n, Đ and DB on % conversion of DMA was studied at $\gamma = 50$ and 50wt% of DMA in dioxane. In ideal SCVP, high molecular weight polymers with the highest DB can only be achieved at very high monomer conversion, owing to the hybrid step/chain growth nature of SCVP.[90] At very low conversion (when $\gamma >> 1$), M_n grows linearly and Đ decreases as it should in a conventional controlled chain-growth polymerisation. After which, both M_n and Đ increase exponentially with conversion due to the nature of linking step-growth reactions.[78] However, the dependence of M_n and Đ on the monomer conversion is greatly influenced by the reactivity of the CTM and the monomer.[110] When CTM is less reactive than the monomer, M_n increases with conversion almost linearly up to very high monomer conversion similar to conventional RAFT with relatively low Đ (Đ < 2) at 99% conversion, indicating the formation of linear macro CTM. When CTM is much more reactive than the monomer, both M_n and Đ strongly increases at low monomer conversion compared with conventional RAFT, as CTMs are consumed fast forming a hyper-branched core.

Figure 2-13 shows the dependence M_n and Đ on the conversion of DMA. Despite the complete conversion of VBPC, no peak of polymer or oligomer were detected before 80 min (20 % conversion of DMA) using DMF GPC. At 20% conversion of DMA, a polymer with M_n of 2,800 Da and Đ of 1.8 was formed. This is much higher than theoretical M_n of 1,100 Da for a conventional RAFT polymerisation, calculated using Equation 2-4, suggesting the formation of the hyper-branched core due to the high reactivity of the VBPC. After which, both M_n and Đ strongly increased throughout the polymerisation. At high monomer conversion, Đ grew exponentially probably due to bimolecular termination. The complete consumption of VBPC at the beginning of the copolymerisation and the low concentration of the monomer made termination reactions the most common pathway, resulting in a polymer with broad molecular weight distribution. Conventional RAFT polymerisation of DMA with BPC resulted in low Đ of 1.13. A slight increase in Đ was observed at ~80% (Figure 2-14).

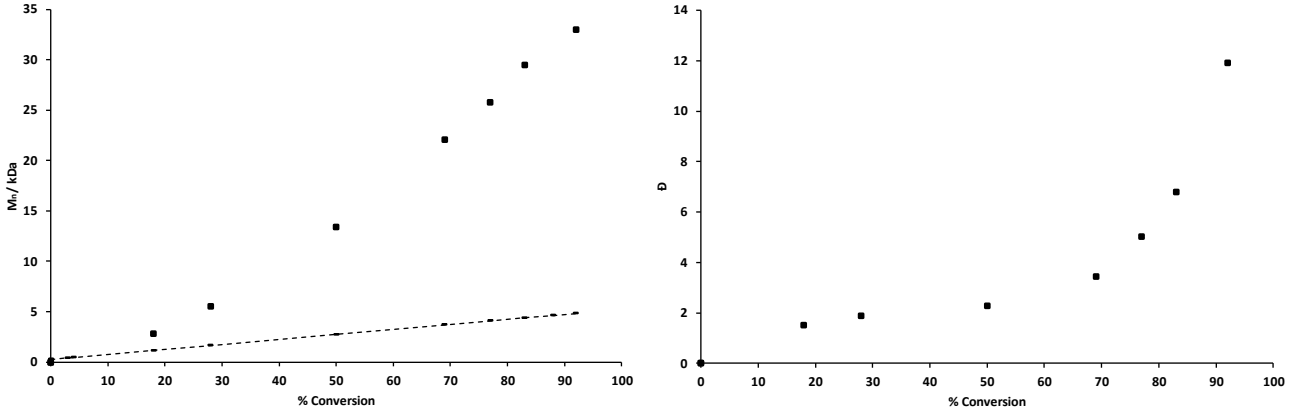

Figure 2-13. Dependence of A) M_n and B) Đ of SHBP-DMA on % conversion. The data presented is for SHB-PDMA50wt%, [DMA]:[VBPC]=50.

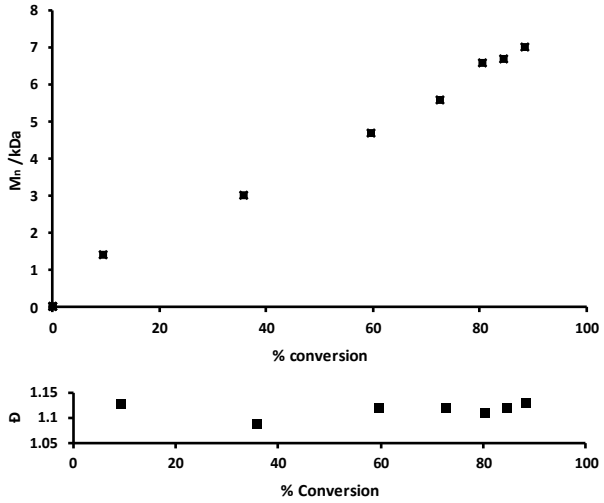

Figure 2-14. A) Dependence of Mn on % conversion B) dependence of Đ on % conversion for RAFT of DMA using non-polymerisable RAFT agent, benzyl-1-pyrrolecarbodithioate (BPC)

As described earlier, in SCVP, the dependence of DB on the monomer conversion is highly dependent on the feed ratio γ (Figure 1-9). Ideally, when γ >> 1, the DB very quickly reaches its final value and then remains constant throughout the polymerisation.

The dependence of DB on DMA conversion shown in Figure 2-15 clearly indicates that the final polymer formed is not the desired segmented hyper-branched structure. The highest DB (DB = 0.405) was reached at low DMA conversion (4% conversion), after which the DB started to decrease. The DB of 0.405 obtained early in the polymerisation is much higher than the maximum value when γ = 50 (DB = 0.039). Considering the kinetic data for the two monomers, this confirms that the VBPC underwent SCVP first probably to form a hyper-branched core. This hyperbranched core then grew linear arms of DMA forming a hyper-star copolymer.

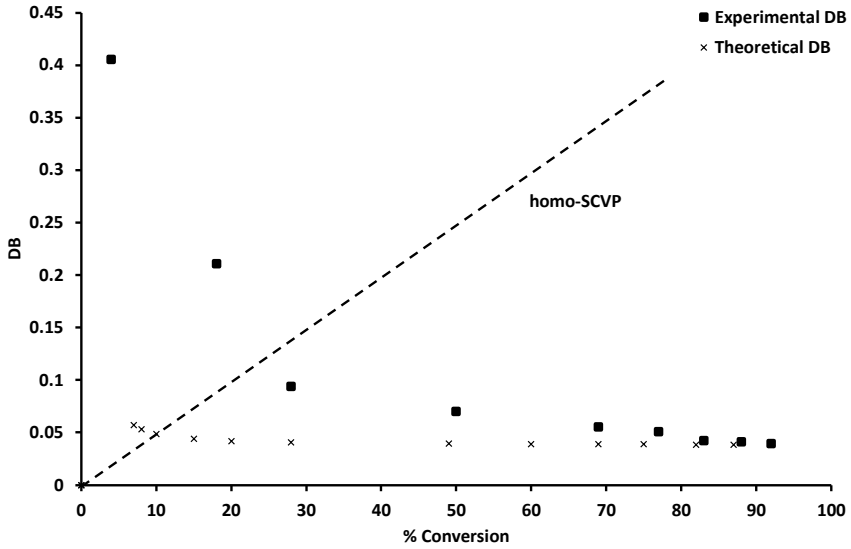

Figure 2-15. Dependence of DB on monomer conversion. The data presented is for SHB-PDMA50wt%, [DMA]:[VBPC]=50.

2.3 Conclusion

The aim of this chapter was to synthesise segmented hyper-branched polymers with high density of thiocarbonylthio terminals required for the installation of the peptide pro-drug. The polymers were simply synthesised via RAFT-SCVP of DMA with polymerisable RAFT agent (VBPC). The effect of: 1) stoichiometry of DMA to VBPC, 2) DMA concentration to dioxane on the degree of branching DB, molecular weight M_n, and Đ were studied.

The different reactivities of VBPC and DMA suggests that a homogeneous distribution of the branch points was not achieved, and SHBP were not formed. Due to its high reactivity, VBPC underwent SCVP first to form a hyper-branched core, which then started to add DMA to form a hyper-star copolymer. These different reactivities not only affect the structure of the final polymer but also affect M_n, Đ and DB at any given conversion. High molecular weight polymers with broad molecular weight distribution were formed early in the polymerisation and both values grew with conversion. In contrast, the DB reached its highest value in the early stages and decreased with time. As the highest DB was achieved earlier, 80% conversion could be targeted to avoid undesired termination and to achieve high fidelity of thiocarbonylthio end group required for the conjugation of peptide via aminolysis/Michael addition reaction.

As both branched[113,162,169] and star[161,167,168] polymers have been found to be good candidates as ^{19}F MRI contrast agents, these polymers will be used to synthesise polymer-peptide conjugates.

Moreover among various feed ratios studied, only polymers with γ = 50 were taken further because of their relative high molecular weight.

2.4 Experimental

2.4.1 Analytical Techniques

2.4.1.1 NMR Spectroscopy

^{1}H and ^{13}C NMR spectra were recorded on Bruker AV400 or Bruker AVIII HD 400 spectrometer at room temperature. Deuterated water and chloroform were used as sample solvent. Chemical shifts of spectrums are estimated in ppm relative to the residual solvent peak and the NMR spectra were examined using Topspin 3.0 NMR software.

^{1}H NMR was used to calculate the DB and monomer conversion. DB was calculated according to the following equation.

$$DB = \frac{2\left(\frac{I_{6.83-7.17}}{4}\right)}{\frac{2(I_{6.83-7.17})}{4} - \frac{(I_{3.28-2.75})}{6}} \qquad \textit{Equation 2-5}$$

Where $I_{6.83-7.17}$ is the integral peak due to styryl protons and $I_{3.28-2.75}$ is the integral peak due to CH_3 of DMA.

The percentage conversion of DMA and VBPC were calculated according to Equation 2-6 and Equation 2-7 respectively.

$$\%\ Conversion_{DMA} = \frac{I_{5.61} \times 100}{I^{\circ}_{5.61}} \qquad \textit{Equation 2-6}$$

where $I_{5.61}$ is the integral value of the peak at 5.61 corresponding to one proton of the vinyl of unreacted DMA, whereas $I^{\circ}_{5.61}$ is the original value before polymerisation.

$$\%\ Conversion_{VBPC} = \frac{I_{5.22} \times 100}{I^{\circ}_{5.22}} \qquad \textit{Equation 2-7}$$

Where $I_{5.22}$ is the integral value of the peak at 5.61 corresponding to one proton of the vinyl of unreacted VBPC, whereas $I^{\circ}_{5.22}$ is the original value before polymerisation.

2.4.1.2 Dynamic Light Scattering

Intensity-average size distributions were determined by Malvern Zetasizer software using a Malvern Zetasizer NanoZS Model ZEN 3600 instrument at a fixed angle of 173°. Measurements were performed at 25 °C on the polymers solutions in water with a concentration of 2 mg mL^{-1}. Three measurements of approximately ten runs of ten seconds duration were made and averaged. DLS autocorrelation function (ACF) curves of SHB-PDMAs are shown in Figure. A-2.

2.4.1.3 Transmission electron microscopy

Transmission electron microscopy (TEM) studies were accomplished using a FEI Tecnai Spirit Microscope operating at an accelerating voltage of 100 kV. Samples were prepared by placing a droplet (5 μL) of the polymer solution 10 mg/ mL on a glow-discharged, carbon-coated grid for approximately one minute and the excess was removed by blotting with filter paper. Samples were stained with a uranyl formate solution (5 μL of a 0.75% w/w solution) and then blotted with filter paper. The samples were additionally dried by vacuum.

2.4.1.4 Gel Permeation Chromatography

The molecular weight distributions were determined by an Agilent 1260 Infinity GPC/SEC system using a solution of dimethylformamide (DMF) with 0.1 % LiBr as eluent at a flow rate of 1.0 mL min^{-1}. The GPC system was equipped with a refractive index detector. Equipment was calibrated with near-monodisperse poly(methyl methacrylate) standards (2.14×10^6 - 1.95×10^3 g mol^{-1} range). Samples were prepared at 1mg ml^{-1} concentration using a solution of DMF 0.1 % LiBr with 0.1 % toluene as a marker reference. Samples were filtered through a 0.45 mm PTFE syringe before injection.

Elemental analysis

Elemental Analysis of the CTM (VBPC) was determined using a Perkin-Elmer 2400 CHNS/O Series 2 Elemental Analyser. The sample was burned in a large excess of oxygen and the resulting water and CO_2 were captured and weighted. Relative amount of each element was determined using a thermal conductivity detector.

Mass Spectrometry

Electron Ionisation (EI) MS of the CTM was accomplished using a VG Autospec Mass Spectrometer.

2.4.2 Materials

Sodium hydride (Sigma Aldrich, 60% in mineral oil dispersion), carbon disulfide (Sigma Aldrich, 99%), 4-vinylbenzyl chloride (Sigma Aldrich, 90%), benzyl 1H-pyrrole-1-carbodithioate (Sigma Aldrich, 97%), magnesium sulfate (Fisher), silica gel (40-63 μm mean particle size, average diameter 60 Å, Fluorochem) diethyl ether (Fisher), acetone (fisher) and hexane (Fisher) were used as received. Dimethyl formamide (DMF) was obtained from the Grubbs dry solvent system. Pyrrole (Sigma Aldrich, 98%) and *N*,*N*-dimethylacrylamide (DMA) (Sigma Aldrich, 99%) were vacuum distilled prior to being used. 4,4′-Azobis(4-cyanovaleric acid) (Sigma Aldrich, ≥98%) was recrystallised prior to being used.

2.4.3 Synthesis of 4-vinylbenzyl *N*–pyrrole carbodithioate (VBPC) (RAFT Agent)

VBPC was synthesised according to the procedure described by Rimmer *et al.*[107] Sodium hydride (3.016 g, 125 mmol) was added to a dried round bottomed flask followed by dry DMF (80 mL) to give a grey suspension. Pyrrole (5.008 g, 74.6 mmol) dissolved in DMF (10 mL) was added to the reaction dropwise over a period of 30 minutes at 0 °C to form a yellow foam. The reaction mixture was stirred at room temperature for 40 minutes. Carbon disulfide (4.500 g, 74.4 mmol) dissolved in DMF (10 mL) was added dropwise over a period of 10 minutes at 0 °C to form a dark red solution. The reaction mixture was stirred at room temperature for approximately 30 minutes. 4-Vinylbenzyl chloride (11.135 g, 72.9 mmol) dissolved in DMF (10 mL) was added dropwise over a period of 20 minutes to form a brown solution. The solution was stirred overnight at room temperature. After completion of the reaction, the crude reaction mixture was dissolved with diethyl ether (100 mL) and extracted with water (100 mL). The organic layer was recovered, and the aqueous layer was extracted with diethyl ether (2 × 100 mL). The combined organic layer extracts were washed with water (2 × 100 mL), dried over anhydrous $MgSO_4$, and filtered. Diethyl ether was removed by rotary evaporator under vacuum giving a brown oil. The crude product was purified by silica gel column chromatography using petroleum ether. Petroleum ether was evaporated under vacuum and the pure product was obtained as a bright yellow solid. The product was stored at -18 °C under nitrogen atmosphere. Yield: 15.7 g (82%); TLC (silica gel; petroleum ether) showed one spot, Rf = 0.25.

Elemental analysis: Expected: C 64.83%, H 5.05%, N 5.40%, S, 24.72%. Found: C 64.79%, H 5.42%, N 5.06%, S 22.32%.

ESI-MS: Expected m/z: 259.3, experimental m/z: 259.0.

^{1}H NMR (400 MHz, $CDCl_3$) δ 7.71 (t, *J* = 2.4 Hz, 2H), 7.46 – 7.34 (m, 4H), 6.73 (dd, *J* = 17.6, 10.9 Hz, 1H), 6.33 (t, *J* = 2.4 Hz, 2H), 5.78 (dd, *J* = 17.6, 0.6 Hz, 1H), 5.29 (dd, *J* = 10.9, 0.5 Hz, 1H), 4.62 (s, 2H).

^{13}C NMR (101 MHz, $CDCl_3$) δ 199.29, 137.37, 136.24, 133.96, 129.63, 126.58, 120.69, 114.36, 114.25, 41.52.

2.4.4 Synthesis of segmented hyper-branched poly(*N*,*N*-dimethylacrylamide) (SHB-PDMA) by varying the concentration to dioxane

N,*N*-dimethylacrylamide (DMA), 4,4'-azobis(4-cyanovaleric acid) and 4-vinylbenzyl *N*-pyrrole carbodithioate were dissolved in different amounts of anhydrous dioxane as shown in Table 2-4. The reaction mixture was then transferred into a Schlenk flask and degassed using 3 freeze-pump-thaw cycles. The flask was backfilled with N_2 and placed in a water bath at 60 °C. After completion of polymerisation, the crude polymer solution was precipitated from diethyl ether/acetone 9:1. The precipitate was isolated by centrifugation (4,500 rpm, for 5 min). The polymer was then dialysed against deionised water (membrane MWCO 3.5 kDa) for 48 h. A yellow solid was obtained after freeze drying.

Table 2-4. Amounts of DMA, VBPC and ACVA used to synthesise SHB-PDMAs by varying the concentration to dioxane

[DMA]:[CTA]:[ACVA]	**DMA**		**CTA**		**ACVA**		**DMA**	**Dioxane**	
	/mmol	**/ g**	**/mmol**	**/ g**	**/mmol**	**/ g**	**wt%**	**/ g**	**/ mL**
50:1:0.2	30	3	0.605	0.165	0.121	0.034	10	27	26.21
50:1:0.2	30	3	0.605	0.165	0.121	0.034	20	12	11.65
50:1:0.2	30	3	0.605	0.165	0.121	0.034	30	7	6.79
50:1:0.2	30	3	0.605	0.165	0.121	0.034	40	4.5	4.37
50:1:0.2	30	3	0.605	0.165	0.121	0.034	50	3	2.91

^{1}H NMR (400 MHz, $CDCl_3$) δ 7.75 – 7.65 (br, 2H), 7.17 – 6.83 (br, 4H), 6.36 – 6.31 (br, 2H), 5.19 – 5.01 (br, 1H), 3.28 – 2.75 (br. m., 6H), 2.77 – 2.03 (br. m., 1H), 2.03 – 1.07 (br. m., 2H).

SHB-PDMA-10 wt%: M_n = 13.5 kDa, Đ = 1.78 (determined by DMF GPC, PMMA standard)

SHB-PDMA-20 wt%: M_n = 19.9 kDa, Đ = 2.70

SHB-PDMA-30 wt%: M_n = 25.5 kDa, Đ = 3.77

SHB-PDMA-40 wt%: M_n = 32.0 kDa, Đ = 8.11

SHB-PDMA-50 wt%: M_n = 33.0 kDa, Đ = 11.92

2.4.5 Synthesis of segmented hyper-branched poly(*N*,*N*-dimethylacrylamide) (SHB-PDMA) at different feed ratios

N,*N*-dimethylacrylamide (DMA), 4,4'-azobis(4-cyanovaleric acid) and 4-vinylbenzyl N-pyrrole carbodithioate were dissolved in anhydrous dioxane as shown in Table 2-5. The flask was sealed with a rubber septum and the reaction mixture was purged with nitrogen through a syringe needle for approximately 30 min, followed by immersing in a 60 °C water bath. After 24 h, the reaction mixture was exposed to air. The crude polymer solution was precipitated from diethyl ether/acetone 9:1. The precipitate was isolated by centrifugation (4,500 rpm, for 5 min). The polymer was then dialysed against deionised water (membrane MWCO 3.5 kDa) for 48 h. A yellow solid was obtained after freeze drying.

Table 2-5. Amounts of DMA, VBPC and ACVA used to synthesise SHB-PDMAs at different feed ratio

[DMA]:[CTA]:[ACVA]	**DMA**		**CTA**		**ACVA**		**DMA**	**Dioxane**	
	/mmol	**/ g**	**/mmol**	**/ g**	**/mmol**	**/ g**	**/wt%**	**/ g**	**/ mL**
20:1:1	20	2	1.009	0.130	1.009	0.141	20	8	7.76
30:1:1	20	2	0.673	0.174	0.672	0.188	20	8	7.76
40:1:1	20	2	0.504	0.130	0.504	0.034	20	8	7.76

^{1}H NMR (400 MHz, D_2O) δ 7.80 – 7.62 (br, 2H), 7.35 – 6.75 (br, 4H), 6.53 – 6.36 (br, 2H), 5.30 – 4.93 (br, *m.*, 1H), 3.17 – 2.74 (br, m., 6H), 2.76 – 2.06 (br, m., 1H), 2.06 – 1.05 (br, *m.*, 1H).

SHB-PDMA, γ= 20: M_n = 7.4 kDa, Đ = 1.75 (determined by DMF GPC, PMMA standard)

SHB-PDMA, γ= 30: M_n = 10.2 kDa, Đ = 2.06

SHB-PDMA, γ= 30: M_n = 14.2 kDa, Đ = 2.37

2.4.6 Synthesis of Linear poly(*N*,*N*-dimethylacrylamide) (L-PDMA) Dp = 50

N,*N*-dimethylacrylamide (DMA) (1 g, 10 mmol), 4,4'-azobis(4-cyanovaleric acid) (0.011 g, 0.040 mmol) and benzyl-1-pyrrolecarbodithioate (0.047 g, 0.202 mmol) were dissolved in anhydrous dioxane (3 g, 2.91 mL). The reaction mixture was then transferred into a Schlenk flask and degassed using 3 freeze-pump-thaw cycles. The flask was backfilled with N_2 and immersed into a water bath at 60 °C. The polymerisation was allowed to proceed for 3 h. The crude polymer solution was precipitated from diethyl ether/acetone 9:1. The precipitate was isolated by centrifugation (4,500 rpm, for 5 min). The polymer was then dialysed against

deionised water (membrane MWCO 3.5 kDa) for 48 h. A yellow solid was obtained after freeze drying.

^{1}H NMR (400 MHz, $CDCl_3$) δ 7.58 – 7.49 (br, 2H), 7.24 – 7.15 (br. m., 2H), 7.15 – 7.06 (br. m., 3H), 6.23 – 6.17 (br, 2H), 5.06 – 4.88 (br, 1H), 3.29 – 2.72 (br. m., 6H), 2.69 – 2.15 (br. m., 1H), 2.02 – 1.01 (br. m., 2H).

M_n =7.5 kDa, Đ = 1.16

Chapter 3 Synthesis of peptide derivative of 5-FU

3.1 Introduction

Since the pioneering work of Emil Fischer[215] with the synthesis of dipeptides, there have been a tremendous progress in peptide synthesis.[216–218] The basic idea of the synthesis of peptides in homogeneous solution involves reversible blocking of the carboxyl group of one amino acid and amino group of another.[216] Moreover, the activation of carboxyl group is essential for the formation of amide bond. In this approach, all intermediates need to be isolated, purified, and characterised prior to starting the following step. Although the classical solution approach has yielded remarkable successes in the synthesis of small peptides,[216] the synthesis of longer peptide chains is rather limited. This is ascribed to solubility problems, and formidable isolation and purification process.[219] In contrast, with the introduction of solid phase peptide synthesis (SPPS) by Merrifield,[220] assembly of longer peptides became possible. The solid phase approach can be carried out more rapidly and nearly to completion using an excess amount of protected amino acids, which can be removed by simple washing. Furthermore, all the coupling and deprotecting reactions can be done in a single reaction vessel allowing the syntheses to be carried out in automated manner.[221,222] The principle of SPPS involves a stepwise addition of protected amino acids to a growing peptide chain linked to a solid support as shown in Scheme 3-1. The process begins with an insoluble resin with a functional group to which the first *N*-protected amino acid can be covalently attached. The protecting group is then cleaved to add the second *N*-protected amino acid. The process then continues in a stepwise manner. Once the desired peptide sequence is synthesised, the bond holding the chain to the solid support along with the side-chain protecting groups are finally cleaved, liberating the product into the solution.[219,220]

The solid phase utilised in SPPS should be carefully selected. Although Merrifield's solid support, cross-linked poly(styrene-divinylbenzene),[220] is still in use, a number of more polar resins have been developed.[223] Grafting PEG chains onto polystyrene beads[224,225] can enhance solubility and decrease the potential aggregation of the growing peptide. The modification of the resin with polar linkers improves the interactions and swelling behaviour with polar solvents.[226] These linkers also determine the C-terminal modification of the peptide synthesised. Most commonly, the peptide is released as an acid or amide but can be released as alcohol, aldehyde, hydrazide and many others.[227] Lightly cross-linked resins, e.g. 1% DVB in PS, is optimum for good accessibility and good swelling properties. A high degree of

crosslinking would reduce the swelling whereas very low degree of crosslinking would cause a considerable loss of mechanical stability in the swollen state.[220]

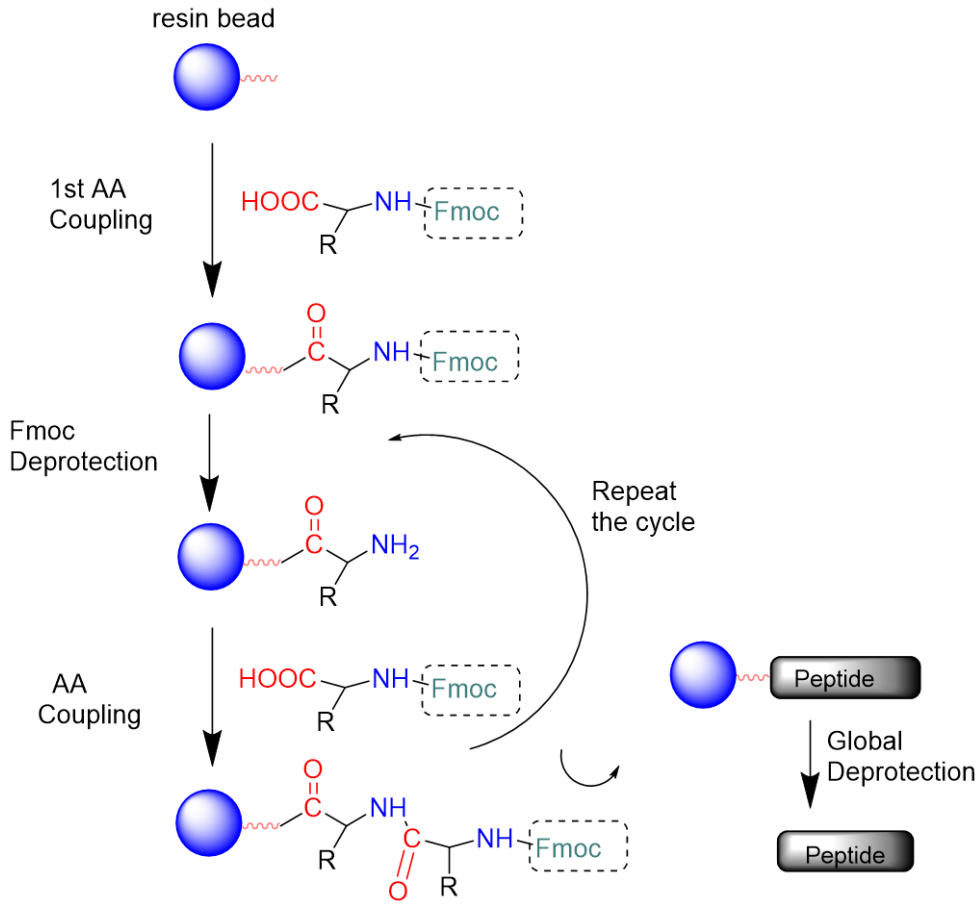

Scheme 3-1. Peptide assembly in Solid Phase Peptide Synthesis using Fmoc protecting group. AA is amino acid and Fmoc is 9-fluorenylmethoxycarbonyl protecting group.

The two major *N*-terminal protecting groups that have been established in SPPS process are *tert*-butyloxycarbonyl (Boc)[228] and 9-fluorenylmethoxycarbonyl (Fmoc).[229] In the Boc method, benzyl-type (Bzl) protecting groups usually serve as permanent protection of the side chains of trifunctional amino acids. Although the Boc/Bzl approach was exclusively used in the first 15 years of SPPS, the hazard of hydrofluoric acid (HF) used for the final cleavage as well as the frequent use of trifluoroacetic acid (TFA) mediated Boc deprotection, which might affect sensitive peptide sequences, limited the use of the technique. The introduction of the Fmoc-group [229] allowed the entire SPPS process to be performed under milder conditions. Fmoc is usually deprotected using mild basic conditions (often piperidine),[230] while the final cleavage of orthogonal *tert*-butyl (*t*-Bu) side-chain protecting groups can be accomplished by TFA.[231,232] Novel side-chain protecting groups of trifunctional amino acids have been also applied in Fmoc/*t*-Bu technique.[233,234]

Notable progress has also been made in the chemistry of peptide bond formation in parallel with the recent development of peptide coupling reagents. Although more traditional carbodiimide-based coupling reagents[220,235] with racemization suppressants, such as 1-hydroxybenzotriazole (HOBt),[236] have been used as the major activators for many decades, coupling reagents such as phosphonium- or uronium-based coupling reagents[237–239] are the most widely used today.

This chapter aims to synthesise the hexa-peptide bearing 5-fluorouracil (5-FU) as α-substituent of terminal glycine moiety, Gly-Phe-Leu-Gly-Leu-Gly-α-(5-FU). The choice of this hexa-peptide was based on its known degradation ability by lysosomal enzymes that the prodrug would encounter in the tumour.[179–182] The synthesis of hexa-peptide was first investigated using the method widely used in peptide chemistry (illustrated in Scheme 3-2). This strategy required the synthesis of the *N*-terminal protected tetra-peptide, Fmoc-Gly-Phe-Leu-Gly, and the *C*-terminal protected dipeptide derivative of 5-FU, Leu-Gly-α-(5-FU)-OMe. After the coupling reaction of the dipeptide and tetra-peptide, Fmoc-protective group was cleaved and *N*-terminal was modified with pentaflourophenyl acrylate to provide vinyl functionality that may be attached to SHB-PDMA via aminolysis/Michael addition reaction This synthetic route, however, resulted in low yield of impure material. Therefore, the tetra-peptide and the dipeptide derivative of 5-FU will be conjugated directly into the polymer (Scheme 4-6). Growing the hexa-peptide on the polymer surface is a good method to avoid undesired side products as the polymer can be purified after each step by simple dialysis. The new synthetic route requires the synthesis of vinyl-modified tetra-peptide, Gly-Phe-Leu-Gly. Furthermore, protecting C-terminal of the dipeptide derivative of 5-FU is not essential. Hence, Leu-Gly-α-(5-FU) will be synthesised.

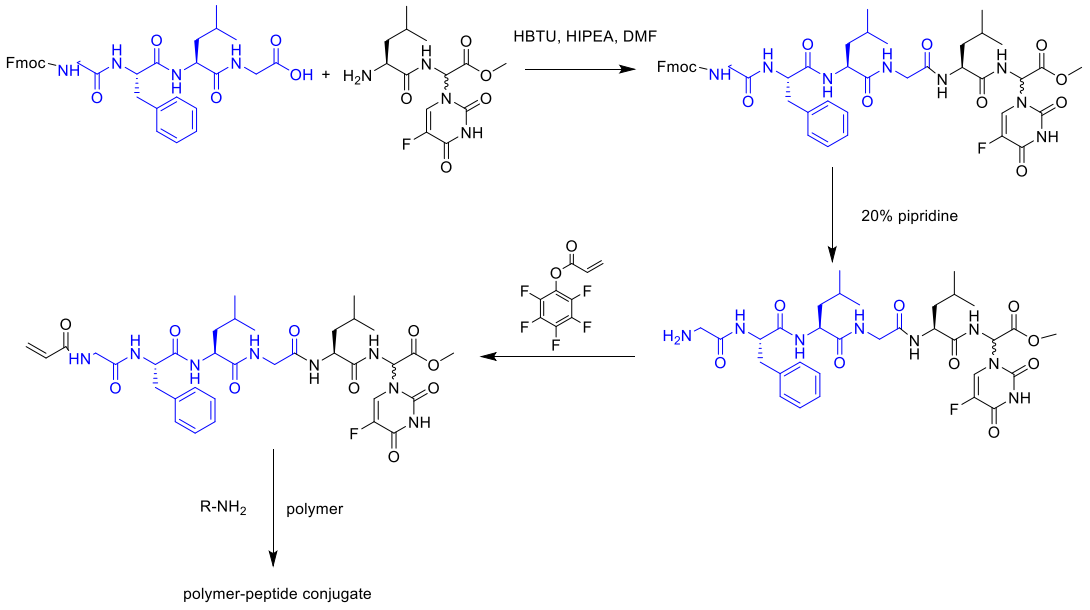

Scheme 3-2 synthetic route to the hexa-peptide bearing 5-fluorouracil (5-FU) as α-substituent of terminal glycine moiety, Gly-Phe-Leu-Gly-Leu-Gly-α-(5-FU) using standard solution coupling method

3.2 Results and discussion

3.2.1 Synthesis and modification of the tetra-peptide Gly-Phe-Leu-Gly

Gly-Phe-Leu-Gly peptide was synthesised using standard 9-fluorenylmethoxycarbonyl (Fmoc) protocols.[192] This was then modified with acrylic acid to provide vinyl functionality. Wang resin (4-Alkoxybenzyl alcohol resin)[240] was chosen as a solid support to synthesise the peptide acid. The cleavage of this resin bearing a hydroxyl group will result in a peptide with acid functionality that may be used to attach to the Leu-Gly-5-FU pro-prodrug. The esterification of Wang resin with the first Fmoc amino acid is a crucial step in SPPS to achieve high conversion. Here, both Wang resin and Fmoc-Gly-Wang resin were investigated to synthesise Gly-Phe-Leu-Gly peptide. The synthesis involved double coupling steps using 5-fold excess amino acid to ensure a quantitative reaction and facilitate high yields. Amino acid coupling was facilitated using *N,N,N′,N′*-tetramethyl-*O*-(1*H*-benzotriazol-1-yl)uronium hexafluorophosphate **(**HBTU) which activated the carboxyl group by forming an activated ester and making nucleophilic attack by an amino group more efficient. The activation by HBTU requires the presence of a base. Diisopropylethylamine (DIPEA) was used for this purpose. The Fmoc group was deprotected under basic condition, piperidine, to give the free amino group which allows coupling of another amino acid. Simple washing of the resin following coupling or deprotection steps allowed the removal of excess reagents and by-products. Gly-Phe-Leu-Gly peptide was modified with acrylic acid to provide vinyl functionality that may be

attached to SHB-PDMA via aminolysis/Michael addition reaction. Final cleavage in the presence of acid resulted in a free peptide with carboxylic functionality at one end and vinyl at the other. The peptide was characterised using ^{1}H NMR spectroscopy, mass spectrometry (MS) and high-performance liquid chromatography (HPLC).

3.2.2 Wang resin versus preloaded Wang resin

The main challenge in the synthesis of Gly-Phe-Leu-Gly peptide was the low yield. Standard Wang resin (**1** in Figure 3-1) was first used as a solid support. Compared to theoretical yield calculated considering Equation 3-1, the standard Wang resin resulted in very low yield (18%).

$$Yield_{theo}\% = Resin\ load\ capacity \times Amount\ of\ resin \times Molecular\ weight\ of\ peptide \qquad Equation\ 3\text{-}1$$

The low yield in SPPS is usually caused by inefficient resin swelling, inefficient first amino acid loading, or complicating synthesis due to long peptide aggregation. Clearly as the aim is to synthesise a short peptide of four amino acids sequences, the aggregation of the growing peptide is not the case. The low yield is probably linked with esterification of Wang resin with first Fmoc amino acids due to the low accessibility of the hydroxyl group of Wang resin. Therefore, the preloaded resin, Fmoc-Gly-Wang resin (**2** in Figure 3-1), was used and the resin swelling time was increased from 15 min to 1 h to ensure diffusion of the reagents and amino acid coupling at all active sites. Pendant glycine will probably increase the swelling of the resin in DMF due to the decrease of the network free energy based on the additional solvation of the amino acid.[241] The synthesis using the preloaded resin resulted in much higher yield (87%).

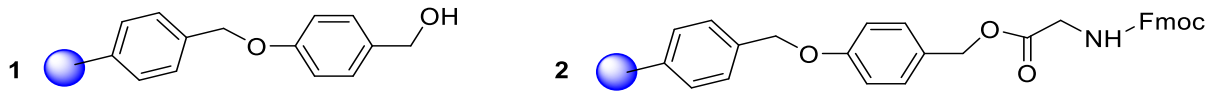

Figure 3-1. 1) Wang resin 2) Fmoc-Gly-Wang resin

3.2.3 The synthesis of vinyl modified peptide

The vinyl-modified peptide was prepared in a similar manner used for coupling a standard amino acid. Once all standard amino acid deprotection and coupling cycles were accomplished and after the cleavage of the *N*-terminus protecting group of the last amino acid, an excess amount of the acrylic acid activated with HBTU in the presence of DIPEA was added (Scheme 3-3).

The synthesis progress of the peptide was followed by the cleaving of a small amount of intermediate product **3**. The purity of vinyl-modified peptide **4** was found to be 81% by high performance liquid chromatography (HPLC) compared with 96% for non-modified peptide **3** as shown in Figure 3-2. The modification was confirmed by ^{1}H NMR spectroscopy and MS.

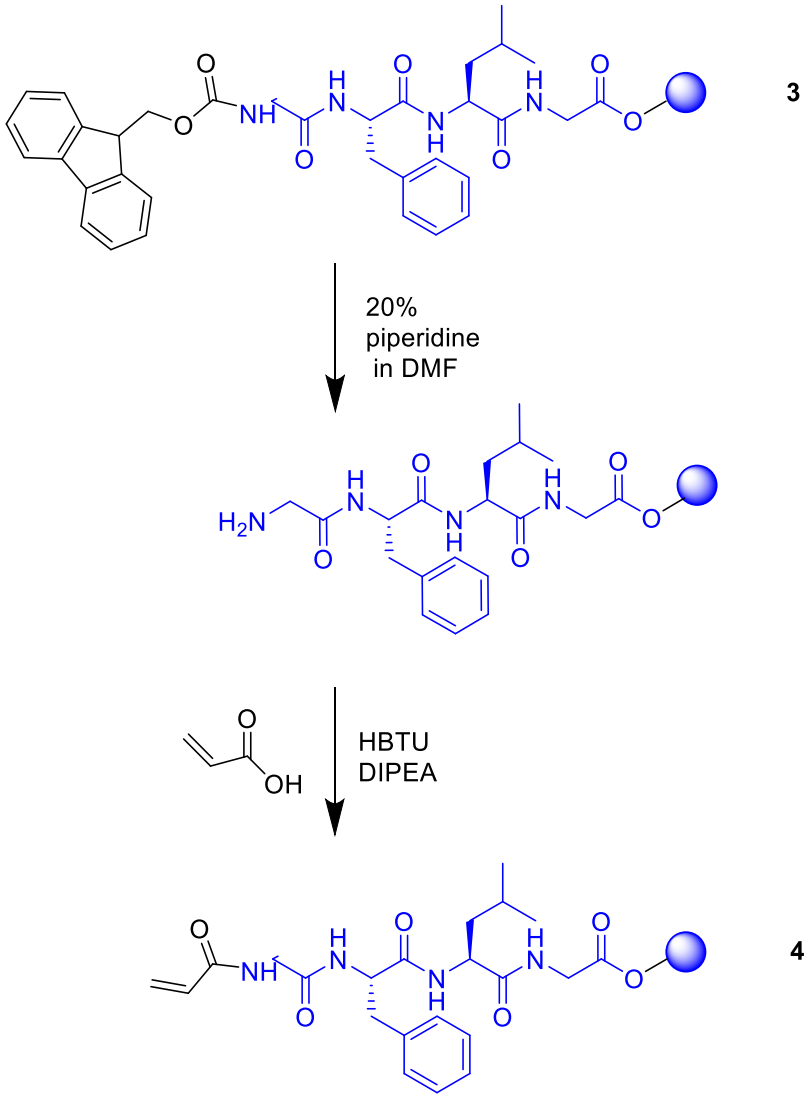

Scheme 3-3. Synthetic route to vinyl-modified peptide 4

The formation of the vinyl-modified peptide **4** was confirmed by ^{1}H NMR spectra as shown in Figure 3-3. Compared with non-modified peptide **3**, the resonances due to Fmoc aromatic protons between 7.12 and 7.97 ppm and Fmoc CH_2 protons at 4.24 ppm almost disappear confirming the successful cleavage. Moreover, the ^{1}H NMR spectrum displays the characteristic resonance signals due to vinyl protons at 5.59, 6.08 and 6.28 ppm confirming the successful modification with acrylic acid. However, the spectrum also shows other resonance signals due to vinyl protons at 5.90 and 6.14 ppm indicating the formation of another product

with vinyl end group. The high purity of non-modified peptide **3** (Figure 3-2) suggests that the impurities were possibly formed during the modification step. ^{1}H NMR spectrum of the acrylic acid used in the modification indicates that the acrylic acid was not a pure monomer (Figure 3-4). The triplets due to **CH$_2$**COOH and **CH$_2$**CH$_2$COOH at 2,06 and 4.26 ppm along with resonance between 5.88-6.32 ppm due to vinyl protons suggest the presence of acrylic acid dimer (3-acryloxypropionic acid). Michael addition reaction of acrylic acid during storage is well known (Scheme 3-4).[242–244] The spectrum also shows other impurities which could be due to the presence of trimer, tetramer etc. Therefore, the impurities seen in the vinyl-modified tetra-peptide were perhaps due to the oligomeric impurities found in the acrylic acid used for the functionalisation as also confirmed by MS (Figure. A-4). As the peptide sequence was not affected (Figure 3-5), the peptide sequence was taken forward without any further purification.

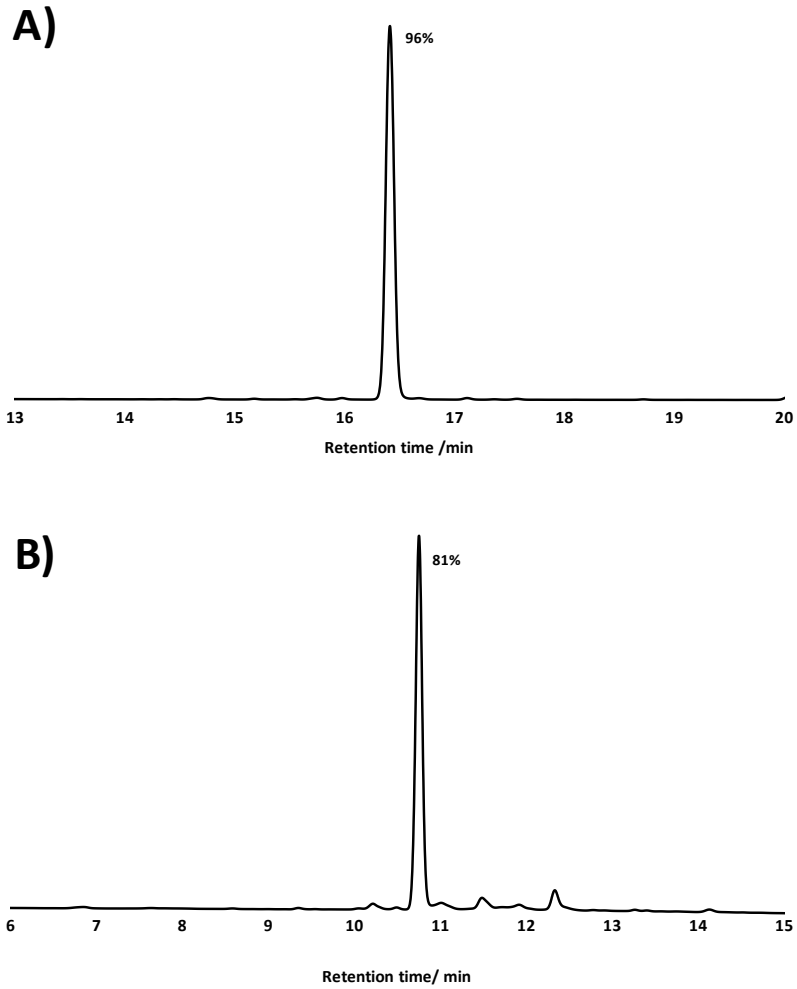

Figure 3-2. HPLC profiles of 1) non-modified peptide 3 2) vinyl-modified peptide. Column: Waters XBridge C18 250 × 4.6 mm. Mobile phase: gradient 5 to 95% acetonitrile (with 0.1% formic acid) over 20 min at a flow rate of 1 mL min^{-1}.

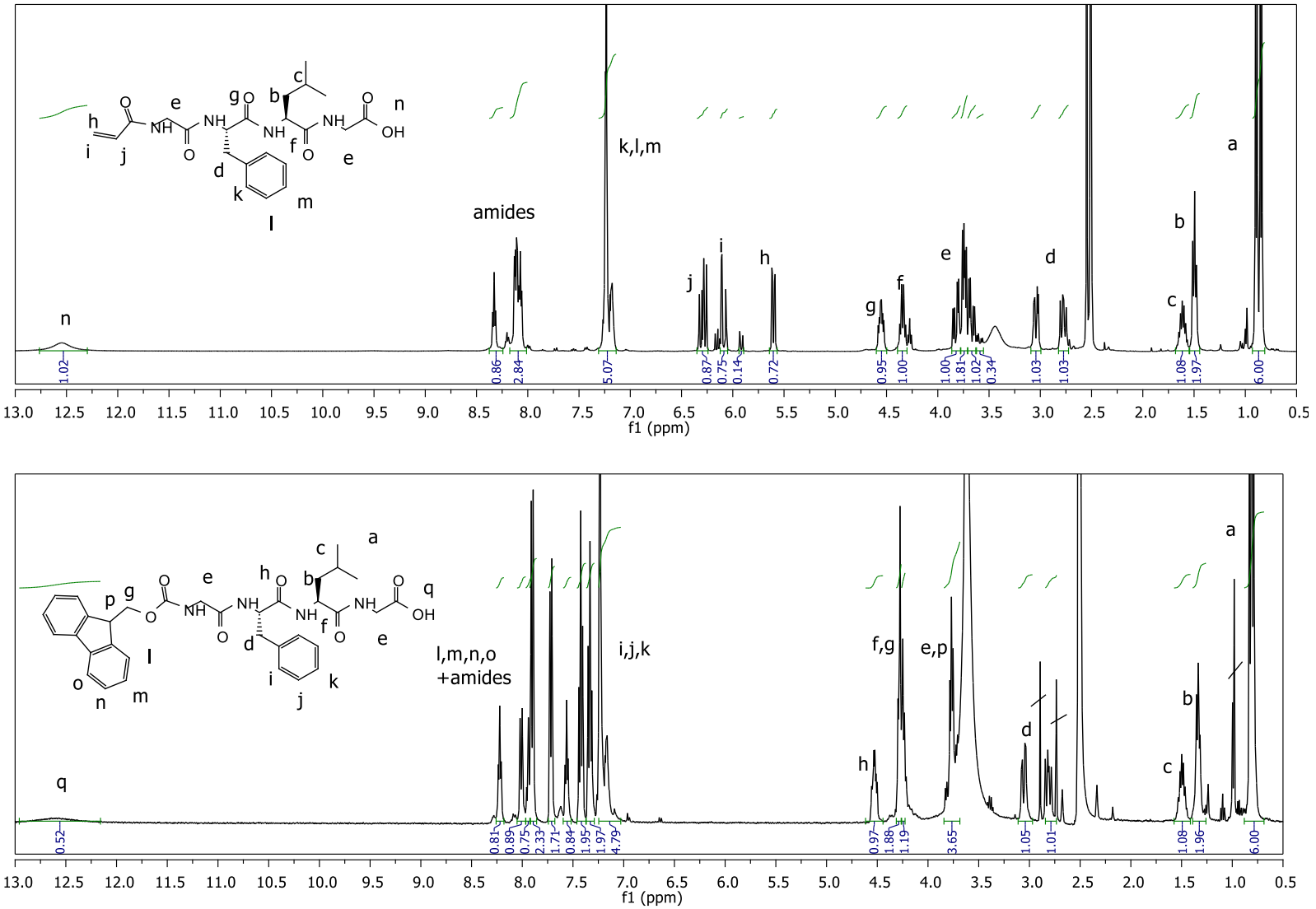

Figure 3-3. ^{1}H NMR of non-modified and vinyl modified peptide in $SO(CD_3)_2$

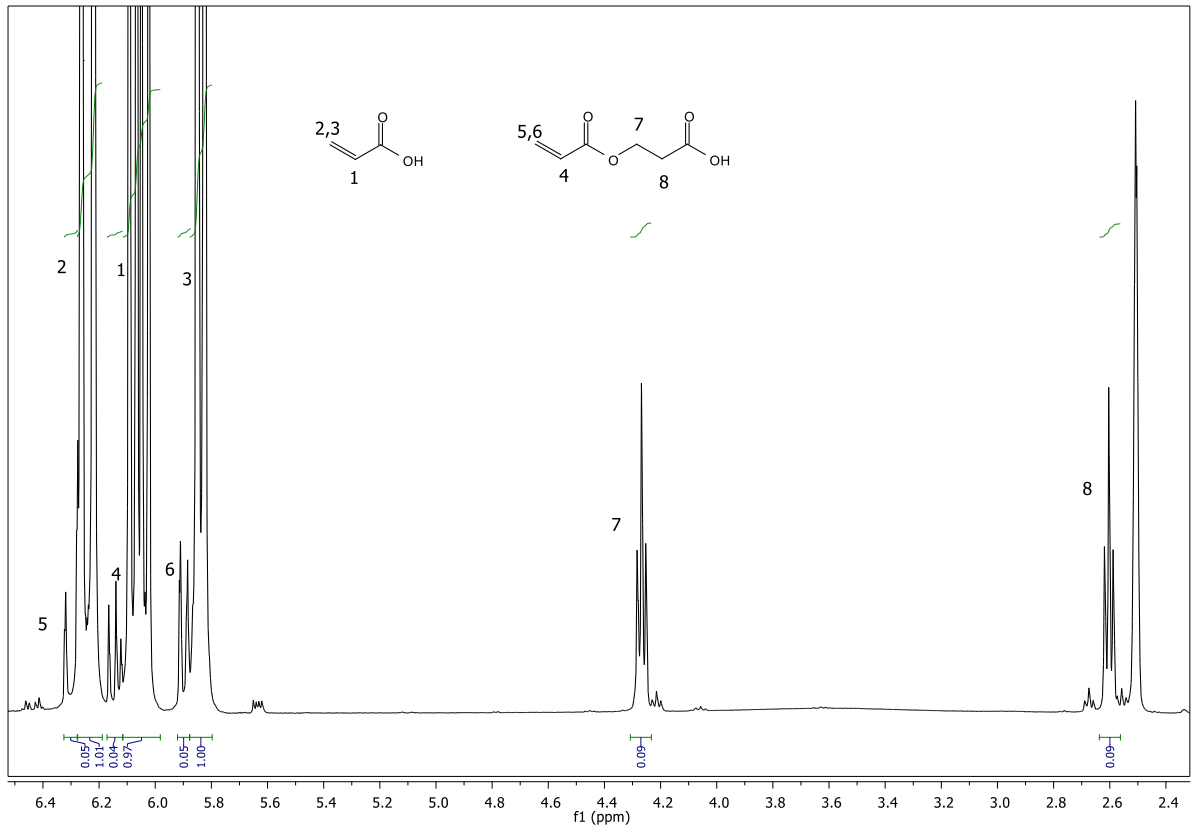

Figure 3-4. ^{1}H NMR of the acrylic acid used for the modification in $SO(CD_3)_2$.

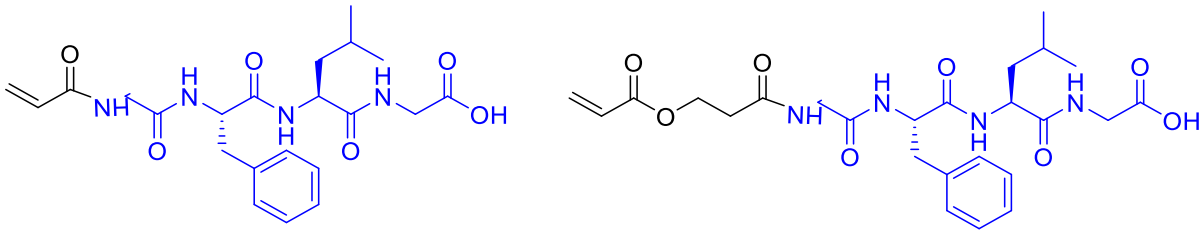

Figure 3-5 The structures of the vinyl-modified tetrapeptides

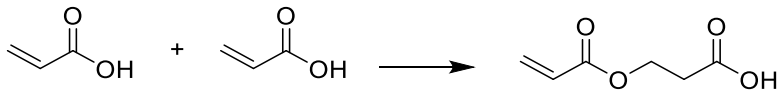

Scheme 3-4. Formation of acrylic acid dimer (3-acryloxypropionic acid) by Michael addition reaction. The reaction might also continue to form a trimer, tetramer etc.

3.2.4 Synthesis of L-Leucyl-2-(5-fluorouracil-l-yl)-L,D-glycine (Leu-Gly(5-FU)):

L-Leucyl-2-(5-fluorouracil-l-yl)-L,D-glycine (Leu-Gly(5-FU)) **9** was synthesised as outlined in Scheme 3-5 following the work of Putnam and Kopecek[179] with some modifications in the Cbz cleavage.

Initially, *N*-(carbobenzyloxy)-L-leucyl serine methyl ester **5** was used as a starting material. The treatment of dipeptide **5** with lead tetraacetate under anhydrous conditions (4 Å molecular sieves, refluxing ethyl acetate) resulted in the α-acetoxy glycine derivative **6** in 44% yield.

Substitution of acetoxy group with 5-FU in the presence of triethylamine at room temperature afforded 5-FU derivative **7** with 5-FU substituted mainly at N1 position of pyrimidine ring. However, substitution at N3 position of 5-FU in similar reactions has been reported.[245] The presence of this isomer (10%) was indicated by both ^{1}H and ^{19}F NMR spectroscopy of the crude material in $(CD_3)_2SO$. These isomers could not be separated using column chromatography and therefore were taken to the following step without any further purification.

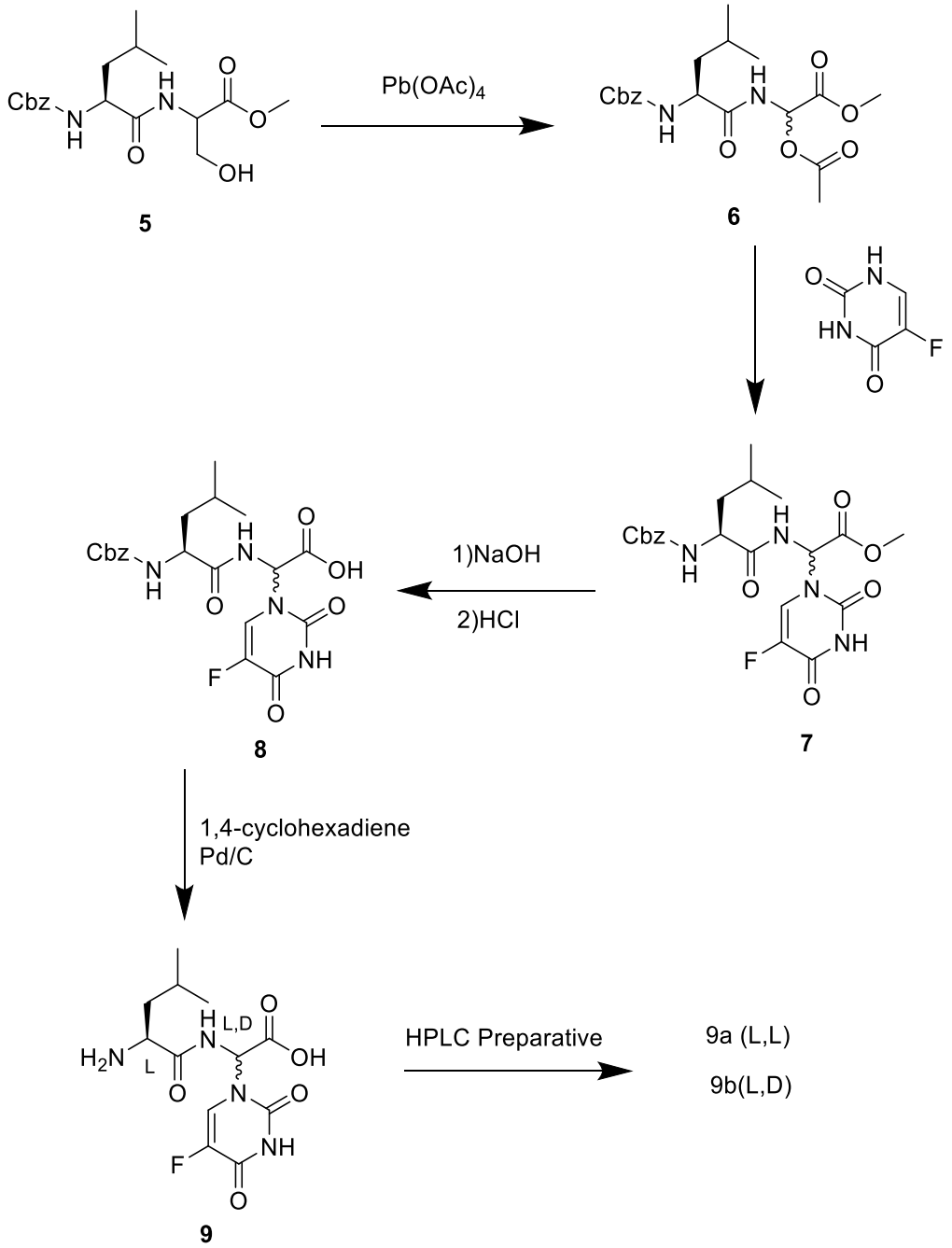

Scheme 3-5. Synthetic route to L-Leucyl-2-(5-fluorouracil-l-yl)-L,D-glycine (Leu-Gly(5-FU))

Methyl ester deprotection of 5-FU derivative **7** was accomplished by basic hydrolysis (0.4 N NaOH) at room temperature as shown in Scheme 3-5. Compared with the methyl ester cleavage from typical amino acids, the cleavage was incredibly fast and was complete in a few minutes, which is also reported for similar 5- FU peptides derivatives.[179] This rapid cleavage might be ascribed to an intramolecular catalysis mechanism induced by the present of the 5-FU (Scheme 3-6).[246]

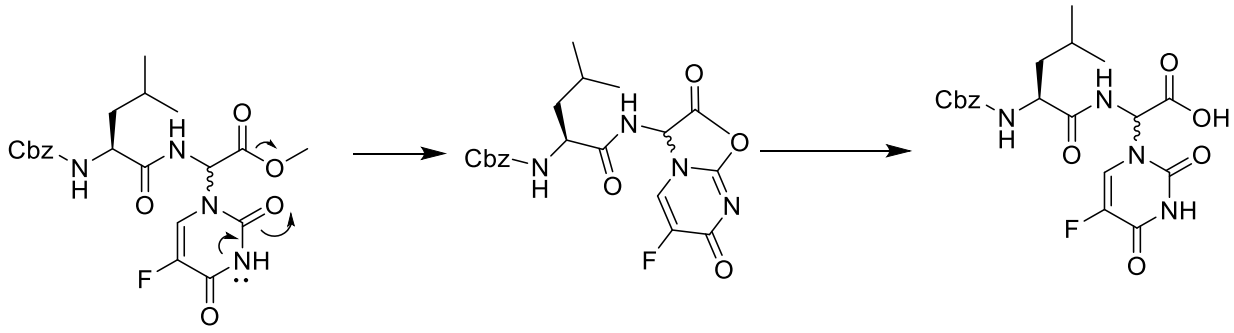

Scheme 3-6. The rapid hydrolysis of methyl ester group is possibly because of the intramolecular catalysis mechanism induced by the presence of 5-FU

3.2.5 Deprotection of Cbz blocking group

Several attempts were made to remove the Cbz protecting group, either before or after the cleavage of methyl ester group, by catalytic hydrogenation in the presence of hydrogen transfer agents; cyclohexene, hydrazide hydrate, formic acid and 1,4- cyclohexadiene. The results are summarised in Table 3-1.

Table 3-1. Cbz deprotection using various hydrogen transfer agents

Cbz-protected peptide	**Hydrogen donor**	**Product**	**Comments**
Cbz-Leu-Gly(5FU)-OMe	Cyclohexene	No reaction	
Cbz-Leu-Gly(5FU)-OMe	Hydrazine	The peptide was destroyed	
Cbz-Leu-Gly(5FU)-OMe	Formic acid	Leu-Gly(5FU)-OMe	Partial hydrogenation of pyrimidine ring
Cbz-Leu-Gly(5FU)-OH	1,4-cyclohexadiene	Leu-Gly(5FU)-OH	

Although successful cleavage of Cbz group for the same dipeptide derivative using cyclohexene as a hydrogen transfer agent has been already reported,[179,191] all attempts using cyclohexene in refluxing methanol failed even with extended reaction times. Experiments carried out using hydrazine in dry methanol at room temperature resulted in partial cleavage with several changes in the structure of the deprotected peptide. MS shows that the product

was destroyed, possibly due to the nucleophilic attack of carbonyl group. MS fragments could not be identified.

Treatment with formic acid in dry methanol at room temperature resulted in a complete cleavage of the Cbz group. This, however, resulted in a side product which was demonstrated by ^{1}H NMR spectroscopy (Figure 3-6). In the ^{1}H NMR spectra of the side product, the disappearance of the doublet at 8.16 ppm due to pyrimidine CH proton was recorded, accompanied with the presence of the resonance signals for CH_2-CHF protons (3.86 and 5.12–5.26 ppm) indicating the hydrogenation of the double bond in the pyrimidine ring. Partial hydrogenation of the double bond in the pyrimidine ring has already been reported during the cleavage of Cbz by catalytic hydrogenation in the presence of H_2 gas.[245] Although internal cyclization to the corresponding diketopiperazines has been observed in similar esterified dipeptide containing C-terminal Gly(5-FU),[245] the formation of this side product was not observed.

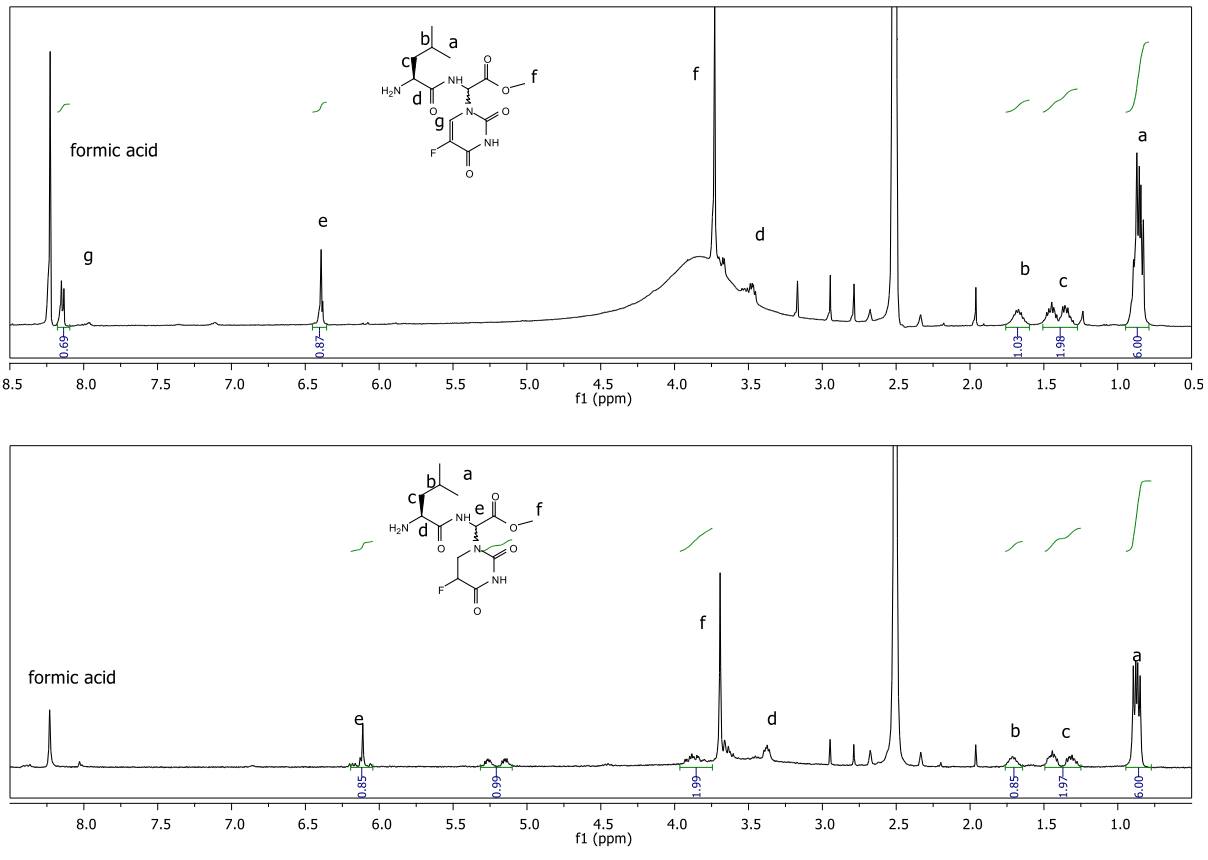

Figure 3-6. ^{1}H NMR spectrum in $SO(CD_3)_2$ of the dipeptide after the hydrogenation with formic acid at room temperature

Cbz group cleavage using 1,4-cyclohexadiene in dry ethanol at room temperature, following the work of Schacht *et al.*[245] was finally attempted. Although, incomplete cleavage of Cbz-

group of about 79% conversion was achieved as calculated by ^{1}H NMR spectroscopy, importantly no side product was formed.

The synthetic route used for dipeptides with 5-FU in its α C-terminal glycine residue[179,191,245] resulted in mixtures of diastereomers, **9a** (L,L) and **9b** (L,D) (Figure 3-7). The isolation of these diastereomers was easily accomplished by preparative HPLC using 5% acetonitrile in 0.1% TFA as eluent. As shown in Figure 3-7, **9a** was eluted first, indicating that it is more hydrophilic than **9b**. Stereochemical assignments of these diastereomers were based on their optical activities[179,191,245] and their degradation ability (see Chapter 5) as the peptide bond cleavage depends on the configuration of the peptide chain. Levorotatory peptides usually are better substrate for enzymes used than the dextrorotatory ones. Using TFA during HPLC purification of the diastereoisomers resulted in TFA salts of the isolated dipeptides as indicated by ^{1}H and ^{19}F NMR spectroscopy in $SO(CD_3)_2$. The ^{19}F NMR spectrum shows two signals at -73.80 and -169.64 ppm due to TFA and 5-FU respectively with relative intensities of 3:1. The ^{1}H NMR shows a signal at 8.24 ppm due to three protons of $-NH_3^+CF_3OO^-$. TFA contaminations were removed by replacement with a stronger acid, HCl.

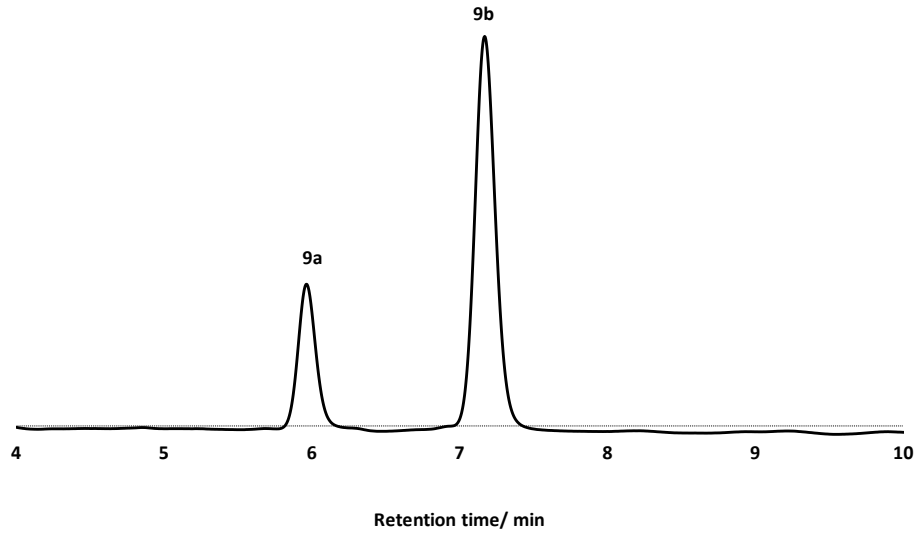

Figure 3-7. HPLC profile of diastereoisomeric mixture of 9. Column: Waters XBridge C18 250 × 4.6 mm. Mobile phase: gradient 5 to 15% acetonitrile (with 0.1% TFA) over 20 min at a flow rate of 1 mL min^{-1}.

3.3 Conclusion

Gly-Phe-Leu-Gly peptide was synthesised according to SPPS and modified by acrylic acid to form peptide with carboxylic group in one end and vinyl group in the other to be attached to the fluorinated drug (Leu-Gly-5-FU) and polymers respectively. It was challenging to obtain a high yield of peptide. The low yield is probably linked with esterification of Wang resin with first Fmoc amino acids. Standard Wang resin, first used as a solid support, resulted in very low yield and to improve the yield preloaded Wang resin (Fmoc-Gly-Wang resin) was used.

Leu- Gly(5-FU) peptide was synthesised as described in the literature.[179] The cleavage of Cbz-protective group was challenging. It was only successful using formic acid or 1,4-cyclohexadiene as hydrogen transfer agent. The treatment with formic acid, however, resulted in partial hydrogenation of pyrimidine ring. Although complete cleavage of Cbz was not achieved using 1,4-cyclohexadiene, no side reaction was formed.

The coupling reaction commonly used in the literature to form the desired hexa-peptide (Scheme 3-2) was unsuccessful. Stepwise conjugation of the tetra-peptide and the dipeptide to the polymer will be used as an alternative. Low molecular weight reagents and by-products can be removed easily by membrane filtration as it will be described in Chapter 4.

3.4 Experimental

3.4.1 Analytical technique

^{1}H and ^{13}C NMR spectra were recorded on Bruker AV400 or Bruker AVIII HD 400 spectrometer at room temperature and examined using Topspin 3.0 NMR software. Elemental Analysis was determined using a Perkin-Elmer 2400 CHNS/O Series 2 Elemental Analyser. Electron Ionisation (EI) mass spectroscopy was accomplished using a VG Autospec Mass Spectrometer. The optical activity of **9a** and **9b** diastereomers of L-Leucyl-2-(5-fluoruracil-l-yl)-L,D-glycine) was determined using polarimeter and calculated considering the following equation.

$$[\alpha] = \frac{\alpha_{obs}}{C \times l} \qquad \textit{Equation 3-2}$$

Where $[\alpha]$ is the specific rotation of the compound, α_{obs} is the observed rotation of light in degrees, C is the concentration in g/mL and l is the cell length in dm.

3.4.2 Materials

1,4-cyclohexadiene (Acros, 97%) was distilled prior to use. Dry *N*,*N*-dimethylformamide (DMF) was obtained from the Grubbs dry solvent system (Puresolve, models SPS 400-6 and SPS200-6). Standard Wang resin (Sigma Aldrich, bead size 100–200 mesh, substitution – 0.80 mmol g^{-1}), Fmoc-Gly-Wang resin (Sigma Aldrich, bead size 100–200 mesh, substitution – 0.56 mmol g^{-1}), DMF peptide synthesis grade (Sigma Aldrich), methylene chloride (Fisher), Fmoc-Gly-OH (Sigma Aldrich, 98%), Fmoc-Phe-OH (Sigma Aldrich, 98%), Fmoc-Leu-OH (Sigma Aldrich, 97%), 1-[bis(dimethylamino)methylene]-1H-benzotriazolium hexafluorophosphate 3-oxide (HBTU) (Alfa Aesar, 98%), *N*,*N*-diisopropylethylamine (Alfa Aesar, 99%), piperidine (Sigma Aldrich, 99%), trifluoroacetic acid (Acros, 99.5%), triisopropylsilane (Sigma Aldrich, 98%), deionised water, diethyl ether (Fisher), cyclohexene (Alfa Aesar, 99%), formic acid (Sigma Aldrich, 98%) , Pd/C 10% (Acros) , 5-fluorouracil (Alfa Aesar, 99%), dry ethanol (Acros, 99.5%), extra dry methanol (Acros, 99.8%), extra dry ethyl acetate (Acros, 95%), triethylamine (Sigma Aldrich, 99%), lead tetraacetate (Acros, 95%) and Cbz-Leu-Ser-OMe (Bachem) were used as received.

3.4.3 Synthesis of Gly-Leu-Phe-Leu using solid phase peptide synthesis (SPPS)

Peptide synthesis was performed manually using standard 9-fluorenylmethoxycarbonyl (Fmoc) protocols.[192] The peptide synthesis usually includes several steps which are described below.

Swelling of the resin:

1 g of either standard Wang resin or Fmoc-Gly-Wang resin was placed into the reaction vessel. DCM (10 mL) was added to the dried resin and the mixture was stirred for 1 h for resin swelling and then removed by vacuum filtration. DMF (10 mL) was added to the resin (washing step) and removed via vacuum filtration.

Deprotection

The Fmoc group was cleaved by solvent mixture of 20% piperidine/DMF (vol/vol) to allow coupling of another amino acid. Double deprotection steps were performed by adding 10 mL of piperidine/DMF mixture, stirring gently for 10 min. Then, the deprotected amino acid on the solid support was washed 5 times with of DMF (10 mL), each time mixing for 1 min.

Amino acid coupling

The amounts of amino acids and activating agent were calculated according to Equation 3-3:

$$n = m_{resin} \times n_{resin\ substitution} \qquad \textit{Equation 3-3}$$

Where n is the number of moles per gram of resin (mmol g^{-1}), m_{resin} is the mass of resin in g, $n_{resin\ substitution}$ is the loading capacity of resin.

The protected amino acid and HBTU were dissolved in DMF (10 mL) prior to loading into the reaction vessel. DIPEA was then added with gentle stirring for 30 min. The solvent was removed by vacuum filtration. Each coupling was repeated twice (double coupling). The resin was washed 5 times with DMF (10 mL), each time mixing for 1 minute.

The coupling and deprotection cycle were repeated to synthesise Gly-Phe-Leu-Gly sequences using the Fmoc-amino acid derivatives shown in Table 3-2 and Table 3-3.

Table 3-2. Amount used in SPPS using 1g of standard Wang Resin (0.8mmol/g)

	Mass/mg	**n.mol/mmol**	**equivalent**	**Volume/µL**
Gly	1117.24	4	5	-
Phe	1549.72	4	5	-
Leu	1413.64	4	5	-
HBTU	1486.621	3.9	4.9	-
DIPEA	1033.92	8	10	1393.4
Acrylic acid	288.24	4	5	274.2

Table 3-3. Amount used in SPPS using 1g preloaded Wang resin (0.56mmol/g)

	Mass/mg	**n.mol/mmol**	**Equivalent**	**Volume/µl**
Gly	782.068	2.8	5	-
Phe	1084.804	2.8	5	-
Leu	989.548	2.8	5	-
HBTU	1040.635	2.7	4.9	-
DIPEA	723.744	5.6	10	975.4
Acrylic acid	201.768	2.8	5	191.9

The synthesis was interrupted before the modification with acrylic acid. To avoid undesired removal of the Fmoc group during storage in DMF, the peptide-resin was washed 5 times with DCM and dried at room temperature. The column was sealed and store at 4 °C. Before the modification, the resin was swollen as described above.

Modification of Gly-Phe-Leu-Gly with acrylic acid

Once Gly-Phe-Leu-Gly was synthesised and Fmoc on the N-terminus was deprotected, acrylic acid and HBTU were added with stirring for 30 s. DIPEA was then added with gentle stirring

for 15 min. The coupling of acrylic acid was made twice. The solvent was removed by filtration and the resin was washed 5 times with DMF (10 mL), each time mixing for 1 min. The resin was then washed four times with DCM (10 mL) and allowed to dry at room temperature.

Final cleavage

10 mL of the cleavage cocktail [TFA/H_2O/TIPS 9.0/0.5/0.5] was added to the dried peptide resin, stirred gently for 30 s and left for 3 h. The cleavage mixture was filtered under vacuum. The filtrate was concentrated and precipitated in diethyl ether (20 mL). After standing for 30 min, the precipitate was isolated by centrifugation (4,500 rpm, for 5 min). This was dried under vacuum at room temperature to a white powder material with the yield of 18% and 87% for standard Wang resin and Fmoc-Gly-Wang resin, respectively.

Gly-Phe-Leu-Gly-Fmoc: ^{1}H NMR (400 MHz, DMSO) δ 12.57 (s, 1H), 8.22 (t, *J* = 5.7 Hz, 1H), 8.01 (d, *J* = 8.4 Hz, 1H), 7.93 (d, *J* = 9.7 Hz, 1H), 7.90 (d, J = 7.6 Hz, 2H), 7.72 (d, *J* = 7.4 Hz, 2H), 7.56 (t, *J* = 6.0 Hz, 1H), 7.42 (t, *J* = 7.4 Hz, 2H), 7.33 (t, *J* = 7.4 Hz, 2H), 7.27 – 7.19 (m, 4H), 7.19 – 7.12 (m, 1H), 4.57 – 4.48 (m, 1H), 4.32 – 4.19 (overlapped, 4H), 3.80 – 3.73 (m, 4H), 3.06 (dd, *J* = 13.9, 4.3 Hz, 1H), 2.81 (dd, *J* = 13.8, 9.8 Hz, 1H), 1.55-1.43 (m, 1H), 1.33 (t, J = 7.2 Hz, 2H), 0.81 (dd, *J* = 10.5, 6.6 Hz, 6H).

ESI-MS: expected m/z: 614.3, experimental m/z: 615.3 (M^+ + H)

Vinyl modified Gly-Phe-Leu-Gly: ^{1}H NMR (400 MHz, DMSO) δ 12.54 (s, 1H), 8.33 (t, *J* = 5.7 Hz, 1H), 8.23 – 7.94 (overlapped, 3H), 7.27 – 7.21 (m, 4H), 7.21 – 7.15 (m, 1H), 6.28 (dd, *J* = 16.9, 10.2 Hz, 1H), 6.09 (dd, *J* = 17.1, 2.1 Hz, 1H), 5.60 (dd, *J* = 10.2, 2.1 Hz, 1H), 4.58 – 4.52 (m, 1H), 4.34 (q, *J* = 7.7 Hz, 1H), 3.87 – 3.61 (m, 4H), 3.04 (dd, *J* = 13.8, 4.2 Hz, 1H), 2.78 (dd, *J* = 13.8, 9.5 Hz, 1H), 1.66 – 1.56 (m, 1H), 1.49 (t, *J* = 7.2 Hz, 2H), 0.87 (dd, *J* = 18.4, 6.5 Hz, 6H).

ESI-MS: expected m/z: 446.2, experimental m/z: 447.2 (M^+ + H)

3.4.4 Synthesis of *N*-(Carbobenzyloxy)-L-leucyl-L,D-2-acetoxygly- cine Methyl Ester Cbz- Leu(α-OAc)-OMe (6)

Cbz-Leu-Gly(α-OAc)-OMe was synthesised according to the method reported by Steglich.[247] Cbz-Leu-Ser-OMe (3.66 g, 10 mmol), lead tetraacetate (6.65 g, 15 mmol), and 4 Å molecular sieves (8 g) were added to a dried round bottomed flask equipped with a stir bar and fitted with rubber septum. Dry ethyl acetate (100 mL) was then added under dry N_2 atmosphere with stirring. The suspension was heated under reflux for 2 hours. The reaction mixture was cooled to room temperature and filtered through Celite to give a brown solution. The filtrate was stirred

with 20% aqueous citric acid (100 mL) for 10 min to give a colourless solution. The resulting mixture was then placed into a separating funnel. The organic layer was recovered, washed with 10% aqueous NaCl (2 × 75 mL), dried over anhydrous $MgSO_4$, and filtered. Ethyl acetate was removed by rotary evaporator under vacuum giving a crude product of a yellowish residue. The product was purified by recrystallisation from ethyl acetate/hexane. Yield: 1.744 g (44%); TLC (silica gel; hexane: ethyl acetate 7:3) showed one spot, Rf = 0.2.

Elemental analysis calc.: C=57.86%, H=6.64%, N=7.10%. Found: C=56.93%, H=6.56%, N=6.83%.

^{1}H NMR (400 MHz, $CDCl_3$) δ 7.59 (dd, *J* = 16.1, 8.7 Hz, 1H), 7.46 – 7.28 (m, 5H), 6.40 (dd, *J* = 8.8, 5.8 Hz, 1H), 5.36 – 5.24 (br, 1H), 5.13 (s, 2H), 4.40 – 4.16 (br, 1H), 3.79 (s, 3H), 2.11 (s, 3H), 1.82 – 1.62 (m, 2H), 1.59 – 1.49 (m, 1H), 0.95 (dd, *J* = 6.1, 3.3 Hz, 6H).

^{13}C NMR (101 MHz, $CDCl_3$) δ 172.45, 170.24, 167.96, 128.57, 128.26, 128.08, 72.07, 67.30, 53.32, 41.25, 24.64, 22.95, 21.87, 20.60.

3.4.5 Synthesis of *N*-(Carbobenzyloxy)-L-leucyl-2-(5-fluorouracil- 1- yl)-L,D-glycine Methyl Ester (7)

The compound was prepared according to the procedure described by Kingsbury.[191] Cbz-Leu(α-OAc)-OMe (**6**) (1.716 g, 4.35 mmol), 5-FU (0.543 g, 4.177 mmol), and triethylamine (0.422 g, 582.1 µL, 4.177 mmol) were dissolved in dry DMF (8 mL) with stirring at room temperature for 20 h. After completion of the reaction, DMF was evaporated under vacuum to give a thick yellowish residue. This was dissolved in ethyl acetate (80 mL) and extracted with water (80 mL). The organic layer was washed with water (2 × 80 mL), dried over anhydrous $MgSO_4$ and filtered. Ethyl acetate was removed by rotary evaporator under vacuum giving a yellowish residue. The intermediate was used directly for the next step without any further purification. Yield: 1.643 g (71%)

Elemental analysis calc.: C=54.31%, H=5.43%, N=12.0. Found: C=54.18%, H=5.79%, N=11.15%.

^{1}H NMR (400 MHz, DMSO) δ 12.10 (t, *J* = 4.8 Hz, 1H), 9.28 (dd, *J* = 13.6, 8.0 Hz, 1H), 8.04 (dd, *J* = 9.4, 6.7 Hz, 1H), 7.61 (dd, *J* = 7.6, 2.8 Hz, 1H), 7.41-7.19 (m, 5H), 6.39 (d, *J* = 7.8 Hz, 1H), 5.03 (d, *J* = 4.7 Hz , 2H), 4.20-4.11 (m, 1H), 3.73 (d, *J* = 3.3 Hz, 3H), 1.73-1.56 (m, 1H), 1.57-1.34 (m, 2H), 0.87 (dd, *J* = 14.5, 7.7 Hz, 6H).

^{13}C NMR (101 MHz, DMSO) δ 174.13, 166.95, 157.52, 156.57, 149.42, 140.88, 138.58, 137.36, 128.77, 128.27, 128.18, 65.93 , 63.00, 60.21, 54.56 – 52.93, 24.64, 23.36, 21.76.

^{19}F NMR (377 MHz, DMSO) δ -168.60.

3.4.6 Synthesis of *N*-(Carbobenzyloxy)-L-leucyl-2-(5-fluorouracil- 1- y1)-L,D-glycine (8)

Cbz-Leu-Gly(5-FU)-OMe (**7**) (1.100 g, 2.36 mmol) was dissolved in methanol (1.5 mL). Then, 0.4 M NaOH (50.4 mL) was added dropwise, stirred for a couple of minutes, and cooled in an ice bath. The solution was then acidified with 5 N HCI giving a cloudy solution. The methanol and HCl were evaporated under vacuum. The cloudy aqueous solution was extracted with ethyl acetate (3 × 50 mL). The combined organic extracts were washed with water (2 × 80 mL), dried over anhydrous $MgSO_4$, and filtered. The ethyl acetate was removed by rotary evaporator under vacuum. The intermediate was used directly for the next step without any further purification. Yield: 436 mg (41%).

^{1}H NMR (400 MHz, DMSO) δ 12.01 (d, *J* = 5.1 Hz, 1H), 9.14 (d, *J* = 7.7 Hz, 1H), 8.08 – 7.93 (m, 1H), 7.68 – 7.54 (m, 1H), 7.45 – 7.17 (m, 5H), 6.26 (d, *J* = 7.9 Hz, 1H), 5.08 – 4.94 (m, 2H), 4.17-4.06 (m, 1H), 1.70-1.56 (m, 1H), 1.54-1.32 (m, 2H), 0.98 – 0.74 (m, 6H).

3.4.7 Synthesis of L-Leucyl-2-(5-fluoruracil-l-yl)-L,D-glycine (9)

The deprotection of the Cbz group was accomplished using 1,4-cyclohexadiene following the procedure described by Schacht.[245] Cbz-Leu-Gly(5-FU) (**8**) (420 mg, 933 mmol) was dissolved in dry ethanol (40 mL), where after 10% Pd/C (420 mg) was added. The reaction mixture was stirred under N_2 atmosphere. Freshly distilled 1,4-cyclohexadiene (806 mg, 6.05 mmol), and acetic acid (0.11 mL) were then added. The reaction progress was monitored by TLC using DCM:MeOH 95:5 as eluent. The crude reaction mixture was filtered through Celite to remove Pd catalyst. The residue in the filter was rinsed with methanol (2 × 50mL) containing 0.01% acetic acid. The filtrate solvent was removed by rotary evaporator under vacuum. Cbz cleavage was about 79% as calculated using ^{1}H NMR. The diastereomers were purified directly by preparative reverse phase chromatography as described below.

3.4.8 Separation of L,L (9a) and L,D (9b) Diastereomers of L-Leucyl-2-(5-fluoruracil-l-yl)-L,D-glycine)

The separation of diastereomers of Leu-Gly(5-FU) was accomplished by the use of preparative reverse phase chromatography (HPLC). About 300 mg of Leu-Gly(5-FU) was dissolved in distilled water: methanol 8:2 (3 mL) and separated via a preparative C18 Waters XBridge 2µm OBD 19 × 250 mm column using gradient 5% to 15% acetonitrile (with 0.1% TFA) as an eluent with UV detection at 240 nm. Both fractions eluting from 6.104 to 7.011 min and from 8.147

to 9.210 min were collected. The first fraction weighed 97 mg, assigned as **9a** (L,L), while the second fraction weighed 144 mg, assigned as **9a** (L,D), following lyophilisation.

To remove TFA counterions from the isolated dipeptide, 50 mg of either **9a** or **9b** was dissolved in 50 mL of 5 mM HCl. This was then nitrogen freezed, and freeze-dried. The process was repeated twice to ensure complete elimination of TFA.

9a (L,L):

$[\alpha]^{25}_{D}$ =+81.0° (c = 1, H_2O) (Lit $[\alpha]^{25}_{D}$ =+94.0° (c = 1, H_2O))[179]

^{1}H NMR (400 MHz, DMSO) δ 12.07 (d, *J* = 3.2 Hz, 1H), 9.82 (d, *J* = 7.9 Hz, 1H), 8.19 (s, 3H), 8.15 (d, *J* = 6.6 Hz, 1H), 6.22 (d, *J* = 7.8 Hz, 1H), 3.95 (br, 1H), 1.73 – 1.62 (m, 1H), 1.59 (t, *J* = 7.0 Hz, 2H), 0.92 (dd, *J* = 10.7, 6.4 Hz, 6H).

^{19}F NMR (377 MHz, DMSO) δ -169.81.

^{13}C NMR (101 MHz, DMSO) δ 170.94, 167.21, 157.66, 149.25, 138.20, 140.49, 130.01, 64.21, 51.06, 24.04, 23.14, 22.27.

EI-MS: expected m/z: 316.12, experimental m/z: 317.1 (M^+ + H)

Elemental analysis calc.: C=39.06%, H=4.22%, N=13.02%. Found: C=37.11%, H=5.88%, N=13.78%.

9b (L,D):

$[\alpha]^{25}_{D}$ = -74.0° (c = 1, H_2O) (Lit $[\alpha]^{25}_{D}$ = -70.6° (c = 1, H_2O))[179]

^{1}H NMR (400 MHz, DMSO) δ 12.08 (d, *J* = 4.7 Hz, 1H), 9.88 (d, *J* = 7.3 Hz, 1H), 8.23 (s, 3H), 8.16 (d, *J* = 6.7 Hz, 1H), 6.26 (d, *J* = 7.3 Hz, 1H), 4.02 (br, 1H), 1.62 – 1.54 (m, 1H), 1.55 – 1.48 (m, 2H), 0.83 (d, *J* = 5.6 Hz, 6H).

^{19}F NMR (377 MHz, DMSO) δ -169.62 (s).

^{13}C NMR (101 MHz, DMSO) δ 170.88, 167.18, 157.56, 149.26, 139.35, 140.48, 129.92, 63.99, 50.91, 23.87, 23.00, 22.37.

EI-MS: expected m/z: 316.12, experimental m/z: 317.1 (M^+ + H)

Elemental analysis calc.: C=39.06%, H=4.22%, N=13.02%. Found: C=38.58%, H=5.73%, N=14.94%.

Chapter 4 Synthesis of the polymer peptide conjugate using aminolysis/Michael addition chemistry

4.1 Introduction

Reversible-addition fragmentation chain transfer (RAFT)[23] is one of the most powerful and versatile controlled radical polymerisation technique for the synthesis of complex architectures.[248–250] The lability of thiocarbonylthio group, which facilitates RAFT process, can be used to add chain end functionalities by a variety of approaches[28,29] including thermolysis,[251] radical-induced reactions[213] and reaction with nucleophiles (Scheme 4-1).[42] End group removal by thermolysis and radical-induced reactions results in sulfur-free unsaturated and saturated ends, respectively. The use of thermolysis is limited to the stability of polymer and functionality under high temperature.[28,252,253] Although radical-induced transformation is more versatile, irreversible chain-chain coupling as a result of termination reaction is the major limitation (Scheme 4-2).[254,255] Reaction with primary or secondary amines[57,89,256] or other nucleophiles such as borohydride,[257–259] is one of the most commonly encountered method for the transformation of thiocarbonylthio groups to a thiol group. However, care needs to be taken during the reaction since the thiols formed can be readily oxidised resulting in higher molecular weight disulfide-coupled species.[260–263,259] Furthermore, the formation of a thiolactone chain end as a result of backbiting of the formed thiol into the ester pendant group of repeating units has been an issue in the case of poly(methyl methacrylate) (Scheme 4-3).[260] These problems can be diminished by the *in situ* reaction with a nucleophile in the presence of a thiol-trapping reagent, e.g. a Michael acceptor[259,261,264,265] or 2,2-dithiodipyridine.[266,267] This one-pot process is an effective approach for the introduction of desired groups into the polymer end and the synthesis of advanced polymer architectures, e.g. stars, block copolymers and bioconjugates.[252,257,259,263,265,268–271]

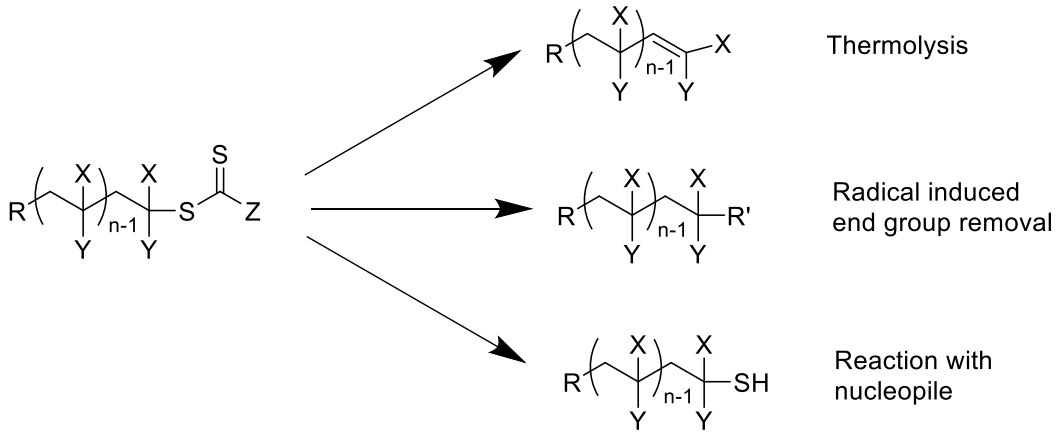

Scheme 4-1 Shemetic representing the main processes for thiocarbonylthio end group transformation

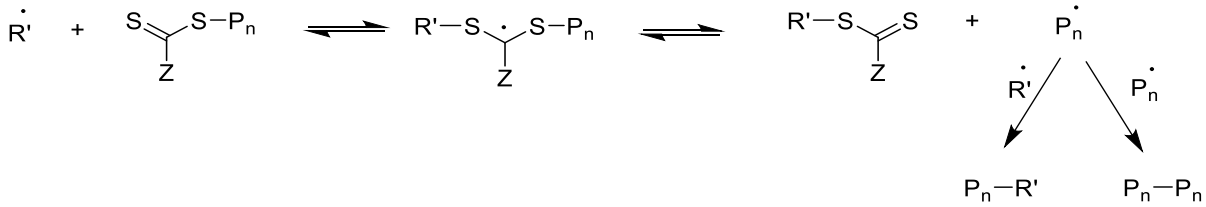

Scheme 4-2 Radical induced removal of thiocarbonylthio end group can result in chain-chain coupling

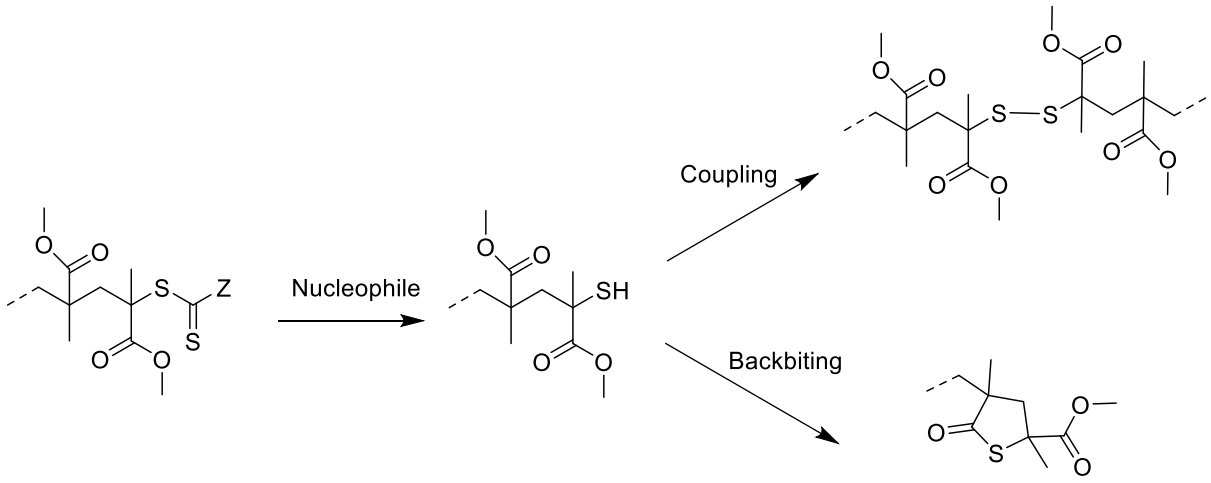

Scheme 4-3 Side products seen in the transformation of thiocarbonylthio end group of poly(methyl methacrylate) PMMA in the presence of nucleophile

This chapter will concern the synthesis of hyper-star poly(*N*,*N*-dimethylacrylamide) that is covalently attached to the oligo-peptide bearing 5-FU in its α C-terminal glycine residue, HS-PDMA-Gly-Phe-Leu-Gly-Leu-Gly-α-(5-FU). The synthesis will involve a couple of steps; the attachment of the vinyl modified-tetra-peptide, Gly-Phe-Leu-Gly, via aminolysis/Michael addition chemistry followed by the attachment of the dipeptide, Leu-Gly-α-(5-FU). *In situ* aminolysis/Michael addition was initially optimised using a commercially available acrylate.

4.2 Results and discussion

4.2.1 The modification of SHB-PDMA via aminolysis/Michael addition reaction

The synthesis and characterisation of hyper-star poly(*N*,*N*-dimethylacrylamide) HS-PDMAs using reversible-addition fragmentation chain transfer mediated vinyl-condensing vinyl polymerisation (SCVP-RAFT) by varying the concentration of DMA to the solvent and keeping the feed ratio [DMA]:[VBPC] 50:1 constant were detailed in Chapter 2. To ensure the presence of thiocarbonylthio end groups required for peptide installation, bimolecular termination was minimised by reducing the amount of initiator (i.e. ACVA) to RAFT agent (i.e. VBPC) to 0.2:1.The fidelity of thiocarbonylthio end groups was calculated using ^{1}H NMR spectroscopy by comparing the ratio of the integrals for the pyrrole proton at 6.33 ppm to styryl proton at 6.83-7.17 ppm considering Equation 4-1. The results varied from 76-67 % (Table 4-1), possibly due to bimolecular termination reaction enhanced by the high conversion achieved during the polymerisation (> 90 % conversion).

$$\%f_{end-group} = \frac{\frac{I_{6.33}}{2} \times 100}{\frac{(I_{6.83-7.17})}{4}} \qquad \textit{Equation 4-1}$$

Table 4-1. Characteristics of HS-PDMAs synthesised by SCVP-RAFT

polymer	γ	Conv / % [a]	M_n / kDa[b]	Đ[b]	Thiocarbonylthio group fidelity %[c]
HS-PDMA-10wt%	50	91	13.5	1.78	67
HS-PDMA-20wt%	50	96	19.9	2.70	76
HS-PDMA-30wt%	50	93	25.5	3.77	75
HS-PDMA-40wt%	50	91	32.0	8.11	72
HS-PDMA-50wt%	50	92	33.0	11.92	73

[a] Conversion as determined by ^{1}H NMR [b] Determined by DMF GPC using PMMA standards [c] Ratio of pyrrole to styryl calculated using ^{1}H NMR

Due to their multifunctional nature, care should be taken when removing the RAFT end group from dendritic polymers. The most commonly used radical-induced approach might lead to irreversible cross-linked material caused by bimolecular termination. Therefore, *in situ*

aminolysis/Michael addition was chosen to eliminate the RAFT end group and conjugate the vinyl-modified peptide in a one-pot process. To optimise the aminolysis/Michael addition reaction required for the installation of the vinyl-modified peptide into HS-PDMAs, the conjugation of a commercially available Michael acceptor, *N*-hydroxyethylacrylamide (HEA), was firstly examined.

4.2.2 Aminolysis in the presence of *N*-hydroxyethylacrylamide (HEA) as a Michael acceptor

The HS-PDMAs with thiocarbonylthio terminals were first functionalised in a one-pot process via primary amine cleavage followed by Michael addition reaction with the acrylamide. This one-pot conversion was achieved using a combination of propyl amine and HEA in *N*,*N*-dimethyl formamide (DMF) as shown in Scheme 4-4. Propyl amine reduced the thiocarbonylthio groups to thiols whereas the HEA reacted with the thiol formed, minimising the occurrence of disulfide formation. The modifications were made at ambient temperature under a nitrogen atmosphere. In this process, a 10-fold molar excess of propyl amine with respect to thiocarbonylthio group[261] was used as it served as a nucleophilic catalyst for the subsequent Michael addition reaction along with its main role for converting the thiocarbonylthio end-groups to the corresponding thiol groups. The propyl amine deprotonates the thiols formed to the corresponding thiolate that adds to the electron deficient double bond. The choice of solvent with high dielectric constant, DMF, was to facilitate the transformation of the thiol to the corresponding thiolate making the reaction faster.[272] As the primary amine is prone to react with the Michael acceptor which could decrease the yield of thiol Michael addition,[265,273,274] HEA was also added in excess. After completion of the reaction, the modified polymer was purified by precipitation followed by dialysis against deionised water to remove excess reagents and by-products.

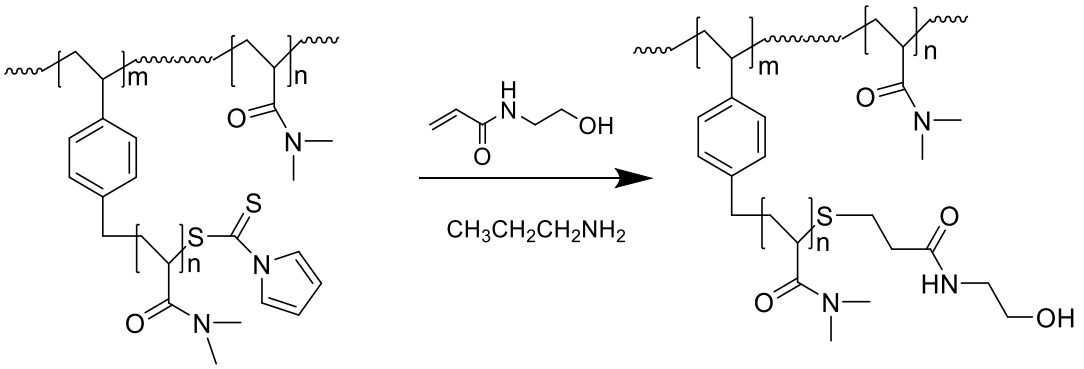

Scheme 4-4. One-pot aminolysis/ Michael addition end group functionalisation

After the isolation of the polymers by precipitation, the high molecular weight polymers, HS-PDMA-30 wt%, HS-PDMA-40 wt% and HS-PDMA-50 wt%, formed gels probably due to aerial oxidation of the thiols to form the disulfide cross-linked species (Scheme 4-5). This suggest that not all thiols were end capped with HEA. The modification of low molecular weight polymers, HS-PDMA-10 wt% and HS-PDMA-20 wt% initially resulted in soluble materials. However, these samples formed cross-linked materials eventually.

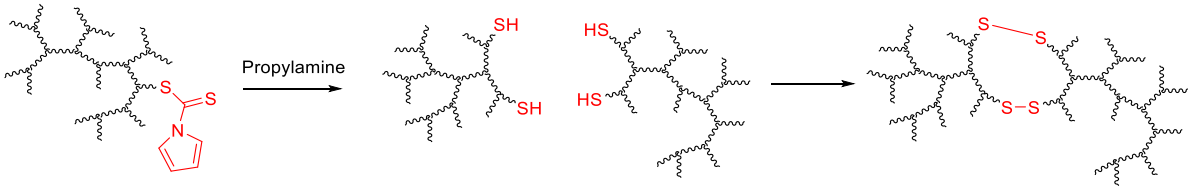

Scheme 4-5. The formation of unwanted disulfide cross-linked species

To avoid the formation of disulfide coupled-species, a reducing agent, phenyldimethylphosphine, Me_2PPh, was used. Me_2PPh also acts as a catalyst for subsequent Michael addition reaction.[275,252,252,276,270] When HS-PDMAs were modified in the presence of Me_2PPh, no cross-linked materials were observed even for high molecular weight polymers.

RAFT end group cleavage was confirmed by several methods. The colour of the polymers changed from yellow to white suggesting the successful cleavage of thiocarbonylthio end group (Figure 4-1). Furthermore, end group removal was evidenced by UV-vis spectroscopy using the characteristic absorbance of the thiocarbonylthio group at ≈300 nm. As shown in Figure 4-2, the original HS-PDMA displays a strong absorbance at 300 nm whilst no absorption is observed in the same region for the acrylamide grafted HS-PDMA conjugate indicating quantitative cleavage of end groups.

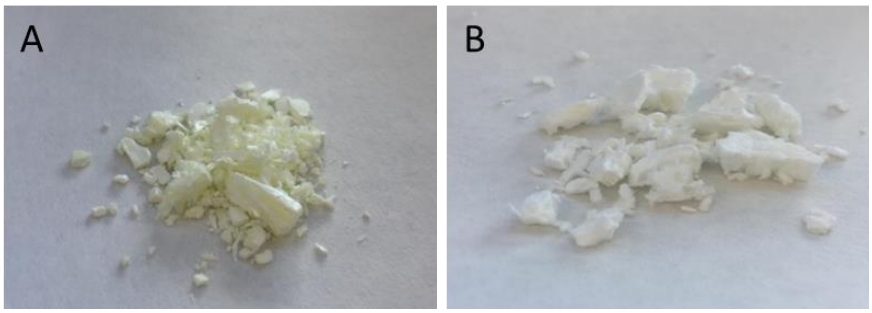

Figure 4-1. The colour of the HS-PDMA (A) before and (B) after aminolysis

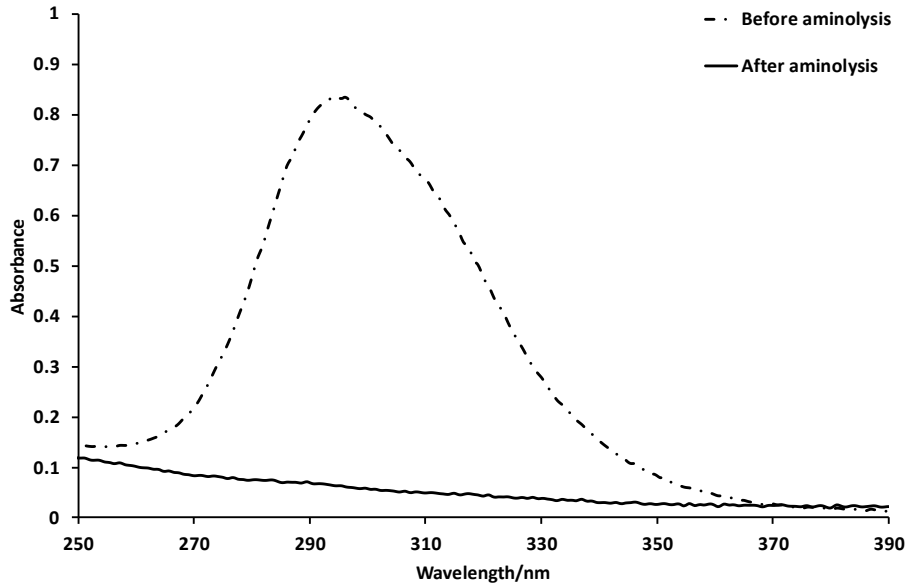

Figure 4-2. UV-vis absorbance spectra of HS-PDMA before and after aminolysis in water

^{1}H NMR spectroscopy before and after the grafting of HEA to HS-PDMA in D_2O (Figure 4-3) also indicates the quantitative cleavage of thiocarbonylthio end-groups as the resonances at 6.33 and 7.72 ppm associated with the pyrrole of the thiocarbonylthio end-group of HS-PDMA are completely absent. Additionally, the vinyl resonance signals of HEA between 5.50 to 6.50 ppm are completely absent confirming the complete elimination of unreacted HEA. The presence of broad resonance signals due to HEA at 3.51 and 3.19 ppm indicates the successful conjugation to the bulky polymer.

An attempt to calculate thioether functionalisation percent using ^{1}H NMR spectroscopy by comparing the integration of methylene protons of HEA at 3.51 ppm relative to the styryl at 6.83-7.17 ppm failed as the methylene signals overlapped with other signals (see Figure 4-3).

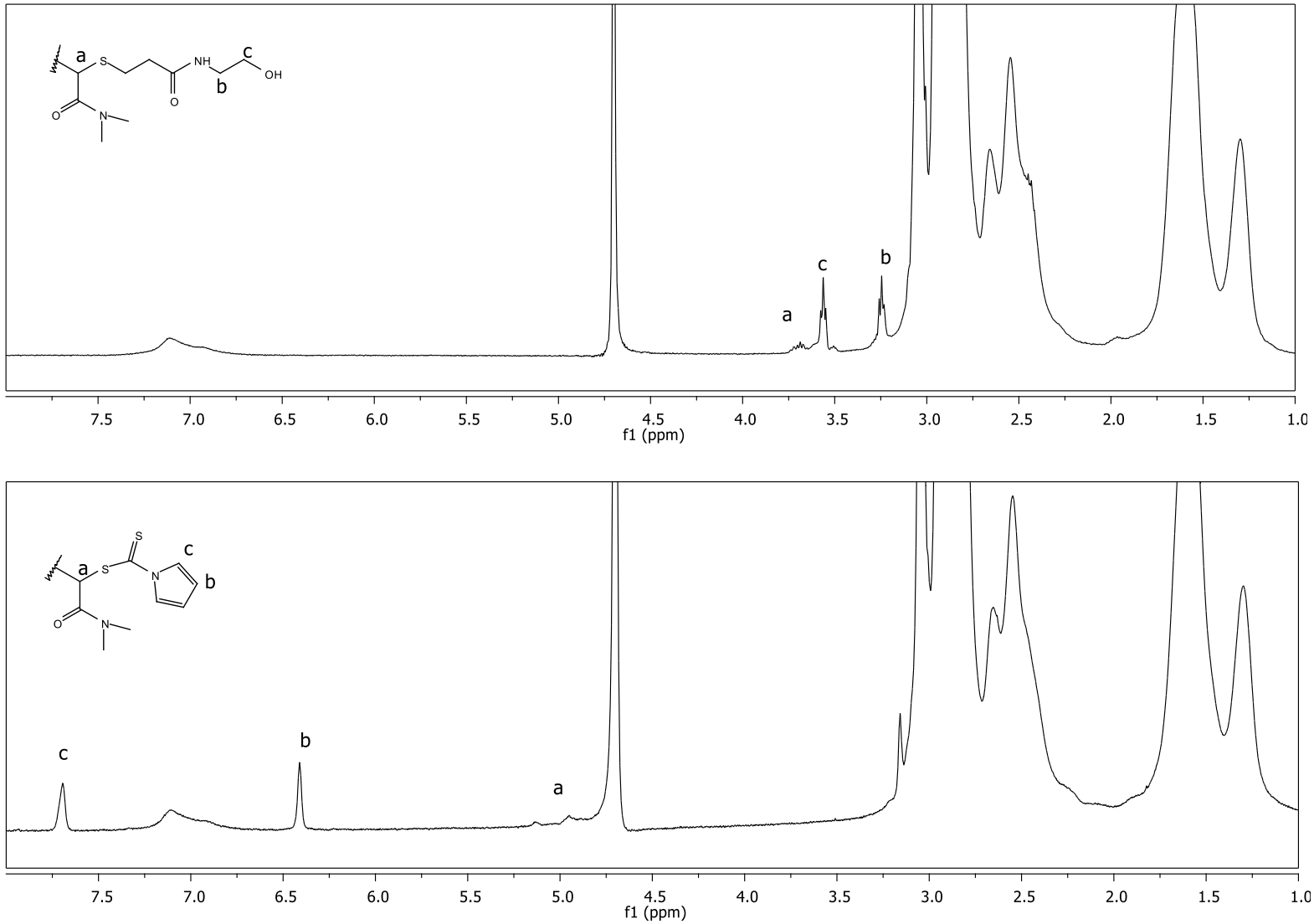

Figure 4-3. ^{1}H NMR spectra in D_2O of HS-PDMA and acrylamide grafted HS-PDMA

The aminolysis products of HS-PDMAs were further analysed by gel permeation chromatography (GPC) as shown in Figure 4-4 and Figure 4-5. The molecular weight distributions of both the original HS-PDMAs and acrylamide grafted HS-PDMAs-1 are multimodal (Figure 4-4) as a characteristic of dendritic polymers synthesised by RAFT-SCVP (see Chapter 3 Chapter 2). The molecular weight distribution for the acrylamide grafted polymers (HS-PDMA-10 wt%-1 and HS-PDMA-20 wt%-1) became even broader with the presence of high molecular weight species indicating the presence of disulfide coupled products. This high molecular weight fraction seems to be more prominent in HS-PDMA-20%-1. It is noteworthy to mention that the high molecular polymers were cross-linked as a result of disulfide formation and therefore no GPC was run for these samples. Such high molecular weight contaminants were completely absence in the presence of a small amount of Me_2PPh (HS-PDMAs-2) indicating that all thiols were end capped with HEA (Figure 4-5). Although, HEA and the cleaved RAFT end group have similar molecular weight, of 115.13 and 111.16 Da respectively, the HEA-grafted polymers show lower molecular weights compared with the starting polymers. This is probably associated with different solubility behaviour of both end groups in DMF resulting in changes in the hydrodynamic volume.

Although the efficiency of Michael addition reaction could not be calculated by ^1H NMR spectroscopy, the absence of high molecular weight disulfide-coupled species, in the presence of Me_2PPh, confirmed that all thiols were end capped with HEA.

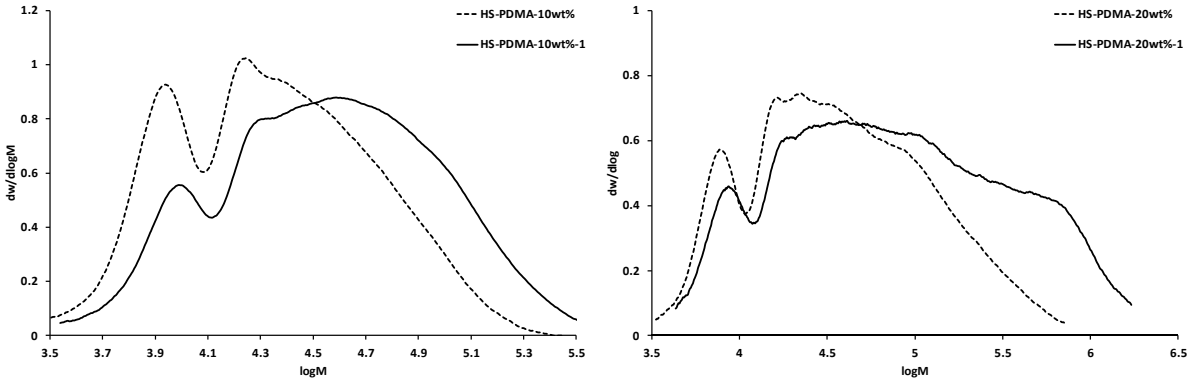

Figure 4-4. DMF GPC molecular weight distributions of SH-PDMA-10 wt% and SH-PDMA-20 wt% before (dotted lines) and after aminolysis/HEA conjugation in the absence Me_2PPh (plain lines).

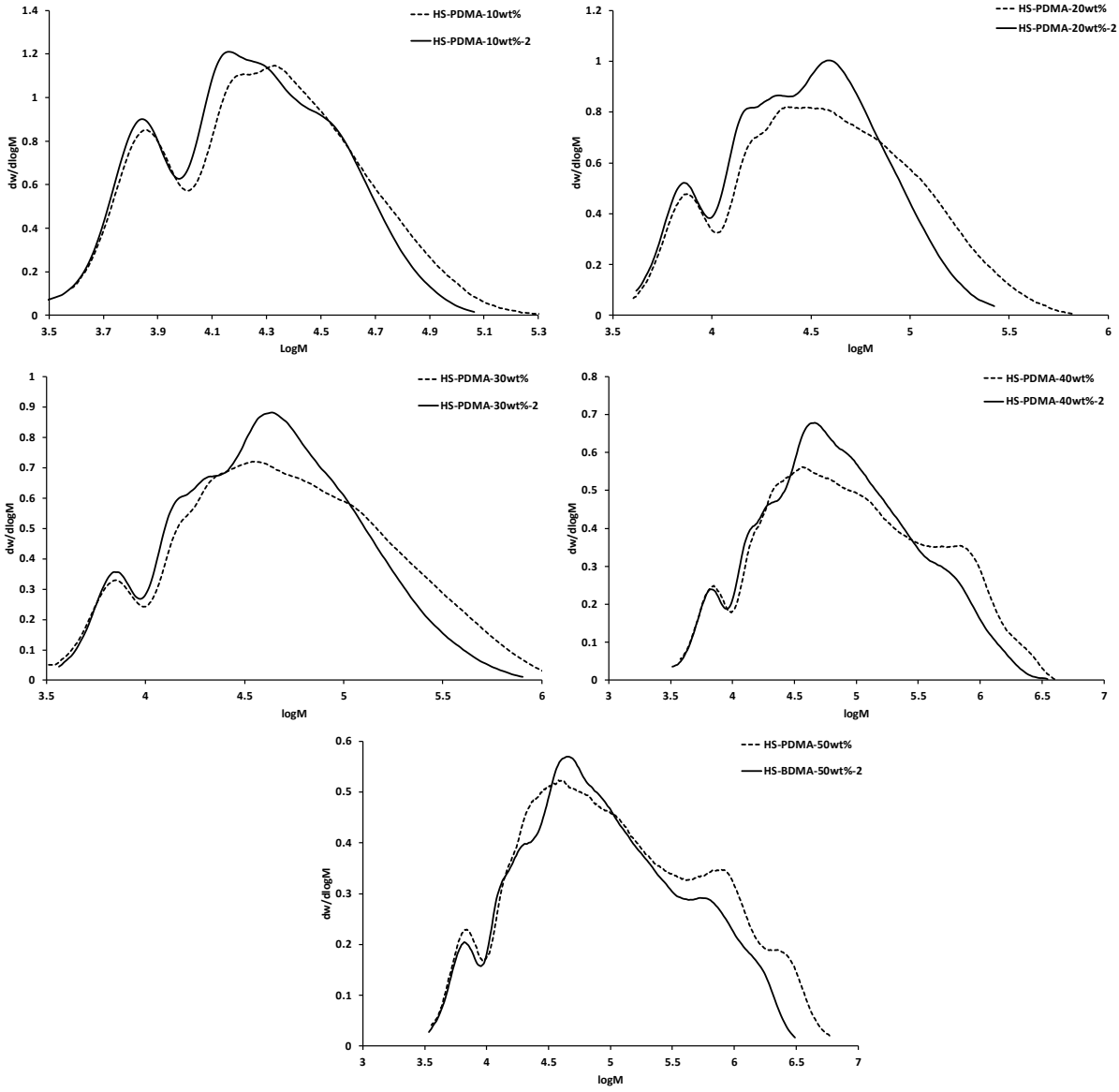

Figure 4-5. DMF GPC molecular weight distribution of HS-PDMAs before (dotted lines) and after aminolysis/HEA conjugation in the presence of Me_2PPh (plain lines).

4.2.3 Synthesis of polymer-peptide conjugates

The synthesis of the polymer-peptide conjugates can be accomplished mainly by two approaches; a divergent approach, where the polymer chain propagates from the peptide macroinitiator or a convergent approach, where a pre-synthesised polymer and peptide are coupled together to form the conjugates.[277–281] Of these, the convergent approach has been the most widely used as it is more versatile and allows complete characterisation of both the polymer and peptide prior to coupling.[280] However, high coupling efficiency under mild conditions is essential to retain peptide activity and avoid contaminating the conjugate with an excess amount of the macromolecule reagent. *In situ* aminolysis/Michael addition might be an example of such an efficient coupling reaction when Me_2PPh is used.

As shown above, HS-PDMAs contain a thiocarbonylthio moiety that can be readily liberated to thiols by aminolysis. A vinyl group was introduced to the peptide backbone by adding acrylic acid to the tetra-peptide, Gly-Leu-Phe-Gly, within SPPS as shown in Chapter 3.

Aminolysis/Michael addition of the vinyl-modified tetra-peptide will be followed by the conjugation of the dipeptide bearing its 5-FU on C-terminal glycine, Leu-Gly-5-FU, after the activation with pentafluorophenol to produce HS-PDMA-Gly-Phe-Leu-Gly-Leu-Gly-α-(5-FU) (Scheme 4-6).

It is worth mentioning that the standard solution method was initially attempted to synthesise the desired hexa-peptide, Gly-Phe-Leu-Gly-Leu-Gly-α-(5-FU). This resulted in low yield of impure material. Therefore, the assembly of the hexapeptide on the HS-PDMA was used as an alternative. The assembly of the peptide on the soluble polymer is well-known as liquid phase peptide synthesis (LPPS). LPPS shares some benefits with solid phase peptide synthesis (SPPS) described earlier in Chapter 3 such as ease of product isolation, and the ability to use an excess of reagents to drive the reaction to completion. Removal of excess amount of reagents and by-products can be accomplished by membrane filtration or re-precipitation.[225,282–285] However, only a few examples of soluble polymer support such as linear poly(ethylene glycol) (PEG)[282–284] and linear polystyrenes[285] have been reported in the literature. The time-consuming process and automation problems as the process could not be carried in a single vessel due to the nature of purification limit the use of the technique especially for the synthesis of polypeptide. Since the synthesis of the polymer-peptide conjugate only involves two steps, the advantages of LPPS over standard solution method is evident.

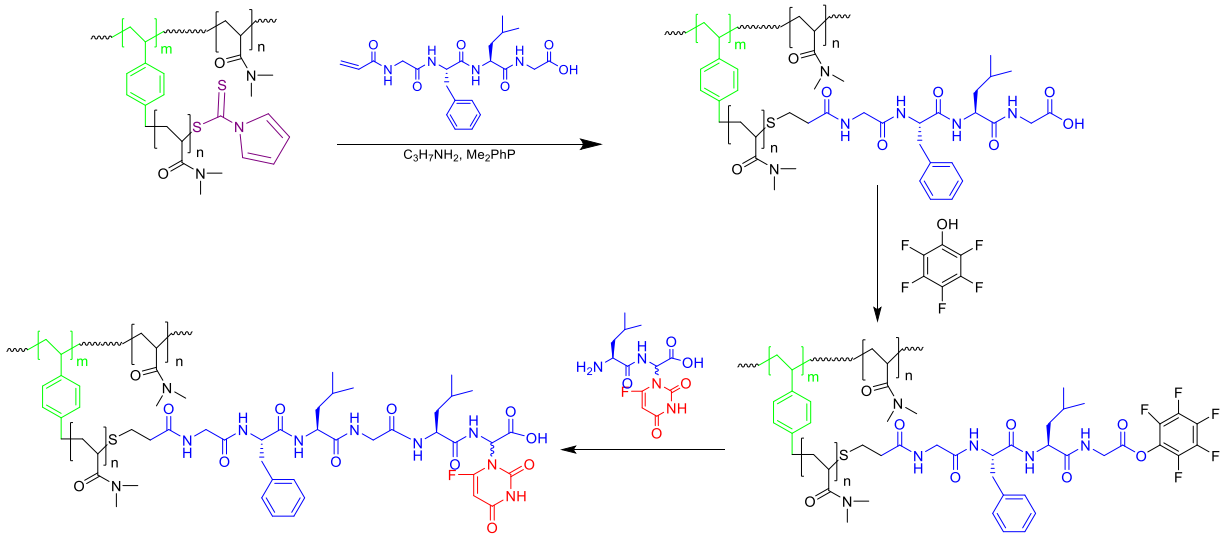

Scheme 4-6. Synthetic route to the polymer-peptide conjugate (HS-PDMA-Gly-Leu-Phe-Gly-Leu-Gly(5-FU))

4.2.3.1 The attachment of vinyl-modified tetra-peptide (Gly-Leu-Phe-Gly)

First, the vinyl-modified tetra-peptide was conjugated to the polymer via aminolysis/Michael addition in the presence of Me_2PPh to avoid the formation of disulfide species (Scheme 4-6). The polymer support used was HS-PDMA-30 wt%. The choice of HS-PDMA-30 wt% was based on its relatively high molecular weight and size (Chapter 2) along with its less probability to undergo gelation during aminolysis/Michael addition reaction.

The loss of yellow colour indicates the successful removal of thiocarbonylthio end groups and the absence of cross-linked material after precipitation indicates that free thiols were end-capped with the peptide. The formation of the polymer-peptide conjugate, HS-PDMA-Gly-Leu-Phe-Gly, was confirmed by ^1H NMR spectroscopy of the purified material in D_2O as shown in Figure 4-6. The disappearance of vinyl resonance signals between 5.50 to 6.50 ppm confirms the complete elimination of unreacted peptide by dialysis. Considering that the tetra-peptide is water insoluble, the observation of resonance signals characteristic to the peptide in D_2O can only be possible after the conjugation to the water-soluble polymer. Moreover, the signals are broad since the attachment of the peptide to the bulky polymer restricts their rotation resulting in broad signals.

^1H NMR spectroscopy suggests quantitative conjugation of the tetra-peptide to HS-PDMA. This was calculated by comparing the integral of the peak at 0.95 ppm due to the methyl leucine of the polymer-peptide conjugate to the integral of the peak at 6.33 ppm due to pyrrole protons of HS-PDMA.

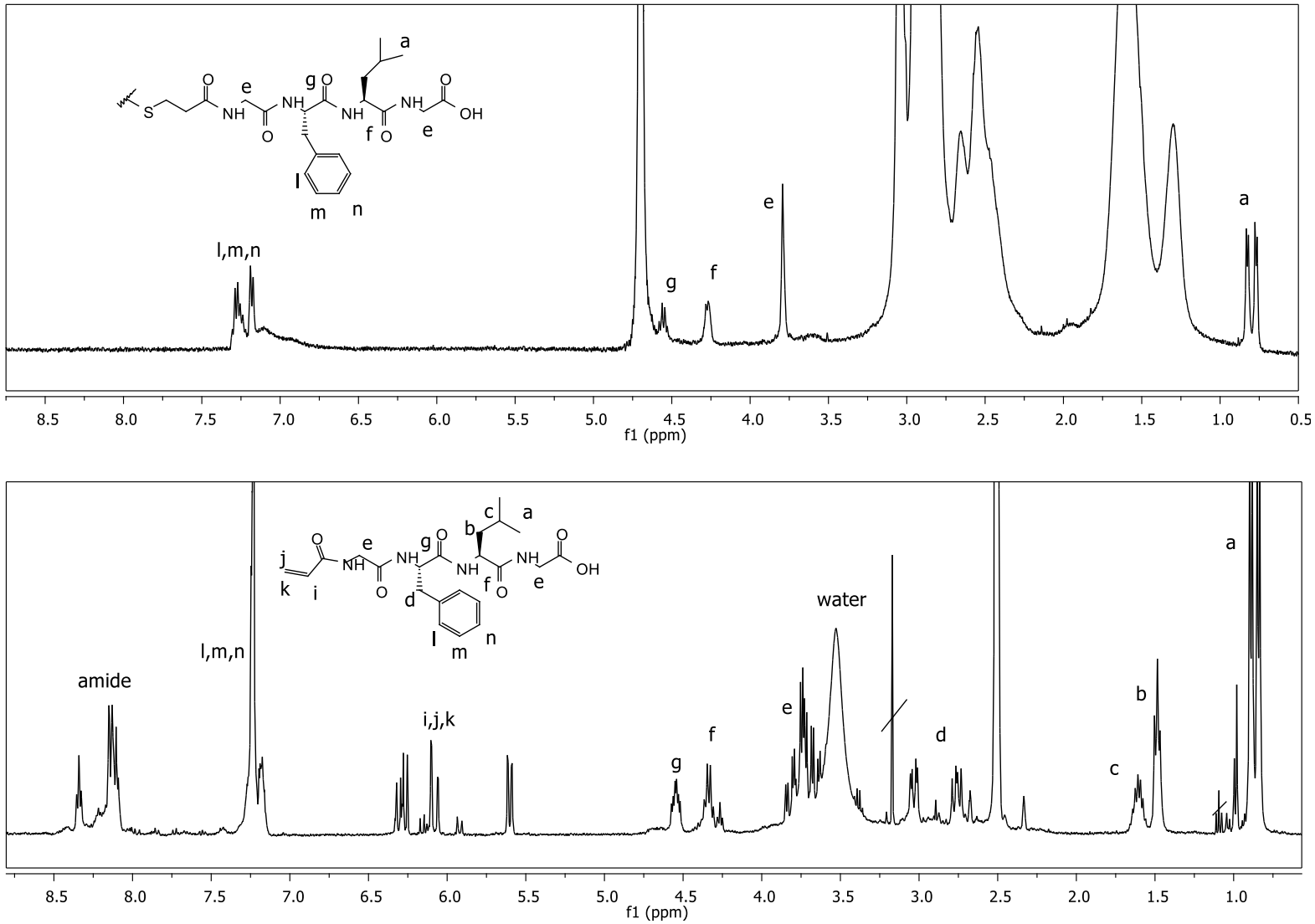

Figure 4-6. [1]H NMR spectra of HS-PDMA-Gly-Leu-Phe-Gly in D_2O and vinyl-modified tetra-peptide (Gly-Leu-Phe-Leu) in $SO(CD_3)_2$

4.2.3.2 The attachment of the dipeptide, Leu-Gly(5-FU)

For selective coupling of the *N*-terminal amine of the dipeptide, Leu-Gly(5-FU), with the *C*-terminal carboxyl of the polymer-peptide conjugate, either the *C*-terminal carboxyl of Leu-Gly(5-FU) should be protected or the *C*-terminal carboxyl of the HS-PDMA-Gly-Leu-Phe-Gly should selectively be activated. As the *C*-terminal protected dipeptide Leu-Gly(5-FU)-OMe was already available it was initially used. Although the HS-PDMA-Gly-Leu-Phe-Gly-Leu-Gly(5-FU)-OMe was successfully formed, subsequent basic hydrolysis to cleave the methyl ester group failed which is probably related to an accessibility issue. Therefore, the *C*-terminal carboxyl group of HS-PDMA-Gly-Leu-Phe-Gly was selectively activated.

The transformation to pentafluorophenyl ester end groups was achieved by the reaction with pentafluorophenol and *N*,*N*-dicyclohexylcarbodiimide (DCC) as coupling agent (Scheme 4-6). The activated conjugate was purified by precipitation several times in diethyl ether.

Three resonance at -153.14, -157.77 and -162.49 ppm due to the pentafluorophenyl ester were visible in the ^{19}F NMR spectrum (Figure 4-7) of the purified material confirming the successful activation. The spectrum also shows other resonance signals which could be due incomplete elimination of unreacted pentafluorophenol. The other possibility is that the original polymer can have carboxylic terminals, as a result of bimolecular termination with ACVA, which can also form a pentafluorophenyl ester. Clearly as the signals were broad and shifted compared with pentafluorophenol, the signal is due to the terminal active ester.

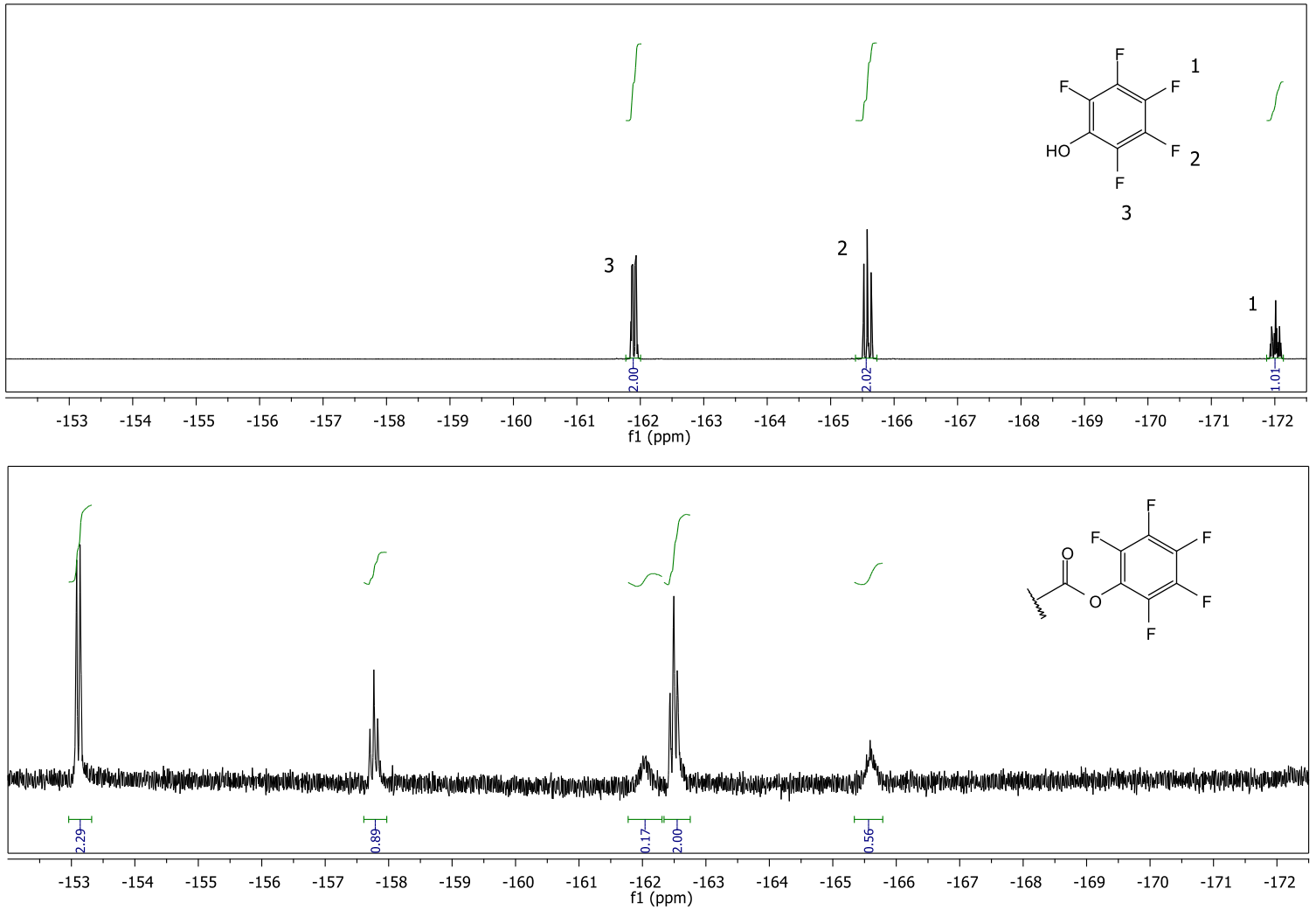

Figure 4-7. ^{19}F NMR of pentafluorophenol and HS-PDMA-Gly-Leu-Phe-Gly with pentafluorophenyl ester end group in $(CD_3)_2SO$

The coupling of active ester with the dipeptide was successfully accomplished in DMF in the presence of *N*,*N*-diisopropylethylamine (DIPEA) and the product was purified by dialysis against deionised water (Scheme 4-6). The successful attachment of the dipeptide was confirmed by ^{1}H and ^{19}F NMR spectroscopy.

The ^{1}H NMR spectrum (Figure 4-8) shows the characteristic resonance signals at 5.87 and 7.75 ppm assigned to glycyl CH and pyrimidine CH proton, respectively, along with the leucine proton signals at 0.95, 1.25, 4.21 and 4.38 ppm. The ^{19}F NMR spectrum shows a signal at -167.56 due to 5-FU, which clearly indicates the successful synthesis of the desired polymer peptide conjugate.

The two signals due to the α-hydrogen of leucine at 4.21 and 4.38 ppm in ^{1}H NMR spectrum, along with the shoulder present in the single ^{19}F NMR peak, indicate different environments due to the formation of the dipeptide and the desired hexa-peptide conjugates. Undesired bimolecular termination with ACVA in the polymerisation process results in carboxylic terminals that can form dipeptide conjugates.

The efficiency of the dipeptide coupling was about 80% as calculated by ^{1}H NMR spectroscopy by comparing the integration of Leu at 0.95 ppm of HS-PDMA-Gly-Leu-Phe-Gly-Leu-Gly(5-FU) to HS-PDMA-Gly-Leu-Phe-Gly.

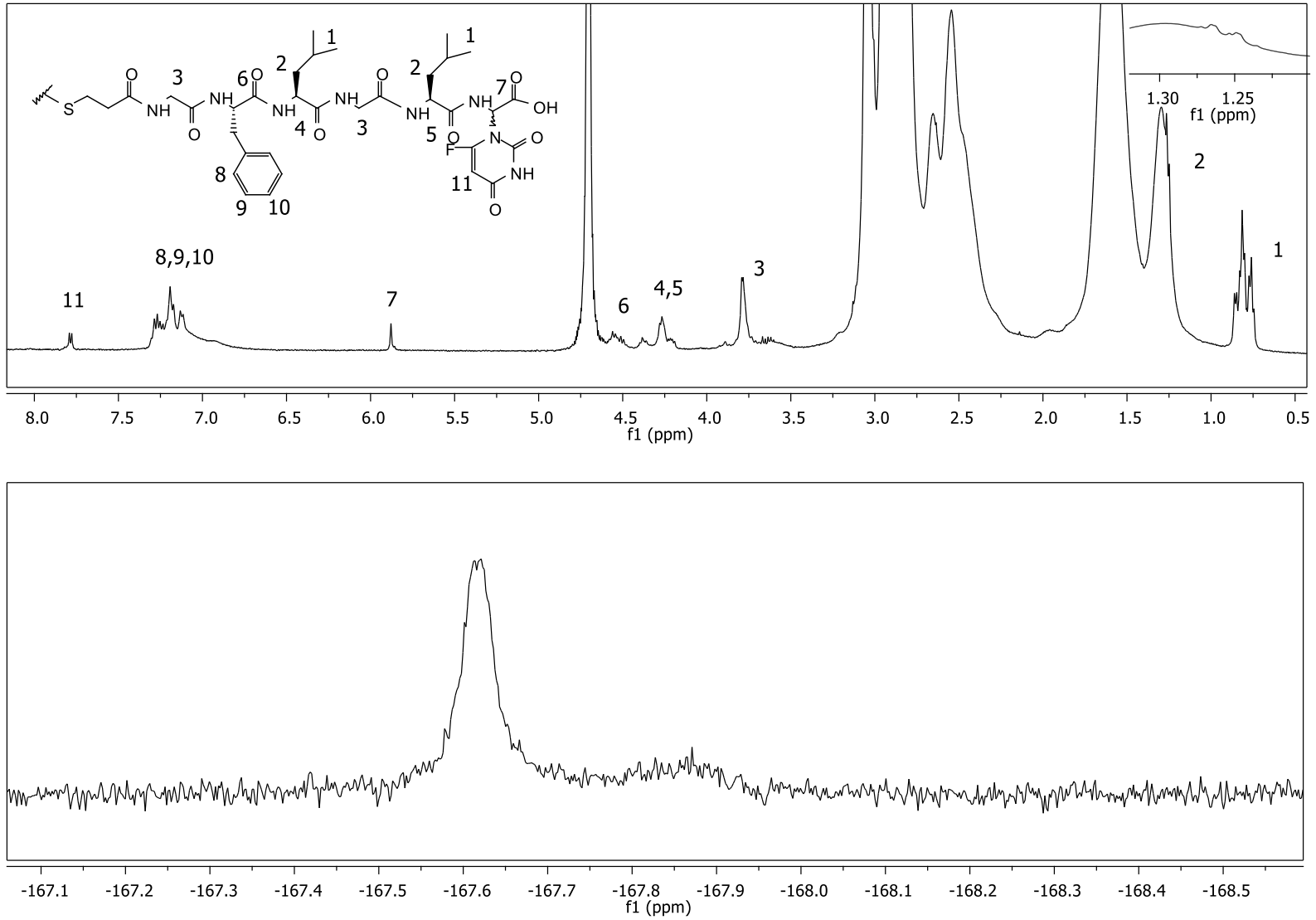

Figure 4-8. ^{1}H NMR and ^{19}F NMR of HS-PDMA-Gly-Leu-Phe-Gly-Leu-Gly(5-FU) in D_2O

4.3 Conclusion

This chapter detailed the synthesis of the polymer peptide conjugate, HS-PDMA-Gly-Phe-Leu-Gly-Leu-Gly-α-(5-FU). The polymer peptide conjugate was synthesised mainly by a couple of steps; the attachment of the vinyl-modified tetrapeptide, Gly-Phe-Leu-Gly, via *in situ* aminolysis/Michael addition chemistry followed by the attachment of the dipeptide, Leu-Gly-α-(5-FU), after the selective activation with pentafluorophenol. Assembly of the peptides on the polymer surface is a good method to avoid undesired side products as excess reagents and by-products can be removed after each step by simple dialysis.

Aminolysis/Michael addition chemistry was initially examined using a commercially available analogue, *N*-hydroxyethyl acrylamide (HEA). The major challenge was the formation of disulfide coupled species either in the form of cross-linked material or high molecular weight contaminants, as suggested by GPC. The formation of such disulfide species was eliminated by the use Me_2PPh which also served as a good catalyst for the thiol Michael addition resulting in a quantitative conjugate as suggested by ^1H NMR spectroscopy.

4.4 Experimental

4.4.1 Instrumentation

^1H and ^{19}F NMR spectra were recorded on Bruker AV400 or Bruker AVIII HD 400 using deuterated solvents at room temperature. Chemical shifts of spectrums are estimated in ppm relative to the residual solvent peak and the NMR spectra were examined using Topspin 3.0 NMR software. UV/Vis absorbance was measured by an Analytik Jena AG Specord S-600 spectrophotometer and Software (WinASPECT) was used for UV/Vis analysis. Molecular weight analysis was performed using a GPC instrument fitted with an RI detector. The instrument was calibrated with PMMA standards using DMF as eluent at a flow rate of 1.0 $ml.min^{-1}$.

4.4.2 Materials

HS-PDMAs were synthesised as described in Chapter 2. Gly-Phe-Leu-Gly and Leu-Gly(5-FU) were synthesised as described in Chapter 3. Dry *N*,*N*-dimethylformamide (DMF) was obtained from the Grubbs dry solvent system (Puresolve, models SPS 400-6 and SPS200-6). Propylamine (Sigma Aldrich, ≥99%), *N*-hydroxyethyl acrylamide (Sigma Aldrich, 97%),

phenyldimethylphosphine (Sigma Aldrich, 99%) 4-(dimethylamino)pyridine (Fluka, 99%), and pentafluorophenol, *N,N′*-dicyclohexylcarbodiimide (Alfa Aesar, 99%) *N,N*-diisopropylethylamine (Alfa Aesar, 99%) and pentafluorophenol (Sigma Aldrich, ≥99%) were used as received without any purification.

4.4.3 Grafting the acrylamide to HS-PDMA

HS-PDMA was dissolved in 3 mL deoxygenated DMF solvent. Propylamine, *N*-hydroxyethylacrylamide and phenyldimethylphosphine were then added (Table 4-2). The reaction mixture was stirred overnight at room temperature under N_2 atmosphere. The crude polymer solution was precipitated from diethyl ether/acetone 9:1. The precipitate was isolated by centrifugation (4,500 rpm, for 5 min). The polymer was then dialysed against deionised water (membrane MWCO 3.5 kDa) for 48 h. A white solid was obtained after freeze drying.

Table 4-2. Amount used in in situ Aminolysis/ Michael addition reaction

	Polymer		**Propyl amine**		**HEA**		**Me_2PPh**	
	µmol	mg	µmol	mg	µmol	mg	µmol	mg
HS-PDMA-10 wt%	7.41	100	62.4	3.7	62.4	7.3	12.5	1.7
HS-PDMA-20 wt%	5.03	100	59.4	3.5	59.4	7.2	11.9	1.6
HS-PDMA-30 wt%	3.92	100	61.2	3.6	61.2	7.0	12.2	1.7
HS-PDMA-40 wt%	3.13	100	63.1	3.7	63.1	7.3	12.6	1.7
HS-PDMA-50 wt%	3.24	100	63.7	3.7	63.7	7.3	12.7	1.7

^{1}H NMR (400 MHz, D_2O) δ 7.11-6.79 (br, 4H), 3.75-3.65 (br. m., 1H), 3.56 (t., J = 5.4 Hz, 2H), 3.52-3.45 (br. m., 2H), 3.24 (t, J = 5.4 Hz, 2H), 3.15 – 2.71 (br. m., 6H), 2.71-2.26 (br. m., 1H), 1.18-1.77 (br. m., 2H).

HS-PDMA-10 wt% conjugate: M_n = 13.1 kDa, Đ = 1.67

HS-PDMA-20 wt% conjugate: M_n = 19.8 kDa, Đ = 2.09

HS-PDMA-30 wt% conjugate: M_n = 24.6 kDa, Đ = 2.91

HS-PDMA-40 wt% conjugate: M_n = 31.7 kDa, Đ = 7.65

HS-PDMA-50 wt% conjugate: M_n = 33.7 kDa, Đ = 5.84

4.4.4 The synthesis of HS-PDMA-Gly-Leu-Phe-Gly

HS-PDMA-30 wt% (0.019 mmol, 500 mg, 25.5kDa, Đ =3.77) was dissolved in 3 ml deoxygenated DMF solvent. Propylamine (0.537 mmol, 31.7 mg) and GLy-Phe-Leu-Gly (0.537 mmol, 239.5 mg) were then added. After 15 min, phenyldimethylphosphine (0.644 mmol, 88.9 mg, 91 µL) was then added. The reaction mixture was stirred at room temperature under N_2 atmosphere. The crude polymer-peptide solution was precipitated from diethyl ether/acetone 9:1. The precipitate was isolated by centrifugation (4,500, for 5 min). The polymer was then dialysed against water (membrane MWCO 3.5 kDa) for 48 h. A white solid was obtained after freeze drying. Yield: 412 mg (85%).

^{1}H NMR (400 MHz, D_2O) δ 7.36 – 7.14 (br. m., 5H), 7.28 – 6.77 (br, 4H), 4.59 – 4.47 (br. m, 1H), 4.27 (s, 1H), 3.79 (s, 4H), 3.27 – 2.71 (m, 6H), 2.77-2.03 (br. m, 1H), 2.03 – 1.07 (br. m, 1H), 0.80 (dd, *J* = 22.2, 5.6 Hz, 6H).

4.4.5 The activation of HS-PDMA-Gly-Leu-Phe-Gly carboxylic group

HS-PDMA-Gly-Phe-Leu-Gly (0.016 mmol, 483 mg), 4-(dimethylamino)pyridine (0.021 mmol, 2.5 mg), and pentafluorophenol (0.207 mmol, 38 mg), were dissolved in 2 mL of DMF, which was then purged with nitrogen for 20 min. Dicyclohexylcarbodiimide (0.207 mmol, 42.8 mg) in 1 mL of DMF was added. The reaction mixture was stirred for 1 h at 0 ^{o}C and for other 20 h at room temperature. After the completion of the reaction, the crude reaction mixture was filtered to remove the insoluble dicyclohexylurea precipitates. The filtrate was concentrated using rotary evaporator under vacuum and purified by precipitation in diethyl ether three times. Traces of solvents were removed under vacuum to give a white solid material. Yield: 355 mg (87%).

^{1}H NMR (400 MHz, DMSO) δ 7.28 – 7.09 (br. m, 5H), 7.14-6.73 (br. m, 4H), 5.57 (d, *J* = 8.0 Hz, 2H), 4.60-4.47 (br. m., 1H), 4.45-4.26 (br. m., 2H), 4.23 – 4.13 (br. m., 1H), 3.78 – 3.64 (br. m., 1H), 3.65-3.49 (br. m., 1H), 3.21 – 2.61 (br. m., 6H), 2.61 – 1.90 (br. m., 1H), 1.89 – 0.93 (br. m., 2H), 0.87 (dd, *J* = 19.4, 6.5 Hz, 6H).

^{19}F NMR (377 MHz, DMSO) δ -153.11, -157.77, -162.49.

4.4.6 The synthesis of HS-PDMA-Gly-Leu-Phe-Gly-Leu-Gly(5-FU)

To a solution of HS-PDMA-Gly-Phe-Leu-Gly (0.015 mmol, 355 mg) in dry DMF, Leu-Gly(5-FU) (0.207 mmol ,89 mg) and *N*,*N*-diisopropylethylamine (0.414 mmol ,53 mg, 72 µL) were added. The reaction mixture was stirred for 24 h at room temperature. The reaction mixture was concentrated by rotary evaporator under vacuum and precipitated in diethyl ether. This was dialyzed against deionised water (membrane MWCO 3.5 kDa) for 24 h and was subsequently freeze-dried to give a white solid material. Yield: 309 mg (81%).

^{1}H NMR (400 MHz, D_2O) δ 7.79 (d, J = 5.7 Hz, 1H), 7.36 – 7.07 (br. m., 1H), 7.32 – 6.73 (br. m., 4H), 5.89 (s, 1H), 4.60-4.46 (br. m., 1H), 4.41-4.33 (br. m., 1H), 4.30-4.23 (br. m., 1H), 4.23-4.16 (br. m., 1H), 3.94 – 3.69 (br. m., 4H), 3.71-3.51 (br. m., 2H), 3.32 – 2.71 (br. m., 6H), 2.71-2.26 (br. m., 1H), 1.18-1.77 (br. m., 2H), 0.91 – 0.67 (br. m., 12H).

M_n=22,000 Da, Đ =2.59

Chapter 5 Monitoring the release of 5-FU by ^{19}F NMR for MRI application

5.1 Introduction

Magnetic resonance imaging (MRI)[116] is arguably the most versatile imaging modality in use in biomedical research. This is owing to its advantages of non-invasiveness, relatively high spatial resolution, visualisation of deep tissues and lack of radioactive nuclides or ionizing radiation.[118] ^{1}H has been the most dominant nucleus in clinical MRI, however, the use of toxic contrast agents, e.g. iron oxide[128] and gadolinium-based chelates,[126,127] is essential to provide contrast within the image. Such contrast is usually subtle due to the high background signal generated from water protons in biological samples.

Alternatively, heteronuclear atoms (e.g. ^{13}C, ^{23}Na, ^{31}P, ^{19}F) can be used. Such atoms can be imaged directly by MRI to give "second colour" images providing anatomical details of living tissues. Of these, ^{19}F is especially attractive due to its favourable NMR properties including 100 % natural abundance, large gyromagnetic ratio, and its high sensitivity. Unlike ^{1}H MRI, ^{19}F MRI provides high image contrast due to the lack of background ^{19}F signal within the body.[148,149] ^{19}F is essentially absent from soft tissues and only found in the form of immobilised fluoride salts in bones and teeth, where its very short T_2 relaxation times result in a signal below the limit of conventional MRI techniques. More interestingly, ^{19}F can be used in several quantitative applications,[137,286] owing to the linear relationship between the ^{19}F MRI signal intensity and the fluorine concentration.

Recently, fluorine-labelled polymers have been considered as a potential new generation of ^{19}F MRI probes. In order to be effective ^{19}F MRI probes, fluorinated polymers should fulfil a number of design requirements including high fluorine content, long T_2 relaxation times and short T_1 relaxation times. Generally, the attachment of ^{19}F nuclei to large polymeric species results in slow tumbling rate leading to crucially shortening both T_1 and T_2 relaxation times of ^{19}F nuclei. Short T_1 relaxation time is favourable as it allows more scans within a certain time-frame and hence results in a better signal-to-noise ratio. Short T_2, however, might lead to signal line-broadening and in some cases, it is difficult to obtain a meaningful signal. T_2 of ^{19}F nuclei within the polymeric contrast agents can be enhanced by increasing the solubility and mobility of fluorinated segments. Generally, incorporating fluorine nuclei within a rigid hydrophobic region significantly restricts their mobility leading to poor image intensity[155,156] whereas

random incorporation of fluorine nuclei within a hydrophilic polymer chain means that the fluorine nuclei are always in a hydrated state.[113,157,158,161,163,164,169] Furthermore, among several classes of partly fluorinated polymeric architectures, including linear,[156,166] branched,[113,157,162–164,169] and star polymers[161,167,168] have been developed, star polymers are especially attractive due to their 3D constrained shape which can frustrate dipole-dipole interactions with nearest ^{1}H and ^{19}F nuclei and aggregation enabling high segmental mobility while maintaining high fluorine content (up to 20 mol % fluorinated monomer).

More recently, significant attention has been paid to the development of smart ^{19}F MRI contrast agents. Such agents undergo switch on in response to specific biological stimuli such as pH,[159,166–168,287] redox[159] or enzyme.[176–178,288,289] In particular, enzyme responsive ^{19}F MRI probes have gained considerable attention to detect enzyme activities. Two types of switchable enzyme responsive ^{19}F MRI probes have been developed: one shows chemical shift change[173–175] and the other exhibits switch on intensity signal after enzymatic treatment. [176–178,288,289] The applications of chemical shift imaging are restricted as sometimes the magnitude of chemical shift alteration is limited. In contrast, most of switchable signal probes are gadolinium-based contrast agents that undergo changes in their relaxation times driven by enzyme catalysed cleavage. Although this approach is promising, polymeric enzyme responsive ^{19}F MRI contrast agents with low cytotoxicity have yet to be developed.

5-Fluorouracil (5-FU)[290] is a chemotherapeutic with an antitumor activity against a wide range of solid tumours.[291–294] However, severe toxic side effects are presented with its administration. The type of linkage used to connect it to the polymer substrate greatly influences the site-specific release of 5-FU. Approaches for the 5-FU using carbamate, amide, carbamoyl or ester bonds have resulted in non-specific chemical hydrolysis within the blood stream.[183] A more affective approach is to use specific oligo-peptides bearing 5-FU in its α C-terminal glycine residue.[179–182] These spacers are designed to be stable in the blood stream but biodegradable by lysosomal enzymes in the target site. Although there has been a considerable development in the controlled release from polymeric device, direct evaluation of release of 5-FU is still in high demand in drug delivery systems.

With the aim of developing a switchable ^{19}F MRI polymeric-based contrast agent induced by enzymatic cleavage for monitoring 5-FU release, hyper-star poly(*N*,*N*-dimethylacrylamide) HS-PDMA that is covalently attached to the oligo-peptide bearing 5-FU in its α C-terminal glycine residue was synthesised. HS-PDMA (M_n = 25.5 kDa, Đ = 3.77) was firstly produced via reversible addition–fragmentation chain transfer mediated self-condensing vinyl polymerisation (RAFT-SCVP) of *N*,*N*-dimethylacrylamide (DMA) with polymerisable RAFT

agent, 4-vinylbenzyl *N*-pyrrole carbodithioate (VBPC), at a feed ratio of [DMA]:[VBPC] 50:1 and 30 wt% concentration as detailed in Chapter 2. The lability of thiocarbonylthio end groups allowed the conjugation of the vinyl modified tetra-peptide, Gly-Leu-Phe-Gly, synthesised by solid-phase chemistry (Chapter 3), via *in situ* aminolysis/ Michael addition in the presence of phenyldimethylphosphine (Me_2PPh) to supress the formation of high molecular weight disulfide coupled species. This was then activated by pentafluorophenol to enable the attachment of the dipeptide, Leu-Gly(5-FU), to form HS-PDMA-Gly-Leu-Phe-Gly-Leu-Gly(5-FU) (M_n = 22.0 kDa, Đ = 2.59), as described in details in Chapter 4.

The aim of this chapter is to examine the principle "the ability of monitoring 5-FU release from polymer carrier using ^{19}F NMR for MRI application". T_2 is an important contrast factor for ^{19}F MRI, since the intensity of the MRI signal directly depends on T_2 relaxation times. ^{19}F nuclei experience slow tumbling rate within the polymer probe resulting in significantly shortened T_2 relaxation time and attenuated ^{19}F MRI signal. Incubation of the polymeric probe with the enzyme should induce the release of free 5-FU accompanied with an extension of T_2 relaxation times and an enhancement in the ^{19}F MRI signal (Scheme 5-1). For optimisation purpose, the release of 5-FU from the dipeptide was firstly studied. Then, the release of 5-FU from the polymer-peptide conjugate was examined. 5-FU release was monitored by ^{19}F NMR along with T_1 and T_2 ^{19}F NMR.

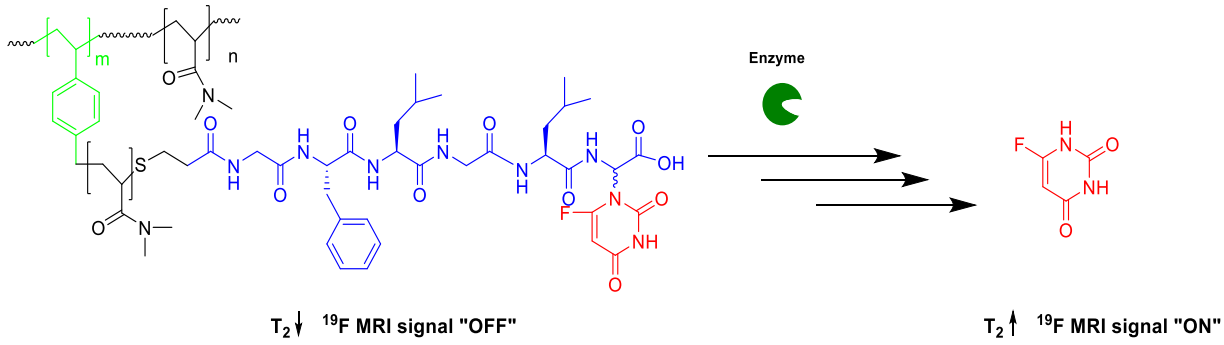

Scheme 5-1. OFF/ ON ^{19}F MRI switch induced by enzymatic catalysed release of 5-FU

5.2 Result and discussion

5.2.1 Proof-of-principle experiments

The suggested mechanism of the enzymatically catalysed release of 5-FU using tritosomes (mixture of lysosomal enzymes known to be overexpressed in many cancer cells) is as follows:[179,180] the catalytic activity of the endopeptidase releases a dipeptide derivative of 5-

FU **2** from the polymer containing 5-FU **1** and the aminopeptidase activity results in a chemically unstable 5-FU derivative **3** that degrades spontaneously to form free 5-FU **4**, as shown in Scheme 5-2. However, the degradation mechanism and the position of cleavage could vary depending on the enzymes used.[181] To avoid the issues of handling animals, the proof-of-principle experiments were performed using commercial S9 fraction from rat liver instead. S9 fraction is a mixture of microsomes and cytosols and contains a wide range of metabolising enzymes.[295]

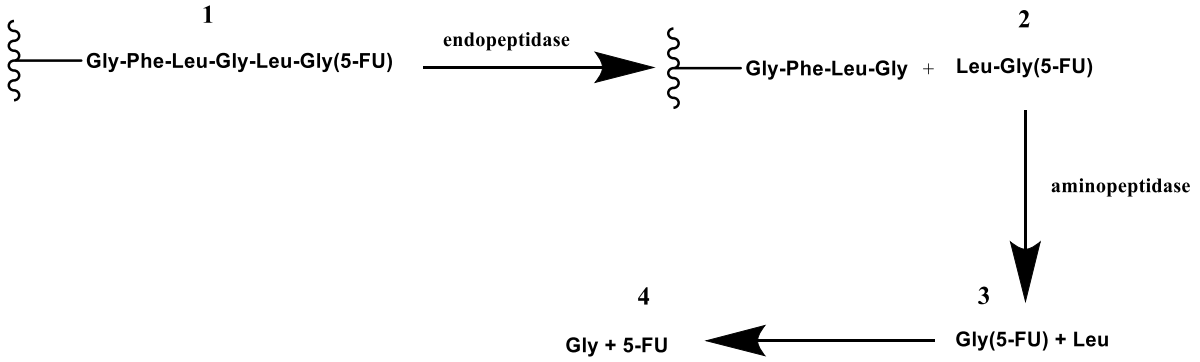

Scheme 5-2. Suggested mechanism of the enzymatically catalysed release of 5-FU[179,180]

5.2.2 Enzyme catalysed release of the dipeptide derivatives of 5-FU

The enzymatically catalysed release of 5-FU from L,L and L,D dipeptide derivatives of 5-FU (Figure 5-1) was firstly studied by incubating an amount containing 15 µM 5-FU with liver S9 fraction in 1:9 D_2O:PBS containing 3 mM $MgCl_2$ (pH 7.4) at 37 °C for 24 h. It is worth mentioning that the dipeptide is present as the HCl salt as explained in Chapter 3. Using TFA during HPLC purification of the dipeptide diastereoisomers resulted in TFA salts that were replaced by HCl. Dissolving this in PBS:D_2O solution resulted in low pH of about 2.87 which was adjusted to the desired pH. As shown in Figure 5-2, the incubation of L,L dipeptide resulted in quantitative degradation (77% release of 5-FU) while the incubation of L,D dipeptide resulted in only 15% release of 5-FU. This indicates that levorotatory peptide is better substrate for S9 enzyme than the dextrorotatory one.

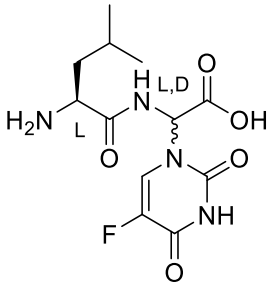

Figure 5-1. The structure of dipeptide derivative of 5-FU

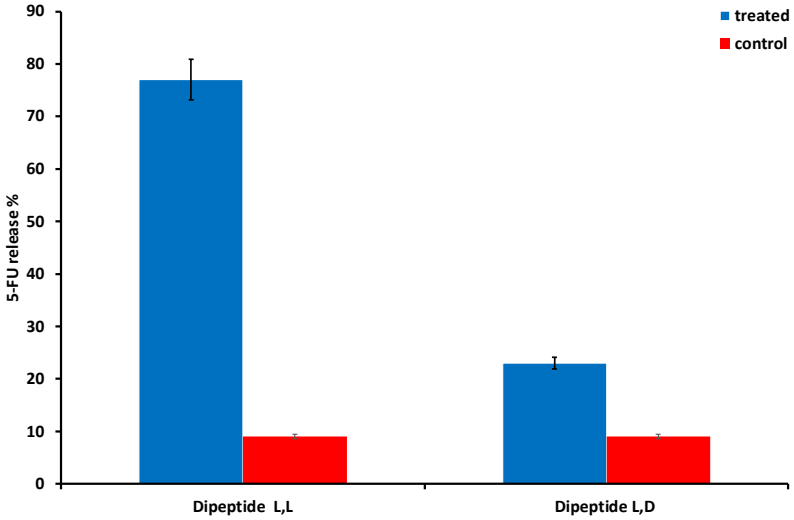

Figure 5-2. Incubation of L,L and L,D dipeptide derivatives of 5-FU with liver S9 fraction at 37° C pH 7.4 for 24 h

^{19}F NMR spectra and the relaxation times were measured before and after incubation of the dipeptide with liver S9 fraction (Figure 5-3). After enzymatic treatment, the singlet broad peak at -166.93 ppm (internal standard: trifluoroacetic acid) disappeared and a new sharp doublet signal due to free 5-FU at -169.16 ppm appeared. This result indicates that ^{19}F nucleus of the dipeptide experiences slow tumbling rate compared with the released 5-FU. The slow tumbling rate effect was explicitly confirmed by longitudinal T_1 and transverse T_2 relaxation times of the reaction sample measured using standard inversion-recovery and Carr–Purcell–Meiboom–Gill pulse sequences, respectively as shown in Figure 5-3-B. After enzyme treatment, the longitudinal T_1 and transverse T_2 ^{19}F relaxation times of the reaction sample became 4.804 s and 0.144 s, respectively. As expected, both of relaxation times showed considerable extension compared to those of the dipeptide. However, the T_2 relaxation time of the released drug is still less than the original value of the free 5-FU shown in Figure 5-10 (T_2 of 0.476 s), possibly because its mobility was hindered by the enzyme. Furthermore, the short T_2 relaxation time could be due to an error in adjusting pH as T_2 of 5-FU greatly influenced by pH (Figure 5-4).

When the relaxation times of 5-FU were measured at various pH, T_2 shortened with pH. The ^{19}F NMR spectrum also shows two other products at -166.42 and -166.10 ppm (+ 2.74 and 3.06 ppm relative to 5-FU). These signals are probably due to metabolites of 5-FU. The change in chemical shift values of the 5-FU metabolites relative to 5-FU can depend on pH, ionic strength, Mg^{2+} concentration and temperature. According to the pH titration curves of 5-FU metabolites reported by Lutz and Hull,[296] the two signals at pH 7.4 are possibly due to 5-fluouridine and 5-fluoro-2-deoxyuridine, respectively.

A)

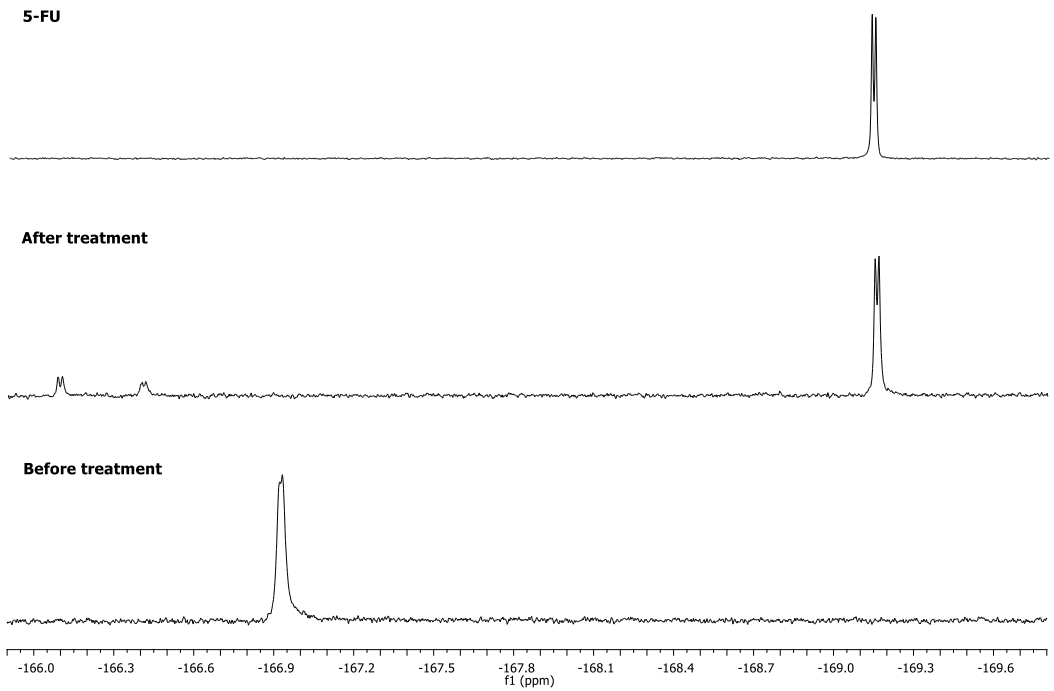

B) ^{19}F T_1

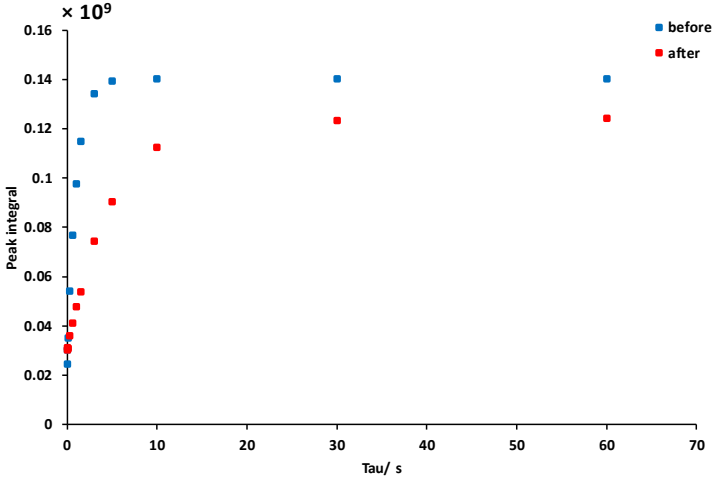

^{19}F T_2

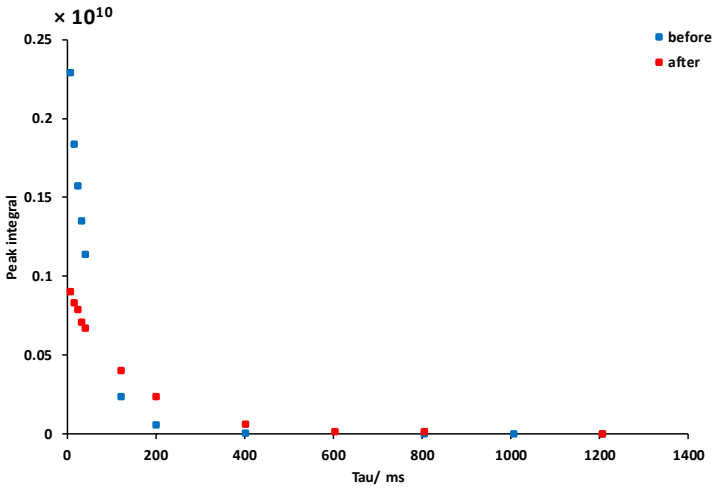

C)

	T_1/ s	T_2/ s
Before treatment	0.997	0.047
After treatment	4.804	0.144

Figure 5-3. A) ^{19}F NMR spectrum of L,L dipeptide derivative of 5-FU before and after the treatment with S9 fraction from liver in PBS:D_2O 9:1 containing 3 mM $MgCl_2$ B) ^{19}F T_1 and T_2 relaxation times curves of L,L dipeptide and the released 5-FU C) list of ^{19}F T_1 and T_2 relaxation times of L,L dipeptide and the released 5-FU

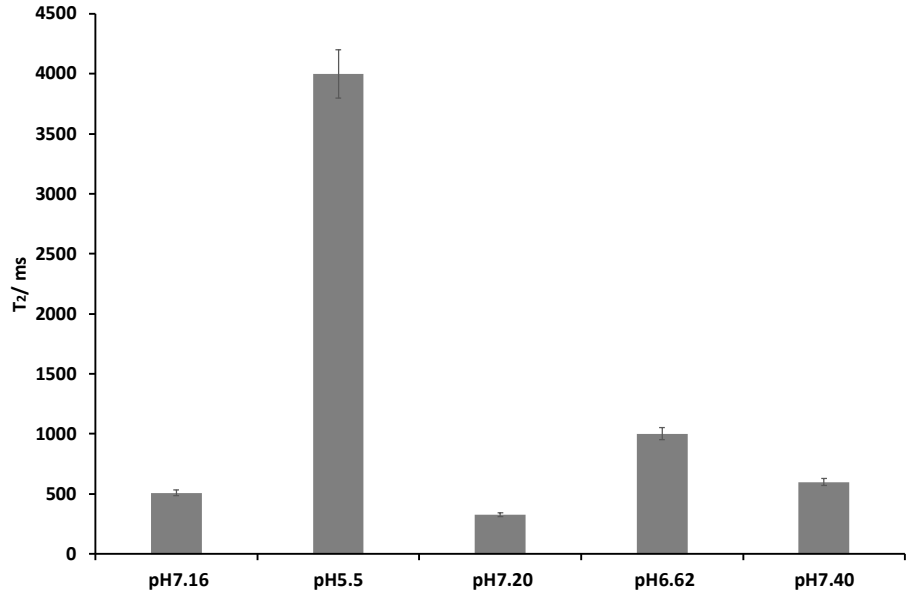

Figure 5-4. T_2 relaxation times of free 5-FU in various pH

5.2.3 Enzyme catalysed release of 5-FU polymer conjugate

As the enzyme is stereochemistry specific, only 5-FU polymer conjugate with L,L configuration was synthesised and analysed. Incubation of 5-FU polymer conjugate with S9 fraction resulted in a very low (9%) conversion to 5-FU (Figure 5-5), compared with the quantitative conversion has been reported using rat liver tritosomes at pH 5.5 to 5-FU and 5-FU derivatives.[179,180]

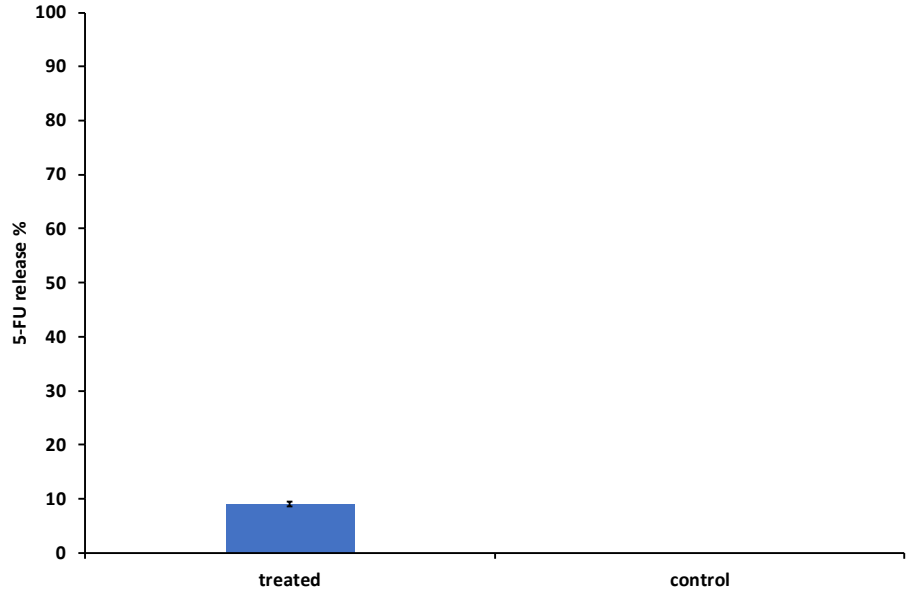

Figure 5-5. Incubation of 5-FU polymer conjugate with liver S9 fraction at 37° C pH 7.4 for 24 h

The low release can be also due to the limited accessibility of S9 fraction to the oligo-peptide spacer due to the relatively compact structure of the polymer at pH 7.4. The particle size of the polymer in PBS was measured using dynamic light scattering (DLS) and shown in Figure 5-6. As the pH was increased from 5.5 to 7.4, the particle size of the polymer progressively decreased by 54% (from 13 to 6 nm) indicating significant dependence of particle size on the pH.

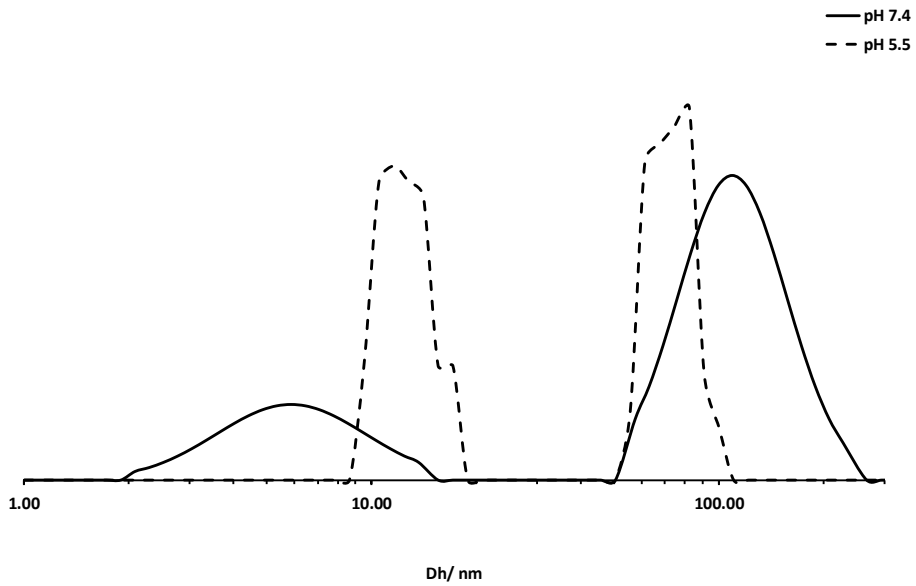

Figure 5-6. Particle size distribution of 5-FU polymer conjugate in PBS at pH 5.5 and 7.4 from DLS operated at 25° C

Figure 5-7-A illustrates the ^{19}F NMR spectra of 5-FU polymer conjugate before and after the incubation with liver S9 fraction. After enzymatic treatment, a sharp doublet peak signal at -169.19 ppm due to the free 5-FU was observed. T_1 and T_2 ^{19}F relaxation times of the cleaved drug showed considerable elongation from 0.846 and 0.038 s to 3.091 and 0.148 s respectively (Figure 5-7-B). This finding indicates an enhancement of the tumbling rate owing to the cleavage of 5-FU. Both T_1 and T_2 relaxation times of the released drug are still less than the original values of the free 5-FU shown in Table 5-1 (4.866 s for T_1 and 0.476 s for T_2). This is perhaps because its mobility was hindered by the enzyme and the high concentration of the polymer (100 mg mL^{-1}). The ^{19}F NMR spectrum shows no signal for the dipeptide suggesting that all the dipeptide was converted to 5-FU which is in a good agreement with the result of the incubation of L,L dipeptide alone with S9 fraction (Figure 5-3).

The spectrum also shows that the signal for 5-FU polymer conjugate at -167.35 is slightly shifted downfield by approximately 0.2 ppm after the treatment with the enzyme, which is possibly due to the fact that 5-FU-containing molecules are sensitive to pH. A slight decrease

in pH was recorded once S9 fraction was added. The effect of pH on the chemical shift and relaxation times was studied and reported in the following section.

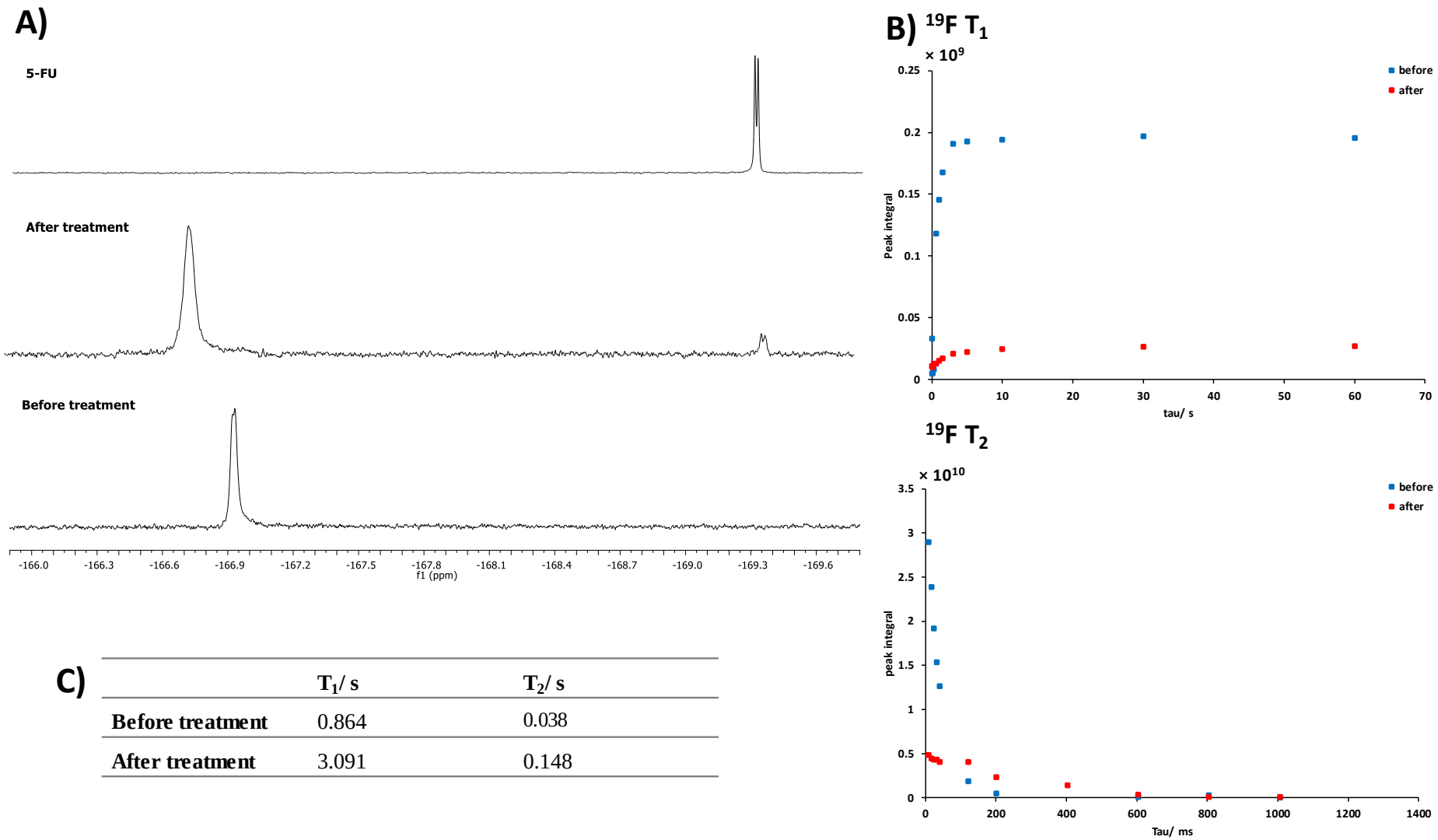

C)

	T_1/ s	T_2/ s
Before treatment	0.864	0.038
After treatment	3.091	0.148

Figure 5-7. ^{19}F NMR spectrum of 5-FU polymer conjugate in PBS:D_2O 9:1 containing 3 mM $MgCl_2$ before and after the treatment with S9 fraction from liver B) ^{19}F T_1 and T_2 relaxation times curves of the polymer and the released 5-FU C) list of ^{19}F T_1 and T_2 relaxation times of the polymer and the released 5-FU

5.2.4 ^{19}F NMR of 5-FU derivatives at different pH

5-FU is a metabolic analogue of uracil with a fluorine atom existing at the C-5 position of the pyrimidine ring. The mechanism underlying its cytotoxicity remains controversial. It has long been hypothesised that the presence of ionised 5-FU might lead to mispairing formation during DNA replication resulting in genetic mutation.[297] Uracil may exist in six tautomeric forms (Figure 5-8) with neutral lactam-keto form with one proton on each nitrogen as the most stable form in neutral pH. At basic pH, uracil deprotonates preferentially at N3-position with a pK_a of 9.1 at 25 °C.[298] Due to the presence of electron-withdrawing fluorine atom, the N3-position becomes more acidic (pK_a = 8)[298] than uracil and hence 5-FU can deprotonate at pH values in the physiological range. Such change from protonated to deprotonated state with pH can be directly witnessed by change in ^{19}F chemical shift.[296,299–301] Furthermore, the line-width of the 5-FU ^{19}F signal has been reported to have pH dependence.[296,302] Since line-width is inversely proportional to T_2 relaxation time, a change in T_2 relaxation times of 5-FU and 5-FU prodrugs with pH is expected. The above proof-of-principle enzyme catalysed release experiment was performed in pH of 7.4. However, lysosomes in cancer cell exhibit a pH as low as 4.5.[165] Therefore, further investigations of ^{19}F NMR properties of 5-FU containing molecules at acidic pH were made. Although the pK_a and hence ^{19}F NMR properties are quite sensitive to temperature and ionic strength, they were not considered as variables.

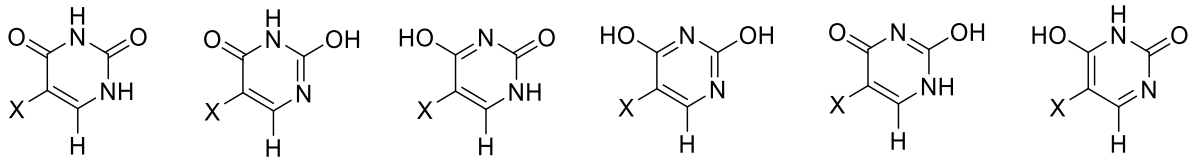

X = H (Uracil)
X = F (5-Fluorouracil)

Figure 5-8 Tautomeric forms of uracil and 5-fluoruracil

^{19}F NMR chemical shift and T_1/ T_2 relaxation times were studied at pH 7.4 and 5.5 simulating the environment of the blood and tumour, respectively. Figure 5-9 illustrates how chemical shifts of the polymer, the dipeptide and 5-FU vary with pH. At pH 5.5, resonance peaks were observed at -167.37, -167.53 and -169.24 ppm, respectively. When the pH was raised to 7.4, their ^{19}F chemical shift was shifted downfield corresponding to the deprotonation of 5-FU group. The resonances of the polymer and the dipeptide show a slight shift downfield by about 0.40 and 0.22 ppm respectively, whereas 5-FU resonance was only 0.02 ppm downfield. This is consistent with several studies on 5-FU and its metabolites.[296,299] The small chemical shift

change observed between protonated and deprotonated form of 5-FU is attributed to the delocalisation effect of the charge in the pyrimidine ring via tautomerization. For the polymer and the dipeptide, ionisation can only occur in N3-position as N1 is attached to Gly and therefore a noticeable chemical shift change was observed.

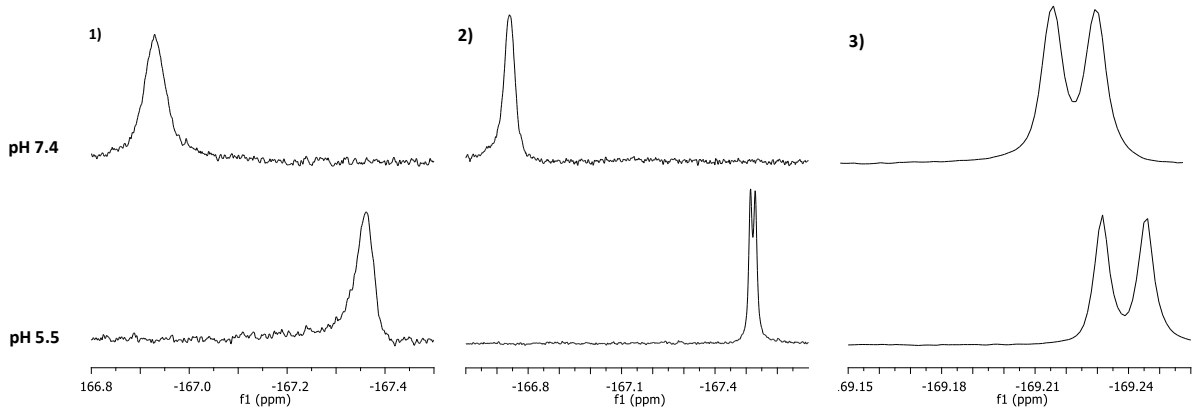

Figure 5-9. ^{19}F NMR spectrum of 1) 5-FU polymer conjugate, 2) dipeptide derivative of 5-FU and 3) free 5-FU in PBS:D_2O 9:1 containing 3mM $MgCl_2$ in pH 5.5 and 7.4. TFA was used as an internal standard reference (-75.43 ppm).

Figure 5-10 illustrates how ^{19}F transverse T_2 relaxation times of 5-FU polymer conjugate, dipeptide derivative of 5-FU and free 5-FU vary with pH. At pH 5.5, they display T_2 relaxation times of 0.057, 0.129 and 3.347 s, respectively. 5-FU shows an extremely long T_2 relaxation time compared with the polymer and the dipeptide indicating a very fast tumbling rate as explained before. When the pH was raised to 7.4, their ^{19}F T_2 relaxation times seem to be shortened indicating slower tumbling rate as a result of chemical exchange effect. This is also in a good agreement with the studies done on 5-FU in PBS[296] and water.[302] The slow tumbling rate of 5-FU has been witnessed by the increasing line-width of the ^{19}F signal with pH. The effect of pH on T_2 relaxation time of 5-FU (reduced by factor of 7) is much greater than those of the polymer and the dipeptide that are reduced by the factor of 1.5 and 2.5, respectively. The ^{19}F NMR signal of the dipeptide lost its doublet feature when pH was raised to 7.4 as shown in Figure 5-9. In contrast, pH shows almost no effect on T_1 relaxation times as illustrated in Table 5-1.

As 5-FU shows very long T_2 relaxation time at low pH compared with physiological pH, more pronounced signal intensity switch would be expected upon catalytic enzymatic cleavage using lysosomal enzyme in tumours.

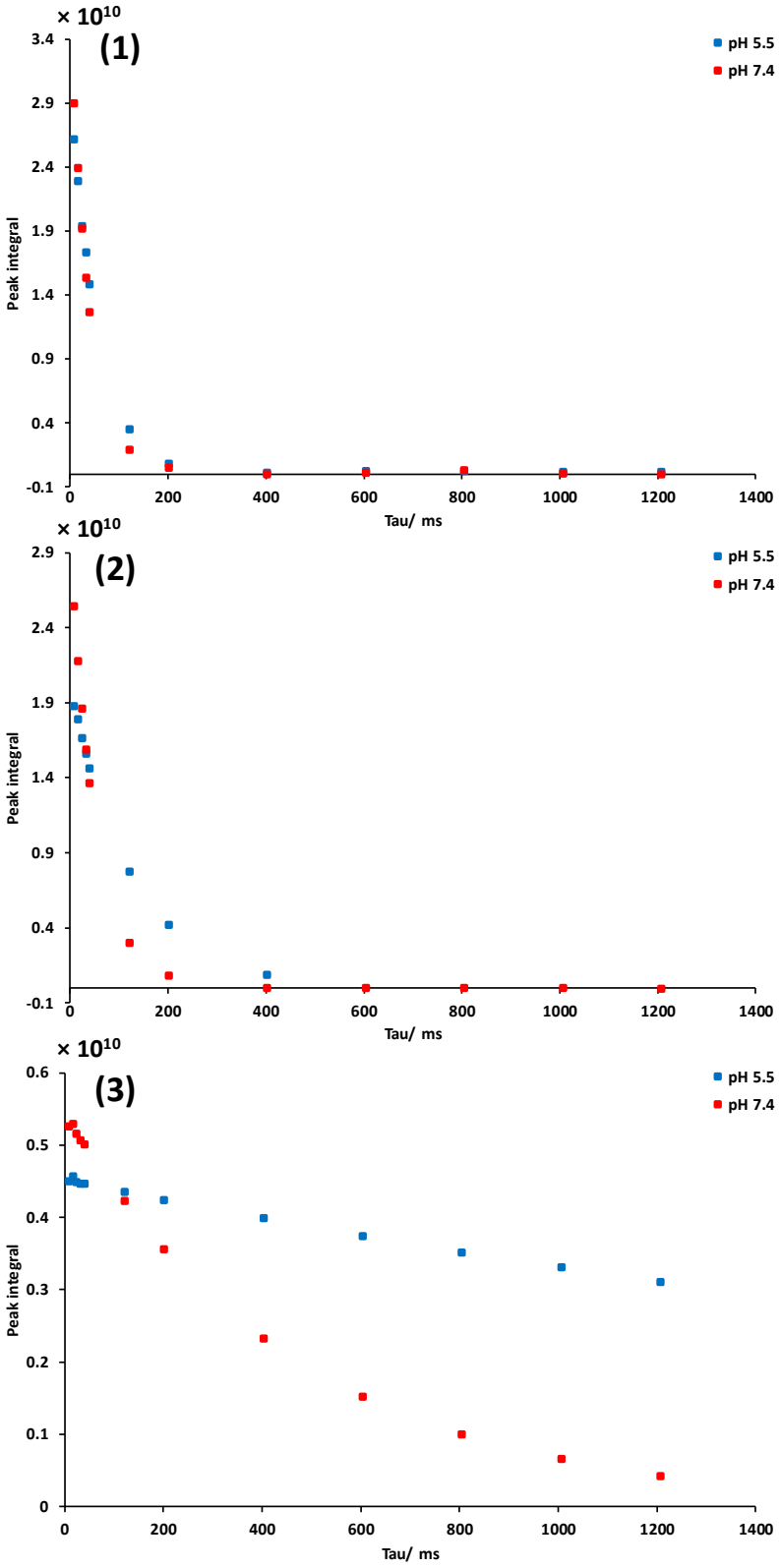

Figure 5-10. ^{19}F Spin-spin T_2 relaxation times of (1) 5-FU polymer conjugate, (2) dipeptide derivative of 5-FU, and (3) free 5-FU at pH 5.5 and 7.4

Table 5-1. List of ^{19}F T_1 and T_2 relaxation times of 5-FU polymer conjugate, dipeptide derivative of 5-FU, and free 5-FU at pH 5.5 and 7.4

	T_1/ s		**T_2/ s**	
	pH 5.5	pH 7.4	pH 5.5	pH 7.4
Free 5-FU	4.866	4.810	3.347	0.476
Dipeptide derivative of 5-FU	1.244	1.049	0.129	0.053
5-FU polymer conjugate	0.837	0.835	0.057	0.038

5.3 Conclusion

This chapter examined the ability of monitoring fluorinated drug release from polymeric carrier by dual increase in ^{19}F MRI intensity. Upon treatment with S9 fraction from liver at pH 7.4, T_2 relaxation time of the released 5-FU showed an elongation from 0.038 s to 0.128 s. As the MRI signal intensity is directly influenced by T_2 relaxation time, switch ON signal is expected upon enzymatic cleavage. ^{19}F MRI phantom could be used to visualise 5-FU release and verify the practical applicability of the probe and its sensing principle.

However, S9 fraction revealed low efficiency of only 9% 5-FU release compared with tritosomes that showed quantitative cleavage to 5-FU and its dipeptide derivatives.[179] This could be due to the limited accessibility of S9 fraction to the peptide linkers as a result of the compacted structure the 5-FU polymer conjugate exhibited at physiological pH compared with acidic pH.

Furthermore, 5-FU shows very long T_2 relaxation time at low pH compared with physiological pH. Therefore, a more pronounced signal intensity switch would be expected upon catalytic enzymatic cleavage using lysosomal enzyme. The proof-of principle experiment could be further investigated using lysosomal enzymes at acidic pH to get better understanding about 5-FU release and ^{19}F MRI properties in a tumour environment.

5.4 Experimental

5.4.1 Material

Dulbecco's phosphate-buffered saline without calcium chloride and magnesium chloride (DPBS) (Sigma Aldrich), S9 from rat liver, pooled (Sigma Aldrich), magnesium Chloride, hexahydrate (Sigma Aldrich, 99%), citric acid (Alfa Aesar, 99%), sodium phosphate dibasic (Sigma Aldrich, ≥99%), ethylenediaminetetraacetic acid (EDTA) (Sigma Aldrich, 98%), glutathione reduced (Sigma Aldrich, ≥98%), trifluoroacetic acid (TFA) (Acros, 99%), and deuterium oxide (Sigma Aldrich, 99 atom % D).

5.4.2 Release of 5-FU from 5-FU polymer conjugate and dipeptide derivatives of 5-FU

5-FU release from of 5-FU polymer conjugate, and L,L and L,D dipeptide derivatives of 5-FU, was studied in 5mm NMR tube. The polymer or the peptides (Table 5-2) were incubated in 1 mL volumes of PBS:D_2O 9:1 containing 3 mM $MgCl_2$ (pH 7.4). 1 µg of S9 fraction from rat liver was then added and the samples were immersed in a water bath at 37 °C for 24 h. The drug release was monitored using 1D ^{19}F NMR along with ^{19}F T_1/T_2. The assignment of the resonance signals for dipeptides and 5-FU was accomplished by comparing the chemical shifts with those of known compounds spectrumed under the same conditions using TFA as an internal standard reference (-75.43 ppm).

*Table 5-2. Masses of the polymer, the dipeptide and the free 5-FU in mg containing 15 µmol of **4***

^{19}F probe	**Weight /mg**	**/µmol of 5-FU**
Free 5-FU	2	15
5-FU dipeptide	5	15
5-FU polymer conjugate	100	15

5.4.3 Instrumentations

NMR Spectroscopy

All NMR experiments were carried out on a Bruker AVIII400 spectrometer fitted with a 5 mm auto-tuneable broad-band (BBFO) probe. Samples were prepared by dissolving an amount

containing 15 mmol of 5-FU in each sample (Table 5-2) in 1 mL volumes of PBS:D_2O 9:1 containing 3 mM $MgCl_2$ at pH 7.4 or 5.5.

1D ^{19}F NMR spectra were acquired at 376.5 MHz without ^{1}H decoupling using a 90° pulse in all measurements. The relaxation delay was 25 s (5 × longest T_1) and the acquisition time was 1.1 s. Data were collected using a spectral width of 59 kHz, and 16-46 scans.

^{19}F spin–lattice relaxation times (T_1) were measured using the standard inversion-recovery (IR) pulse sequence.[120] The relaxation delay was 30 s and the acquisition time was 1.1 s. Data were collected using a spectral width of 59 kHz, and 32-128 scans. For each measurement, the recovery times were from 1 ms to 60 s and 12 points were collected. T_1 was then calculated by TopSpin 3 using area type fitting. A single-component exponential recovery fit was used (Equation 5-1).

$$I(\tau) = I(0) + P\exp(-\frac{\tau}{T_1}) \qquad \textit{Equation 5-1}$$

^{19}F spin–spin relaxation times (T_2) were measured using the Carr–Purcell–Meiboom–Gill (CPMG).[120] The relaxation delay was 20 s and the acquisition time was 1.1 s. Data were collected using a spectral width of 9.4 kHz, and 128-512 scans. For each measurement, the delay times ranged from 8 ms to 1.2 s and 12 points were collected. T_2 was then calculated by TopSpin 3 using area type fitting. A single-component exponential decay fit was used (Equation 5-2).

$$I(\tau) = P\exp\left(-\frac{\tau}{T_2}\right) \qquad \textit{Equation 5-2}$$

Dynamic Light Scattering

Hydrodynamic diameters of the 5-FU polymer conjugate in PBS at pH 5.5 and 7.4 were determined by dynamic light scattering (DLS) using a Brookhaven NanoBrook Ver. 2.2 instrument operated at 25 ˚C. All measurements were made in triplicate. DLS autocorrelation function (ACF) curve of 5-FU polymer conjugate is shown in Figure. A-5

Chapter 6 Conclusions and future work

6.1 Conclucions

The aim of this project was to develop a new ^{19}F MRI contrast agent based upon SHBPs conjugated with degradable peptide containing 5-FU in its α C-terminal glycine residue.

Initially, a series of SHBP-DMAs were synthesised by RAFT copolymerisation of DMA with polymerisable CTM, i.e. VBPC. For comparison, homo L-PDMA using non-polymerisable CTA, BPC, was also synthesised. Very high molecular weight SHB-PDMAs (13.5 – 33.0 kDa) with high Đ in the range of 1.8 – 11.9 were obtained different from L-PDMA that has a controlled Đ of 1.13. Both the effect of the feed ratio and the reaction concentration on RAFT-SCVP were evaluated. The feed ratio affected the degree of branching and the chain length hence the molecular weight. In contrast, the reaction concentration did not influence the degree of branching but greatly influenced both the molecular weight and dispersity: higher concentrations led to higher molecular weight polymers but greater dispersity.

Kinetic study revealed that styryl polymerisable group of VBPC completely consumed at early stage of the polymerisation accompanied with little polymerisation activity of DMA. As a result of the unequal reactivity, the reaction probably did not proceed by an ideal SCVP mechanism and the polymer formed was more likely a hyperstar polymer. If SHBPs are desired, an acrylamide based CTM with similar reactivity with DMA would be more appropriate to be copolymerised with DMA. Since star polymers exhibit similar desirable properties of SHBPs such as 3-D constrained shape and large number of end groups, these polymers were taken further to synthesise 5-FU polymer conjugates. Furthermore, among various polymers, only $\gamma = 50$ was taken further because of their high molecular weight compared with other systems.

These polymers contained the thiocarbonylthio moiety at the chain ends for the conjugation of peptide containing 5-FU. The retention of thiocarbonylthio end groups was 76-86%, possibly due to bimolecular termination reaction enhanced by the high conversion achieved during the polymerisation. Lower conversion could be targeted to avoid undesired termination and to achieve high fidelity of thiocarbonylthio terminals.

With the aim to synthesise Gly-Leu-Phe-Gly-Leu-Gly-5-FU, the dipeptide, Leu-Gly-α-(5-FU), and the vinyl modified tetra-peptide, Gly-Phe-Leu-Gly were synthesised. The coupling reaction in solution to form the desired hexapeptide resulted in a low concentration of impure product. Therefore the tetrapeptide and dipeptide were directly conjugated to HS-PDMAs. This

was accomplished by a couple of steps; the attachment of the tetrapeptide via aminolysis/Michael addition chemistry and the attachment of the dipeptide after the activation with pentafluorophenol. Growing the peptides on the polymer surface helped to avoid undesired side products as the polymer was purified after each step by simple dialysis. Aminolysis/Michael addition was firstly investigated using a commercially available analogue, *N*-hydroxyethyl acrylamide (HEA). Aminolysis of thiocarbonylthio end groups and Michael addition of HEA were performed *in situ* without isolation of the thiol intermediates. The major challenge was the formation of disulfide coupled species as a result of thiol oxidation. This was observed as cross-linked material for high molecular weight polymers or high molecular weight contaminants as suggested by GPC for low molecular weight polymers. The formation of such disulfide species was eliminated by the use of Me_2PPh. Based on these results, 5-FU polymer conjugate was synthesised using HS-PDMA-30 wt% as a polymer carrier because of its reasonable molecular weight and size along with its less probability to form cross-linked material. Furthermore, the conjugation of the vinyl-modified peptide was carried out in the presence of Me_2PPh giving quantitative conjugation.

Finally, the ability to monitor the release of 5-FU from the polymer carrier was examined. ^{19}F nuclei within 5-FU polymer conjugate and the free 5-FU have significantly different mobility due to their different molecular sizes. This different in change was measured by ^{19}F T_2 relaxation times. Upon treatment with S9 fraction, free 5-FU was released accompanied with a significant increase of its T_2 relaxation times from 0.038 s to 0.128 s. However, S9 fraction showed low efficiency of only 9% 5-FU release. Therefore, 5-FU release could not be further evaluated using ^{19}F MRI phantom imaging. 5-FU release must be maximized to enhance the signal-to-noise ratio as the fluorine concentration is directly proportional to ^{19}F MRI signal intensity. Furthermore, 5-FU showed very long T_2 relaxation time at pH 5.5 compared with physiological pH. Thus, a more pronounced signal intensity switch would be expected upon enzymatic hydrolysis using lysosomal enzyme. The proof-of principle experiment could be further investigated using lysosomal enzymes at acidic pH to get better understanding about 5-FU release and ^{19}F MRI properties in a tumour environment.

In principle, this approach is not limited for monitoring 5-FU release but could be applicable to monitor the release of other fluorinated drugs[303] and using other responsive linkers such as pH and redox.[165,170–172]

6.2 Future work

Based on the findings and conclusions of this work, the following future extensions are suggested:

- Although the ability of monitoring 5-FU release based on the change in T_2 relaxation times has been proofed using S9 at pH 7.4, it is crucial to evaluate the release of the drug at pH 5.5 using lysosomal cocktail that are usually overexpressed in the tumour (e.g. tritosomes and Cathepsin B). Putnam and Kopecek[179] reported a quantitative release of 5-FU and its derivatives from 5-FU polymer conjugates containing the same oligopeptide side chain using tritosomes (50.1 % free 5-FU) within 24 h. Furthermore, studying the release at low pH allows better understanding about the ^{19}F NMR switch in the tumour.
- In attempt even to increase the release of free 5-FU, 5-FU polymer conjugates with oligopeptide chains, having a (5-FU) glycine ethyl ester residue at the C-terminus could be synthesised. Nichifor *et al.*[181] reported that these conjugates showed greate instability in the presence of cathepsin B (50% free 5-FU release) and tritosomes (90% free 5-FU) within 4h. The dipeptide with ethyl ester can undergo chemical hydrolysis (due to the formation of diketopepridizine) along with the enzymatic hydrolysis increasing the release of free 5-FU.
- To attempt ^{19}F MRI phantom in order to visualise 5-FU release and verify the practical applicability of the probe and its sensing principle
- The original polymer formed was probably an ill-defined hyper-star polymer. It would be interesting to synthesise uniform hyper-branched polymer by using an acrylamide based chain transfer monomer that should have similar reactivity to DMA.
- To increase the loading of 5-FU required for enhancing ^{19}F MRI signal intensity. High 5-FU capacity can be achieved by tuning [DMA]:[VBPC] ratio. Low [DMA]:[VBPC] ratio will result in higher number of terminals for higher concentration of 5-FU. High concentration of fluorine is expected to increase the signal-to-noise ratio and hence the intensity of the image but in the same time can cause an aggregation reducing T_2 relaxation times. Therefore, this should be finely tuned and further studied.

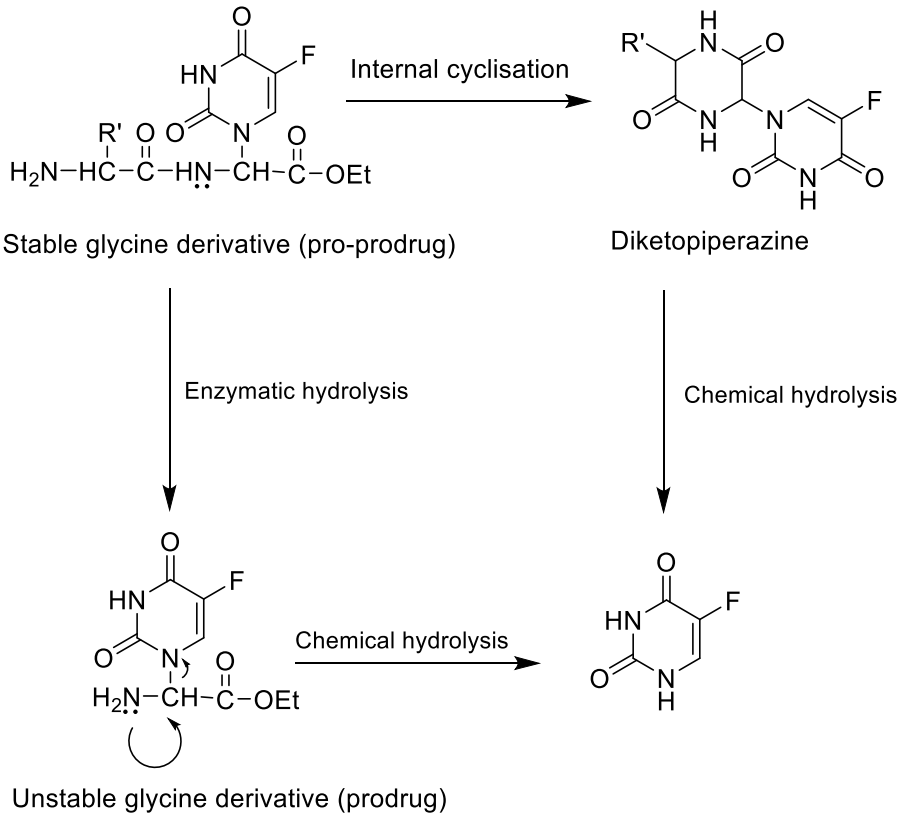

Scheme 6-1.The dipeptide with glycine ethyl ester residue can undergo enzymatic or chemical hydrolysis to release 5-FU.

References

1 G. Patterson, *A Prehistory of Polymer Science*, Springer, 2012.

2 M. M. Coleman and P. C. Painter, *Fundamentals of Polymer Science: An Introductory Text, Second Edition*, CRC Press, 2nd edn., 1998.

3 F. W. Billmeyer, *Textbook of Polymer Science, 3rd Edition*, John Wiley & Sons, 3rd edn., 1984.

4 R. D. Deanin, *Polymer structure, properties, and applications*, Boston, Cahners Books, 1972.

5 W.-F. Su, *Principles of Polymer Design and Synthesis*, 2013, vol. 82.

6 W. H. Carothers, *J. Am. Chem. Soc.*, 1929, **51**, 2548–2559.

7 P. J. Flory, *Chem. Rev.*, 1946, **39**, 137–197.

8 W. H. Carothers, *Chem. Rev.*, 1931, **8**, 353–426.

9 H. Carothers, *Trans. Faraday Soc*, 1936, **32**, 39–49.

10 W. H. Carothers and G. J. Berchet, *J. Am. Chem. Soc.*, 1930, **52**, 5289–5291.

11 E. Saldivar-Guerra and E. Vivalodo-Lima, *Handbook of Polymer Synthesis, Characterization, and Processing*, John Wiley & Sons, 2013.

12 G. Odian, *Principle of Polymerization*, John Wiley & Sons, Fourth Edi., 2004.

13 K. Ziegler and K. Buehr, *Berichte der Dtsch. Chem. Gesellschaft A B Ser.*, 1928, **61**, 253–263.

14 M. Szwarc, *Nature*, 1956, **178**, 1168–1169.

15 G. Polymeropoulos, G. Zapsas, K. Ntetsikas, P. Bilalis, Y. Gnanou and N. Hadjichristidis, *Macromolecules*, 2017, **50**, 1253–1290.

16 N. Hadjichristidis, H. Iatrou, S. Pispas and M. Pitsikalis, *J. Polym. Sci. Part A Polym. Chem.*, 2000, **38**, 3211–3234.

17 J.-E. Rempp, P; Franta, E; Herz, *Adv. Polym. Sci.*, 1988, **86**, 145–173.

18 K. Matyjaszewski, *Handbook of Radical Polymerization*, John Wiley & Sons, 2002.

19 J. S. Wang and K. Matyjaszewski, *Macromolecules*, 1995, **28**, 7901–7910.

20 J. S. Wang and K. Matyjaszewski, *J. Am. Chem. Soc.*, 1995, **117**, 5614–5615.

21 M. Kato, M. Kamigaito, M. Sawamoto and T. Higashimura, *Macromolecules*, 1995, **28**, 1721–1723.

22 M. K. Georges, R. P. N. Veregin, P. M. Kazmaier and G. K. Hamer, *Macromolecules*, 1993, **26**, 2987–2988.

23 J. Chiefari, Y. K. Chong, F. Ercole, J. Krstina, J. Jeffery, T. P. T. Le, R. T. A.

Mayadunne, G. F. Meijs, C. L. Moad, G. Moad, E. Rizzardo and S. H. Thang, *Macromolecules*, 1998, **31**, 5559–5562.

24 K. Matyjaszewski, *ACS Symp. Ser.*, 1998, **685**, 2–30.

25 W. A. Braunecker and K. Matyjaszewski, *Prog. Polym. Sci.*, 2007, **32**, 93–146.

26 K. Matyjaszewski, *Adv. Mater.*, 2018, **30**, 1–22.

27 D. J. Keddie, *Chem. Soc. Rev.*, 2014, **43**, 496–505.

28 H. Willcock and R. K. O'Reilly, *Polym. Chem.*, 2010, **1**, 149–157.

29 G. Moad, E. Rizzardo and S. H. Thang, *Polym. Int.*, 2011, **60**, 9–25.

30 D. J. Keddie, G. Moad, E. Rizzardo and S. H. Thang, *Macromolecules*, 2012, **45**, 5321–5342.

31 S. Perrier, *Macromolecules*, 2017, **50**, 7433–7447.

32 M. R. Hill, R. N. Carmean and B. S. Sumerlin, *Macromolecules*, 2015, **48**, 5459–5469.

33 S. Perrier and P. Takolpuckdee, *J. Polym. Sci. Part A Polym. Chem.*, 2005, **43**, 5347–5393.

34 K. Matyjaszewski, *Macromol. Symp.*, 2012, **45**, 4015–4039.

35 R. B. Grubbs and R. B. Grubbs, *Polym. Rev.*, 2011, **51**, 104–137.

36 G. Moad, J. Chiefari, Y. K. Chong, J. Krstina, R. T. A. Mayadunne, A. Postma, E. Rizzardo and S. H. Thang, *Polym. Int.*, 2000, **49**, 993–1001.

37 G. Moad, J. Chiefari, R. T. A. Mayadunne, C. L. Moad, A. Postma, E. Rizzardo and S. H. Thang, *Macromol. Symp.*, 2002, **182**, 65–80.

38 T. Yildirim, A. C. Rinkenauer, C. Weber, A. Traeger, S. Schubert and U. S. Schubert, *J. Polym. Sci. Part A Polym. Chem.*, 2015, **53**, 2711–2721.

39 S. Harrisson, X. Liu, J.-N. Ollagnier, O. Coutelier, J.-D. Marty and M. Destarac, *Polymers (Basel).*, 2014, **6**, 1437–1488.

40 M. Destarac, *Polym. Rev.*, 2011, **51**, 163–187.

41 G. Moad, E. Rizzardo and S. H. Thang, *Aust. J. Chem.*, 2009, **62**, 1402–1472.

42 R. T. A. Mayadunne, E. Rizzardo, J. Chiefari, J. Krstina, G. Moad, A. Postma and S. H. Thang, *Macromolecules*, 2000, **33**, 243–245.

43 R. T. A. Mayadunne, E. Rizzardo, J. Chiefari, Y. K. Chong, G. Moad and S. H. Thang, *Macromolecules*, 1999, **32**, 6977–6980.

44 M. Destarac, D. Charmot, X. Franck and S. Z. Zard, *Macromol. Rapid Commun.*, 2000, **21**, 1035–1039.

45 M. H. Stenzel, L. Cummins, G. E. Roberts, T. P. Davis, P. Vana and C. Barner-Kowollik, *Macromol. Chem. Phys.*, 2003, **204**, 1160–1168.

46 D. J. Keddie, C. Guerrero-Sanchez, G. Moad, E. Rizzardo and S. H. Thang, *Macromolecules*, 2011, **44**, 6738–6745.

47 M. Benaglia, M. Chen, Y. K. Chong, G. Moad, E. Rizzardo and S. H. Thang, *Macromolecules*, 2009, **42**, 9384–9386.

48 D. J. Keddie, C. Guerrero-Sanchez, G. Moad, R. J. Mulder, E. Rizzardo and S. H. Thang, *Macromolecules*, 2012, **45**, 4205–4215.

49 M. Benaglia, J. Chiefari, Y. K. Chong, G. Moad, E. Rizzardo and S. H. Thang, *J. Am. Chem. Soc.*, 2009, **131**, 6914–6915.

50 M. J. Monteiro and H. De Brouwer, *Macromolecules*, 2001, **34**, 349–352.

51 M. J. Monteiro, R. Bussels, S. Beuermann and M. Buback, *Aust. J. Chem.*, 2002, **55**, 433–437.

52 B. Y. K. Chong, J. Krstina, T. P. T. Le, G. Moad, A. Postma, E. Rizzardo and S. H. Thang, *Macromolecules*, 2003, **36**, 2256–2272.

53 L. I. Chunzhao and B. C. Benicewicz, *J. Polym. Sci. Part A Polym. Chem.*, 2005, **43**, 1535–1543.

54 M. S. Donovan, A. B. Lowe, B. S. Sumerlin and C. L. McCormick, *Macromolecules*, 2002, **35**, 4123–4132.

55 S. Perrier, C. Barner-Kowollik, J. F. Quinn, P. Vana and T. P. Davis, *Macromolecules*, 2002, **35**, 8300–8306.

56 M. Benaglia, E. Rizzardo, A. Alberti and M. Guerra, *Macromolecules*, 2005, **38**, 3129–3140.

57 G. Moad, Y. K. Chong, A. Postma, E. Rizzardo and S. H. Thang, *Polymer (Guildf).*, 2005, **46**, 8458–8468.

58 D. A. Tomalia and J. M. J. Fréchet, *J. Polym. Sci. Part A Polym. Chem.*, 2002, **40**, 2719–2728.

59 D. A. Tomalia, *Prog. Polym. Sci.*, 2005, **30**, 294–324.

60 A. Carlmark, C. Hawker, A. Hult and M. Malkoch, *Chem. Soc. Rev.*, 2009, **38**, 352–362.

61 D. A. Tomalia, H. Baker, J. Dewald, M. Hall, G. Kallos, S. Martin, J. Roeck, J. Ryder and P. Smith, *Polym. J.*, 1985, **17**, 117–132.

62 C. J. Hawker and J. M. J. Fréchet, *J. Am. Chem. Soc.*, 1990, **112**, 7638–7647.

63 V. Gupta and S. K. Nayak, *J. Appl. Pharm. Sci.*, 2015, **5**, 117–122.

64 G. M. Dykes, *J. Chem. Technol. Biotecnol.*, 2001, **76**, 903–918.

65 C. Gao and D. Yan, *Prog. Polym. Sci.*, 2004, **29**, 183–275.

66 R. M. England and S. Rimmer, *Polym. Chem.*, 2010, **1**, 1533.

67 B. Voit, B. I. Voit and A. Lederer, *Chem. Rev.*, 2009, **109**, 5924–5973.
68 P. J. Flory, *J. Am. Chem. Soc.*, 1952, **74**, 2718–2723.
69 P. A. Gunatillake, G. Odian and D. A. Tomalia, *Macromolecules*, 1988, **21**, 1556–1562.
70 Y. H. Kim and O. W. Webster, *J. Am. Chem. Soc.*, 1990, **112**, 4592–4593.
71 Y. H. Kim and O. W. Webster, *Macromolecules*, 1992, **25**, 5561–5572.
72 T. Emrick, H.-T. Chang and J. M. J. Fréchet, *Macromolecules*, 1999, **32**, 6380–6382.
73 N. O'Brien, A. McKee, D. C. Sherrington, A. T. Slark and A. Titterton, *Polymer (Guildf).*, 2000, **41**, 6027–6031.
74 P. . Costello, I. . Martin, A. . Slark, D. . Sherrington and A. Titterton, *Polymer (Guildf).*, 2002, **43**, 245–254.
75 M. Liu, N. Vladimirov and J. M. J. Fréchet, *Macromolecules*, 1999, **32**, 6881–6884.
76 D. Yan, J. Hou, X. Zhu, J. J. Kosman and H. S. Wu, *Macromol. Rapid Commun.*, 2000, **21**, 557–561.
77 J. M. J. Frechet, M. Henmi, I. Gitsov, S. Aoshima, M. R. Leduc and R. B. Grubbs, *Science*, 1995, **269**, 1080–1083.
78 G. I. Litvinenko, P. F. W. Simon and A. H. E. Müller, *Macromolecules*, 1999, **32**, 2410–2419.
79 J. A. Alfurhood, P. R. Bachler and B. S. Sumerlin, *Polym. Chem.*, 2016, **7**, 3361–3369.
80 G. I. Litvinenko and A. H. E. Müller, *Macromolecules*, 2002, **35**, 4577–4583.
81 D. Baskaran, *Macromol. Chem. Phys.*, 2001, **202**, 1569–1575.
82 D. Baskaran, *Polymer (Guildf).*, 2003, **44**, 2213–2220.
83 C. J. Hawker, J. Dao, J. M. J. Fréchet and R. B. Grubbs, *J. Am. Chem. Soc.*, 1995, **117**, 10763–10764.
84 Y. Tao, J. He, Z. Wang, J. Pan, H. Jiang, S. Chen and Y. Yang, *Macromolecules*, 2001, **34**, 4742–4748.
85 S. G. Gaynor, S. Edelman and K. Matyjaszewski, *Macromolecules*, 1996, **29**, 1079–1081.
86 K. Matyjaszewski, S. G. Gaynor and A. H. E. Müller, *Macromolecules*, 1997, **30**, 7034–7041.
87 M. W. Weimer, J. M. J. Fréchet and I. Gitsov, *J. Polym. Sci. Part A Polym. Chem.*, 1998, **36**, 955–970.
88 R. W. Graff, X. Wang and H. Gao, *Macromolecules*, 2015, **48**, 2118–2126.
89 Z. Wang, J. He, Y. Tao, L. Yang, H. Jiang and Y. Yang, *Macromolecules*, 2003, **36**, 7446–7452.

90 X. Wang and H. Gao, *Polymers (Basel).*, 2017, **9**, 188.

91 S. Carter, B. Hunt and S. Rimmer, *Macromolecules*, 2005, **38**, 4595–4603.

92 A. J. Heidenreich, J. E. Puskas, W. F. Reed and A. M. Alb, *J. Polym. Sci. Part A Polym. Chem.*, 2008, **46**, 7621–7627.

93 M. Rikkou-Kalourkoti, M. Elladiou and C. S. Patrickios, *J. Polym. Sci. Part A Polym. Chem.*, 2015, **53**, 1310–1319.

94 L. Platt, L. Kelly and S. Rimmer, *J. Mater. Chem. B.*, 2014, **2**, 494–501.

95 S. Carter, S. Rimmer, A. Sturdy and M. Webb, *Macromol. Biosci.*, 2005, **5**, 373–378.

96 U. Haldar, S. G. Roy and P. De, *Polym. (United Kingdom)*, 2016, **97**, 113–121.

97 J. Schmitt, N. Blanchard and J. Poly, *Polym. Chem.*, 2011, **2**, 2231.

98 S. Ghosh Roy and P. De, *Polym. Chem.*, 2014, **5**, 6365–6378.

99 S. Rimmer, S. Carter, R. Rutkaite, J. W. Haycock and L. Swanson, *Soft Matter*, 2007, **3**, 971–973.

100 L. Shallcross, K. Roche, C. J. Wilcock, K. T. Stanton, T. Swift, S. Rimmer, P. V. Hatton and S. G. Spain, *J. Mater. Chem. B*, 2017, **5**, 6027–6033.

101 J. Han, S. Li, A. Tang and C. Gao, *Macromolecules*, 2012, **45**, 4966–4977.

102 C. Zhang, Y. Zhou, Q. Liu, S. Li, S. Perrier and Y. Zhao, *Macromolecules*, 2011, **44**, 2034–2049.

103 Y. Zhang, B. M. Teo, A. Postma, F. Ercole, R. Ogaki, M. Zhu and B. Städler, *J. Phys. Chem. B*, 2013, **117**, 10504–10512.

104 Y. Zhuang, H. Deng, Y. Su, L. He, R. Wang, G. Tong, D. He and X. Zhu, *Biomacromolecules*, 2016, **17**, 2050–2062.

105 C. Li, H. Liu, D. Tang and Y. Zhao, *Polym. Chem.*, 2015, **6**, 1474–1486.

106 J. A. Alfurhood, H. Sun, P. R. Bachler and B. S. Sumerlin, *Polym. Chem.*, 2016, **7**, 2099–2104.

107 R. Plenderleith, T. Swift and S. Rimmer, *RSC Adv.*, 2014, **4**, 50932–50937.

108 X. Zhou, J. Zhu, M. Xing, Z. Zhang, Z. Cheng, N. Zhou and X. Zhu, *Eur. Polym. J.*, 2011, **47**, 1912–1922.

109 Y. Sudo, R. Kawai, Y. Nabae, T. Hayakawa and M. aki Kakimoto, *Appl. Surf. Sci.*, 2018, **3**, 166.

110 G. I. Litvinenko, P. F. W. Simon and A. H. E. Müller, *Macromolecules*, 2001, **34**, 2418–2426.

111 S. Li, J. Han and C. Gao, *Polym. Chem.*, 2013, **4**, 1774–1787.

112 X. Hu, G. Liu, Y. Li, X. Wang and S. Liu, *J. Am. Chem. Soc.*, 2015, **137**, 362–368.

121

113 K. Wang, H. Peng, K. J. Thurecht, S. Puttick and A. K. Whittaker, *Biomacromolecules*, 2015, **16**, 2827–2839.

114 J. Huang, L. Lin, H. Liang and J. Lu, *Polym. Chem.*, 2015, **6**, 4020–4029.

115 A. P. Vogt, S. R. Gondi and B. S. Sumerlin, *Aust. J. Chem.*, 2007, **60**, 396–399.

116 P. C. Lauterbur, *Nature*, 1973, **242**, 190.

117 M. L. James and S. S. Gambhir, *Physiol. Rev.*, 2012, **92**, 897–965.

118 P. Debbage and W. Jaschke, *Histochem. Cell Biol.*, 2008, **130**, 845–875.

119 Z. Y. Chen, Y. X. Wang, Y. Lin, J. S. Zhang, F. Yang, Q. L. Zhou and Y. Y. Liao, *Biomed Res. Int.*, , DOI:10.1155/2014/819324.

120 R. K. Harris, *Nuclear Magnetic Resonance Spectroscopy: A Physicochemical View*, Pitman, 1983.

121 T. L. James, *Control*, 1998, **27**, 1–31.

122 D. J. Wink, *J. Chem. Educ.*, 1989, **66**, 810.

123 R. B. Lauffer, *Chem. Rev.*, 1987, **87**, 901–927.

124 M. Bottrill, L. Kwok and N. J. Long, *Chem. Soc. Rev.*, 2006, **35**, 557–571.

125 D. V Hingorani, A. S. Bernstein and M. D. Pagel, *Contrast Media Mol. Imaging 2015*, 2015, **10**, 245–265.

126 P. Caravan, J. J. Ellison, T. J. McMurry and R. B. Lauffer, *Chem. Rev.*, 1999, **99**, 2293–2352.

127 S. Aime, M. Botta and E. Terreno, *Adv. Inorg. Chem.*, 2005, **57**, 173–237.

128 J. W. M. Bulte and D. L. Kraitchman, *NMR Biomed.*, 2004, **17**, 484–499.

129 S. Laurent, D. Forge, M. Port, a Roch, C. Robic, L. V Elst and R. N. Muller, *Chem. Rev.*, 2008, **108**, 2064–2110.

130 X. H. Peng, X. Qian, H. Mao, a Y. Wang, Z. G. Chen, S. Nie and D. M. Shin, *Int. J. Nanomedicine*, 2008, **3**, 311–321.

131 R. F. Code, J. E. Harrison, K. G. Mcneill and M. Szyjkowski, *Magn. Reson. Med*, 1990, **13**, 358–369.

132 F. A. Bovey, *Nuclear Magnetic Resonance Spectroscopy*, Academic Press, 2nd edn., 1988.

133 G. . Holland, P. . Bottomley and W. . Hinshaw, *J. Magn. Reson.*, 1977, **28**, 133–136.

134 E. McFarland, J. A. Koutcher, B. R. Rosen, B. Teicher and T. J. Brady, *J. Comput. Assist. Tomogr.*, 1985, **9**, 8–15.

135 Z. Bober, D. Aebisher, Ł. Ożóg, J. Tabarkiewicz, P. Tutka and D. Bartusik-Aebisher, *Eur. J. Clin. Exp. Med.*, 2017, **15**, 109–119.

136 D. Zhao, A. Constantinescu, L. Jiang, E. W. Hahn and R. P. Mason, *Am. J. Clin. Oncol. Cancer Clin. Trials*, 2001, **24**, 462–466.

137 M. Srinivas, A. Heerschap, E. T. Ahrens, C. G. Figdor and I. J. M. de Vries, *Trends Biotechnol.*, 2010, **28**, 363–370.

138 M. Srinivas, P. Boehm-Sturm, C. G. Figdor, I. J. de Vries and M. Hoehn, *Biomaterials*, 2012, **33**, 8830–8840.

139 H. Amiri, M. Srinivas, A. Veltien, M. J. van Uden, I. J. M. de Vries and A. Heerschap, *Eur. Radiol.*, 2015, **25**, 726–735.

140 J. Yu, V. Kodibagkar, W. Cui and R. Mason, *Curr. Med. Chem.*, 2005, **12**, 819–848.

141 J. Chen, G. M. Lanza and S. A. Wickline, *Wiley Interdiscip. Rev. Nanomedicine Nanobiotechnology*, 2010, **2**, 431–440.

142 U. Nöth, S. P. Morrissey, R. Deichmann, S. Jung, H. Adolf, A. Haase and J. Lutz, *Artif. Cells. Blood Substit. Immobil. Biotechnol.*, 1997, **25**, 243–254.

143 M. L. Gregory, M. W. Patrick, M. N. Anne and A. W. Shelton, D. Caruthers Franklin, D. Hockett Samuel, *Curr. Top. Dev. Biol.*, 2005, **70**, 57–76.

144 X. Fan, J. N. River, A. S. Muresan, C. Popescu, M. Zamora, R. M. Culp and G. S. Karczmar, *Phys. Med. Biol.*, 2006, **51**, 211–220.

145 X. Fan, J. N. River, M. Zamora, H. A. Al-Hallaq and G. S. Karczmar, *Int. J. Radiat. Oncol. Biol. Phys.*, 2002, **54**, 1202–1209.

146 R. Díaz-López, N. Tsapis and E. Fattal, *Pharm. Res.*, 2010, **27**, 1–16.

147 T. D. Tran, S. D. Caruthers, M. Hughes, J. N. Marsh, T. Cyrus, P. M. Winter, A. M. Neubauer, S. A. Wickline and G. M. Lanza, *Int J Nanomedicine*, 2007, **2**, 515–526.

148 J. C. Knight, P. G. Edwards and S. J. Paisey, *RSC Adv.*, 2011, **1**, 1415.

149 I. Tirotta, V. Dichiarante, C. Pigliacelli, G. Cavallo, G. Terraneo, F. B. Bombelli, P. Metrangolo and G. Resnati, *Chem. Rev.*, 2015, **115**, 1106–1129.

150 R. E. Hendrick, *Magn. Reson. Imaging*, 1987, **5**, 31–37.

151 Z. Jiang, X. Liu, E. Jeong and Y. B. Yu, *Chem. Int. Ed.*, 2009, **48**, 4755–4758.

152 P. A. Mirau, *A Practical Guide to Undertanding the NMR of Polymers*, John Wiley & Sons, 2005.

153 N. Bloembergen, E. M. Purcell and R. V. Pound, *Phys. Rev.*, 1948, **73**, 679–712.

154 M. E. M. E. Smith and J. H. H. Strange, *Meas. Sci. Technol.*, 1996, **7**, 449–475.

155 A. M. Nystrom, J. W. Bartels, W. Du and K. L. Wooley, *J. Polym. Sci. Part A Polym. Chem.*, 2008, **47**, 1023–1037.

156 H. Peng, I. Blakey, B. Dargaville, F. Rasoul, S. Rose and A. K. Whittaker, 2009, 374–

381.

157 W. J. Du, A. M. Nystrom, L. Zhang, K. T. Powell, Y. L. Li, C. Cheng, S. A. Wickline and K. L. Wooley, *Biomacromolecules*, 2008, **9**, 2826–2833.

158 W. Zhao, H. T. Ta, C. Zhang and A. K. Whittaker, *Biomacromolecules*, 2017, **18**, 1145–1156.

159 C. Fu, S. Herbst, C. Zhang and A. K. Whittaker, *Polym. Chem.*, 2017, 4585–4595.

160 C. Zhang, S. S. Moonshi, Y. Han, S. Puttick, H. Peng, B. J. A. Magoling, J. C. Reid, S. Bernardi, D. J. Searles, P. Král and A. K. Whittaker, *Macromolecules*, 2017, **50**, 5953–5963.

161 K. Wang, H. Peng, K. J. Thurecht and A. K. Whittaker, *Macromol. Chem. Phys.*, 2016, **217**, 2262–2274.

162 K. Wang, H. Peng, K. J. Thurecht, S. Puttick and A. K. Whittaker, *Polym. Chem.*, 2016, **7**, 1059–1069.

163 B. E. Rolfe, I. Blakey, O. Squires, H. Peng, N. R. B. Boase, C. Alexander, P. G. Parsons, G. M. Boyle, A. K. Whittaker and K. J. Thurecht, *J. Am. Chem. Soc.*, 2014, **136**, 2413–2419.

164 K. J. Thurecht, I. Blakey, H. Peng, O. Squires, S. Hsu, C. Alexander and A. K. Whittaker, *J. Am. Chem. Soc.*, 2010, **132**, 5336–5337.

165 S. Ganta, H. Devalapally, A. Shahiwala and M. Amiji, *J. Control. Release*, 2008, **126**, 187–204.

166 L. Nurmi, H. Peng, J. Seppala, D. M. Haddleton, I. Blakey and A. K. Whittaker, *Polym. Chem.*, 2010, **1**, 1039–1047.

167 K. Wang, H. Peng, K. J. Thurecht, S. Puttick and A. K. Whittaker, *Polym. Chem.*, 2013, **4**, 4480.

168 K. Wang, H. Peng, K. J. Thurecht, S. Puttick and A. K. Whittaker, *Polym. Chem.*, 2014, **5**, 1760–1771.

169 A. V. Fuchs, A. P. Bapat, G. J. Cowin and K. J. Thurecht, *Polym. Chem.*, 2017, **8**, 5157–5166.

170 M. Mittal, M. R. Siddiqui, K. Tran, S. P. Reddy and A. B. Malik, 2014, **20**, 1126–1167.

171 K. Sugamura and J. F. Keaney, *Free Radic. Biol. Med.*, 2011, **51**, 978–992.

172 B. Kumar, S. Koul, L. Khandrika, R. B. Meacham and H. K. Koul, 2008, **68**, 1777–1786.

173 V. D. Kodibagkar, J. Yu, L. Liu, H. P. Hetherington and R. P. Mason, *Magn. Reson. Imaging*, 2006, **24**, 959–962.

174 L. Liu, V. D. Kodibagkar, J.-X. Yu and R. P. Mason, *FASEB J.*, 2007, **21**, 2014–2019.
175 J. Yu, P. Otten, Z. Ma, W. Cui, L. Liu and R. P. Mason, *Bioconjug. Chem.*, 2004, **15**, 1334–1341.
176 S. Mizukami, R. Takikawa, F. Sugihara, Y. Hori, H. Tochio, M. Wälchli, M. Shirakawa and K. Kikuchi, *J. Am. Chem. Soc.*, 2008, **130**, 794–795.
177 S. Mizukami, R. Takikawa, F. Sugihara, M. Shirakawa and K. Kikuchi, *Angew. Chemie - Int. Ed.*, 2009, **48**, 3641–3643.
178 S. Mizukami, H. Matsushita, R. Takikawa, F. Sugihara, M. Shirakawa and K. Kikuchi, *Chem. Sci.*, 2011, **2**, 1151–1155.
179 D. Putnam and J. Kopeček, *Bioconjug. Chem.*, 1995, **6**, 483–492.
180 D. A. Putnam, J. G. Shiah and J. Kopeček, *Biochem. Pharmacol.*, 1996, **52**, 957–962.
181 M. Nichifor, E. H. Schacht and L. W. Seymour, *J. Control. Release*, 1997, **48**, 165–178.
182 M. Nichifor, E. H. Schacht and L. W. Seymour, *J. Control. Release*, 1996, **39**, 79–92.
183 T. Ouchi, A. Fujino, K. Tanaka and T. Banba, *J. Control. Release*, 1990, **12**, 143–153.
184 J. L. Grem, *Invest. New Drugs*, 2000, **18**, 299–313.
185 D. B. Longley, D. P. Harkin and P. G. Johnston, *Nat. Rev. Cancer*, 2003, **3**, 330–338.
186 M. Malet-Martino and R. Martino, *Oncologist*, 2002, **7**, 288–323.
187 S. Ozaki and T. Akiyama, *Polym. J.*, 1989, **21**, 955–958.
188 K. H. T. Ouchi, T. I. M.Keashima and T. Tashiro, *J. Control. Release*, 1988, **8**, 141–150.
189 Y. OHYA, K. INOSAKA and T. OUCHI, *Synthesis and antitumor activity of 6-O-carboxymethyl chitin fixing 5-fluorouracils through pentamethylene, monomethylene spacer groups via amide, ester bonds*, 1992, vol. 40.
190 M. Nichifor, V. Coessens and E. H. Schacht, *J. Bioact. Compat. Polym.*, 1995, **10**, 199–222.
191 W. D. Kingsbury, J. C. Boehm, R. J. Mehta, S. F. Grappel and C. Gilvarg, *J. Med. Chem.*, 1984, **27**, 1447–1451.
192 I. Coin, M. Beyermann and M. Bienert, *Nat. Protoc.*, 2007, **2**, 3247–3256.
193 M. Jikei and M. Kakimoto, *Prog. Polym. Sci.*, 2001, **26**, 1233–1285.
194 M. Calderón, M. A. Quadir, S. K. Sharma and R. Haag, *Adv. Mater.*, 2010, **22**, 190–218.
195 L. R. Hutchings, J. M. Dodds and S. J. Roberts-Bleming, *Macromolecules*, 2005, **38**, 5970–5980.
196 L. R. Hutchings, J. M. Dodds and S. J. Roberts-Bleming, *Macromol. Symp.*, 2006, **240**, 56–67.

197 L. R. Hutchings, J. M. Dodds, D. Rees, S. M. Kimani, J. J. Wu and E. Smith, *Macromolecules*, 2009, **42**, 8675–8687.

198 S. Unal, I. Yilgor, E. Yilgor, J. P. Sheth, G. L. Wilkes and T. E. Long, *Macromolecules*, 2004, **37**, 7081–7084.

199 S. Unal and T. E. Long, *Macromolecules*, 2006, **39**, 2788–2793.

200 A. R. Fornof, T. E. Glass and T. E. Long, *Macromol. Chem. Phys.*, 2006, **207**, 1197–1206.

201 K. Matyjaszewski, S. G. Gaynor, A. Kulfan and M. Podwika, *Macromolecules*, 1997, **30**, 5192–5194.

202 P. R. Bachler, K. E. Forry, C. A. Sparks, M. D. Schulz, K. B. Wagener and B. S. Sumerlin, *Polym. Chem.*, 2016, **7**, 4155–4159.

203 C. J. Hawker, R. Lee and J. M. J. Frechet, *J. Am. Chem. Soc.*, 1991, **113**, 4583–4588.

204 D. Holtel, A. Burgath and H. Frey, *Acta Polym.*, 1997, **48**, 30–35.

205 D. Yan and A. H. E. Mu, *Macromolecules*, 1997, **30**, 7024–7033.

206 L. J. Hobson and W. J. Feast, *Chem. Commun.*, 1997, **0**, 2067–2068.

207 G. M. I, C. Zech, B. Voit and H. Kornbe, *Macromol. Chem. Phys.*, 1998, **199**, 2655–2664.

208 C. M. Nunez, B. Sen Chiou, A. L. Andrady and S. A. Khan, *Macromolecules*, 2000, **33**, 1720–1726.

209 P. F. W. Simon, A. H. E. Müller and T. Pakula, *Macromolecules*, 2001, **34**, 1677–1684.

210 P. J. Wyatt, *Anal. Chim. Acta*, 1993, **272**, 1–40.

211 P. J. Wyatt, *J. Chromatogr. A*, 1993, **648**, 27–32.

212 Z. Grubisic, P. Rempp and H. Benoit, *J. Polym. Sci. Part B Polym. Lett.*, 1967, **5**, 753–759.

213 S. Perrier, P. Takolpuckdee and C. A. Mars, *Macromolecules*, 2005, **38**, 2033–2036.

214 C. Barner-Kowollik, J. F. Quinn, D. R. Morsley and T. P. Davis, *J. Polym. Sci. Part A Polym. Chem.*, 2001, **39**, 1353–1365.

215 E. Fischer, *Berichte der Dtsch. Chem. Gesellschaft*, 1901, **34**, 433–454.

216 M. Bergmann and L. Zervas, *Berichte der Dtsch. Chem. Gesellschaft (A B Ser.*, 1932, **65**, 1192–1201.

217 G. W. Anderson, J. Blodinger and A. D. Welcher, *J. Am. Chem. Soc.*, 1952, **74**, 5309–5312.

218 V. Du Vigneaud, C. Ressler, J. M. Swan, C. W. Roberts, P. G. Katsoyannis and S. Gordon, *J. Am. Chem. Soc.*, 1953, **75**, 4879–4880.

219 B. Merrifield, *Science*, 1986, **232**, 341–347.
220 R. B. Merrifield, *J. Am. Chem. Soc.*, 1963, **85**, 2149–2154.
221 R. B. Merrifield, *Science*, 1965, **150**, 178–85.
222 V. Mäde, S. Els-Heindl and A. G. Beck-Sickinger, *Beilstein J. Org. Chem.*, 2014, **10**, 1197–1212.
223 E. Atherton, D. L. J. Clive and R. C. Sheppard, *J. Am. Chem. Soc.*, 1975, **97**, 6584–6585.
224 S. Zalipsky, J. L. Chang, F. Albericio and G. Barany, *React. Polym.*, 1994, **22**, 243–258.
225 E. Bayer, *Angew. Chemie - Int. Ed.*, 1991, **30**, 113–129.
226 R. Santini, M. C. Griffith and M. Qi, *Tetrahedron Lett.*, 1998, **39**, 8951–8954.
227 J. Alsina and F. Albericio, *Biopolym. - Pept. Sci. Sect.*, 2003, **71**, 454–477.
228 L. A. Carpino, *J. Am. Chem. Soc.*, 1957, **79**, 98–101.
229 L. A. Carpino and G. Y. Han, *J. Am. Chem. Soc.*, 1970, **92**, 5748–5749.
230 J. Meienhofer, M. Waki, E. P. Heimre, T. J. Lambros, R. C. Makofske and C.-D. Chang, *Int. J. Pept. Protein Res.*, 2009, **13**, 35–42.
231 G. W. Anderson and F. M. Callahan, *J. Am. Chem. Soc.*, 1960, **82**, 3359–3363.
232 C. Chang, M. Waki, M. Ahmad, J. Meienhofer, E. O. Lundell and J. D. Haug, *Int. J. Pept. Protein Res.*, 1980, **15**, 59–66.
233 R. Behrendt, P. White and J. Offer, *J. Pept. Sci.*, 2016, **22**, 4–27.
234 J. M. Palomo, *RSC Adv.*, 2014, **4**, 32658–32672.
235 J. Izdebski, A. Orlowska, R. Anulewicz, E. Witkowska and D. Fiertek, *Int. J. Pept. Protein Res.*, 2009, **43**, 184–189.
236 W. König and R. Geiger, *Chem. Ber.*, 1970, **103**, 788–798.
237 J. Coste, D. Le-Nguyen and B. Castro, *Tetrahedron Lett.*, 1990, **31**, 205–208.
238 R. Knorr, A. Trzeciak, W. Bannwarth and D. Gillessen, *Tetrahedron*, 1989, **30**, 1927–1930.
239 L. A. Carpino, *J. Am. Chem. Soc.*, 1993, **115**, 4397–4398.
240 S. sun Wang, *J. Am. Chem. Soc.*, 1973, **95**, 1328–1333.
241 V. K. Sarin, S. B. H. Kent and R. B. Merrifield, *J. Am. Chem. Soc.*, 1980, **102**, 5463–5470.
242 F. M. Wampler, *Plant/Operations Prog.*, 1988, **7**, 183–189.
243 S. Pokorný and J. Dneboský, *J. Dent.*, 1988, **16**, 76–79.
244 M. Fujita, Y. Iizuka and A. Miyake, *J. Therm. Anal. Calorim.*, 2017, **128**, 1227–1233.
245 M. Nkhifor and E. H. Schacht, *Tetrahedron*, 1994, **50**, 3747–3760.
246 A. J. Nollet and U. K. Pandit, *Tetrahedron Lett.*, 1969, **53**, 4605–4606.

247 G. Apitz and W. Steglich, *Tetrahedron Lett.*, 1991, **32**, 3163–3166.

248 A. M. Bivigou-Koumba, J. Kristen, A. Laschewsky, P. Müller-Buschbaum and C. M. Papadakis, *Macromol. Chem. Phys.*, 2009, **210**, 565–578.

249 J. F. Quinn, R. P. Chaplin and T. P. Davis, *J. Polym. Sci. Part A Polym. Chem.*, 2002, **40**, 2956–2966.

250 J. Xu, L. Tao, J. Liu, V. Bulmus and T. P. Davis, *Macromolecules*, 2009, **42**, 6893–6901.

251 A. Postma, T. P. Davis, G. Moad and M. S. O'Shea, *Macromolecules*, 2005, **38**, 5371–5374.

252 S. Matsumura, A. R. Hlil, C. Lepiller, J. Gaudet, D. Guay, Z. Shi, S. Holdcroft and A. S. Hay, *Am. Chem. Soc. Polym. Prepr. Div. Polym. Chem.*, 2008, **49**, 511–512.

253 Y. Liu, J. He, J. Xu, D. Fan, W. Tang and Y. Yang, *Macromolecules*, 2005, **38**, 10332–10335.

254 M. Chen, G. Moad and E. Rizzardo, *J. Polym. Sci. Part A Polym. Chem.*, 2009, **47**, 6704–6714.

255 M. Chen, G. Moad and E. Rizzardo, *J. Polym. Sci. Part A Polym. Chem.*, 2009, **47**, 6704–6714.

256 V. Lima, X. Jiang, J. Brokken-Zijp, P. J. Schoenmakers, B. Klumperman and R. Van Der Linde, *J. Polym. Sci. Part A Polym. Chem.*, 2005, **43**, 959–973.

257 C. W. Scales, A. J. Convertine and C. L. McCormick, *Biomacromolecules*, 2006, **7**, 1389–1392.

258 B. S. Sumerlin, A. B. Lowe, P. A. Stroud, P. Zhang, M. W. Urban and C. L. McCormick, *Langmuir*, 2003, **19**, 5559–5562.

259 J. M. Spruell, B. A. Levy, A. Sutherland, W. R. Dichtel, J. Y. Cheng, F. J. Stoddart and A. Nelson, *J. Polym. Sci. Part A Polym. Chem.*, 2009, **47**, 346–356.

260 J. Xu, J. He, D. Fan, X. Wang and Y. Yang, *Macromolecules*, 2006, **39**, 8616–8624.

261 X. P. Qiu and F. M. Winnik, *Macromol. Rapid Commun.*, 2006, **27**, 1648–1653.

262 X. P. Qiu and F. M. Winnik, *Macromolecules*, 2007, **40**, 872–878.

263 M. R. Whittaker, Y. K. Goh, H. Gemici, T. M. Legge, S. Perrier and M. J. Monteiro, *Macromolecules*, 2006, **39**, 9028–9034.

264 J. W. Chan, C. E. Hoyle and A. B. Lowe, *J. Am. Chem. Soc.*, 2009, **131**, 5751–3.

265 G. N. Grover, S. N. S. Alconcel, N. M. Matsumoto and H. D. Maynard, *Macromolecules*, 2009, **42**, 7657–7663.

266 C. Boyer, V. Bulmus and T. P. Davis, *Macromol. Rapid Commun.*, 2009, **30**, 493–497.

267 G.-H. Hsiue, H.-Z. Chiang, C.-H. Wang and T.-M. Juang, *Bioconjug. Chem.*, 2006, **17**, 781–786.

268 J. W. Chan, B. Yu, C. E. Hoyle and A. B. Lowe, *Chem. Commun.*, 2008, **0**, 4959–4961.

269 M. Li, P. De, H. Li and B. S. Sumerlin, *Polym. Chem.*, 2010, **1**, 854–859.

270 J. W. Chan, B. Yu, C. E. Hoyle and A. B. Lowe, *Polymer (Guildf).*, 2009, **50**, 3158–3168.

271 D. P. Nair, M. Podgórski, S. Chatani, T. Gong, W. Xi, C. R. Fenoli and C. N. Bowman, *Chem. Mater.*, 2014, **26**, 724–744.

272 A. B. Lowe, *Polym. Chem.*, 2010, **1**, 17–36.

273 J. F. Brière, P. Charpentier, G. Dupas, G. Quéguiner and J. Bourguignon, *Tetrahedron*, 1997, **53**, 2075–2086.

274 M. R. Saidi, Y. Pourshojaei and F. Aryanasab, *Synth. Commun.*, 2009, **39**, 1109–1119.

275 J. W. Chan, B. Yu, C. E. Hoyle and A. B. Lowe, *Chem. Commun.*, 2008, 4959.

276 G.-Z. Li, R. K. Randev, A. H. Soeriyadi, G. Rees, C. Boyer, Z. Tong, T. P. Davis, C. R. Becer and D. M. Haddleton, *Polym. Chem.*, 2010, **1**, 1196.

277 H. G. Börner, *Prog. Polym. Sci.*, 2009, **34**, 811–851.

278 B. Le Droumaguet and J. Nicolas, *Polym. Chem.*, 2010, **1**, 563–598.

279 H. A. Klok, *Macromolecules*, 2009, **42**, 7990–8000.

280 S. Dehn, R. Chapman, K. A. Jolliffe and S. Perrier, *Polym. Rev.*, 2011, **51**, 214–234.

281 M. A. Gauthier and H.-A. Klok, *Chem. Commun.*, 2008, **0**, 2591–2611.

282 H. Han, M. M. Wolfe, S. Brenner and K. D. Janda, *Proc. Natl. Acad. Sci. U. S. A.*, 1995, **92**, 6419–6423.

283 M. Mutter, *Tetrahedron Lett.*, 1978, **19**, 2839–2842.

284 P. Wentworth Jr, A. M. Vandersteen and K. D. Janda, *Chem. Commun.*, 1997, **0**, 759–760.

285 M. M. Shamyeki, Y. A. Ovchinnikov, A. A. Kinyushkin and I. V. Kozhevnikova, *Tetrahedron Lett.*, 1965, **0**, 2323–2327.

286 J. Chen, G. M. Lanza and S. A. Wickline, 2015, 1–16.

287 P. K. Senanayake, A. M. Kenwright, D. Parker and S. K. Van Der Hoorn, *Chem. Commun.*, 2007, **0**, 2923–2925.

288 A. Keliris, I. Mamedov, G. E. Hagberg, N. K. Logothetis, K. Scheffler and J. Engelmann, *Contrast Media Mol. Imaging*, 2012, **7**, 478–483.

289 Y. Takaoka, T. Sakamoto, S. Tsukiji, M. Narazaki, T. Matsuda, H. Tochio, M. Shirakawa and I. Hamachi, *Nat. Chem.*, 2009, **1**, 557–561.

290 J. A. Montgomery and K. Hewson, *J. Am. Chem. Soc.*, 1957, **79**, 4559–4560.

291 J. L. Grem, *Cancer Treat Res*, 1998, **98**, 293–338.

292 P. J. O. Dwyer and J. P. Stevenson, *Cancer Treat Res*, 1998, **98**, 111–152.

293 J. A. Egan, *Rocky Mt Med J*, 1952, **49**, 129.

294 J. A. M. Van Laar, Y. M. Rustum, S. P. Ackland, C. J. Van Groeningen and G. J. Peters, *Eur. J. Cancer*, 1998, **34**, 296–306.

295 J. B. Taylor and D. J. Triggle, *Comprehensive medicinal chemistry II*, Elesevier, 2nd edn., 2007.

296 N. W. Lutz and W. E. Hull, *NMR Biomed.*, 1999, **12**, 237–248.

297 E. Freese, *J. Mol. Biol.*, 1959, **1**, 87–105.

298 G. C. Daher, B. E. Harris and R. B. Diasio, *Pharmacol. Ther.*, 1990, **48**, 189–222.

299 M. O. F. Fasoli, D. Kerridge, P. G. Morris and A. Torosantucci, *Antimicrob. Agents Chemother.*, 1990, **34**, 1996–2006.

300 R. E. Loomis and J. L. Alderfer, *Biopolymers*, 1986, **25**, 571–600.

301 A. B. Kremer, T. Mikita and G. P. Beardsley, *Biochemistry*, 1987, **26**, 391–397.

302 N. Markova, V. Enchev and G. Ivanova, *J. Phys. Chem. A*, 2010, **114**, 13154–13162.

303 J. Wang, J. Luis, C. Pozo, A. E. Sorochinsky, S. Fustero, V. A. Soloshonok and H. Liu, *Chem. Commun.*, 2014, **114**, 2432–2506.

Appendix A

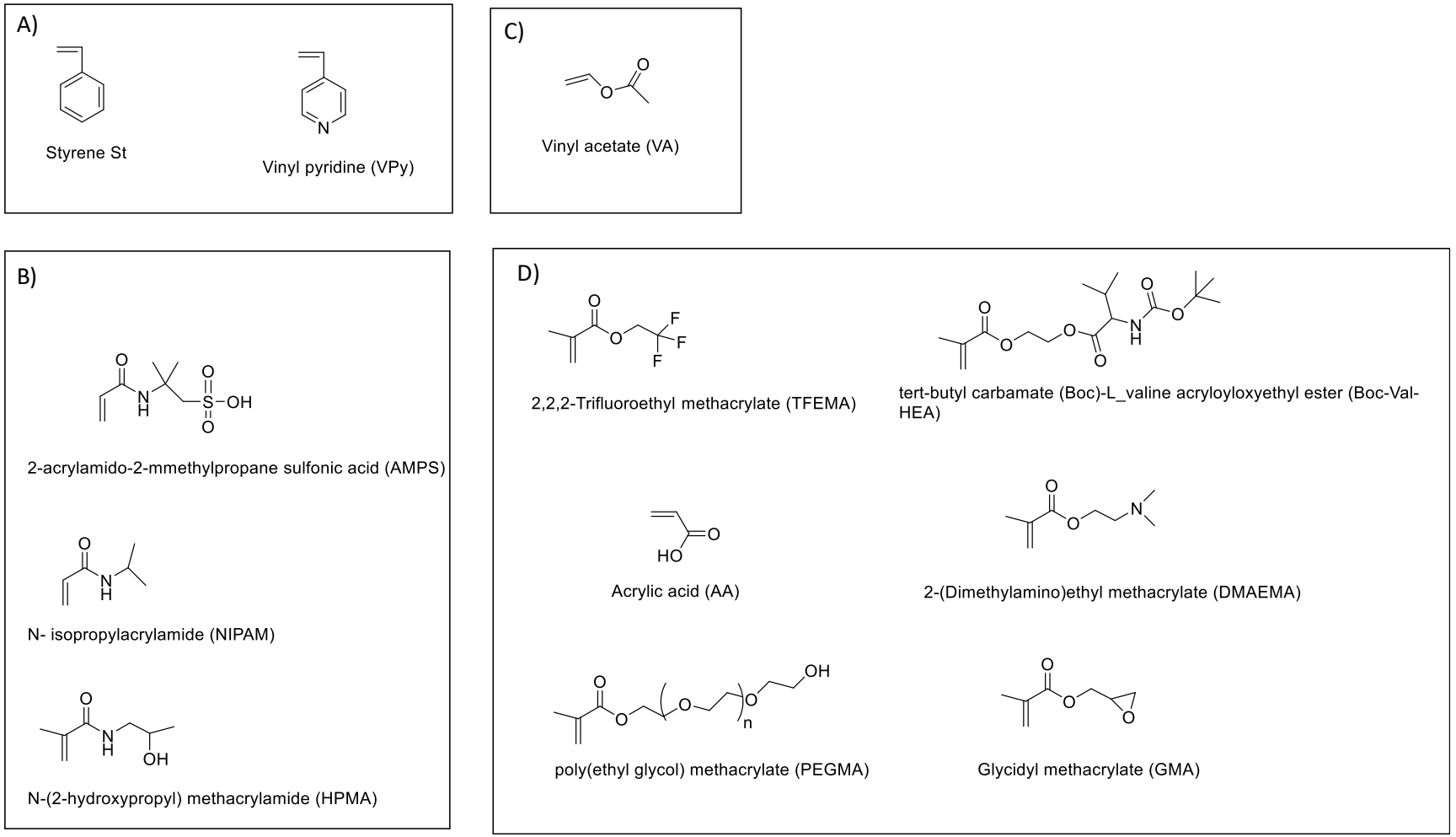

Figure. A-1. Monomers have been polymerised by RAFT-SCVP, A) styrene, B) (meth)acrylamide C)vinyl acetate D) (meth)acrylate monomers

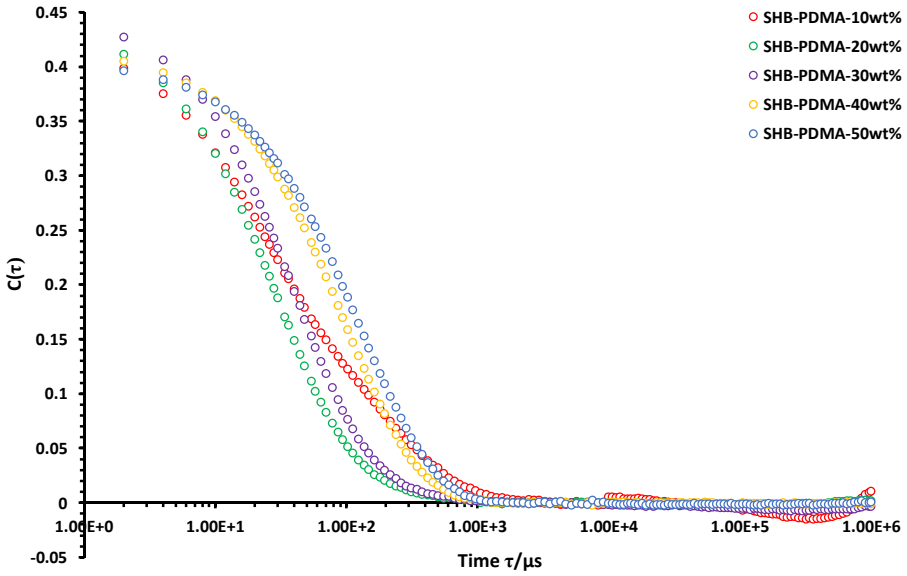

Figure. A-2. DLS autocorrelation function (ACF) curves of SHB-PDMAs in water

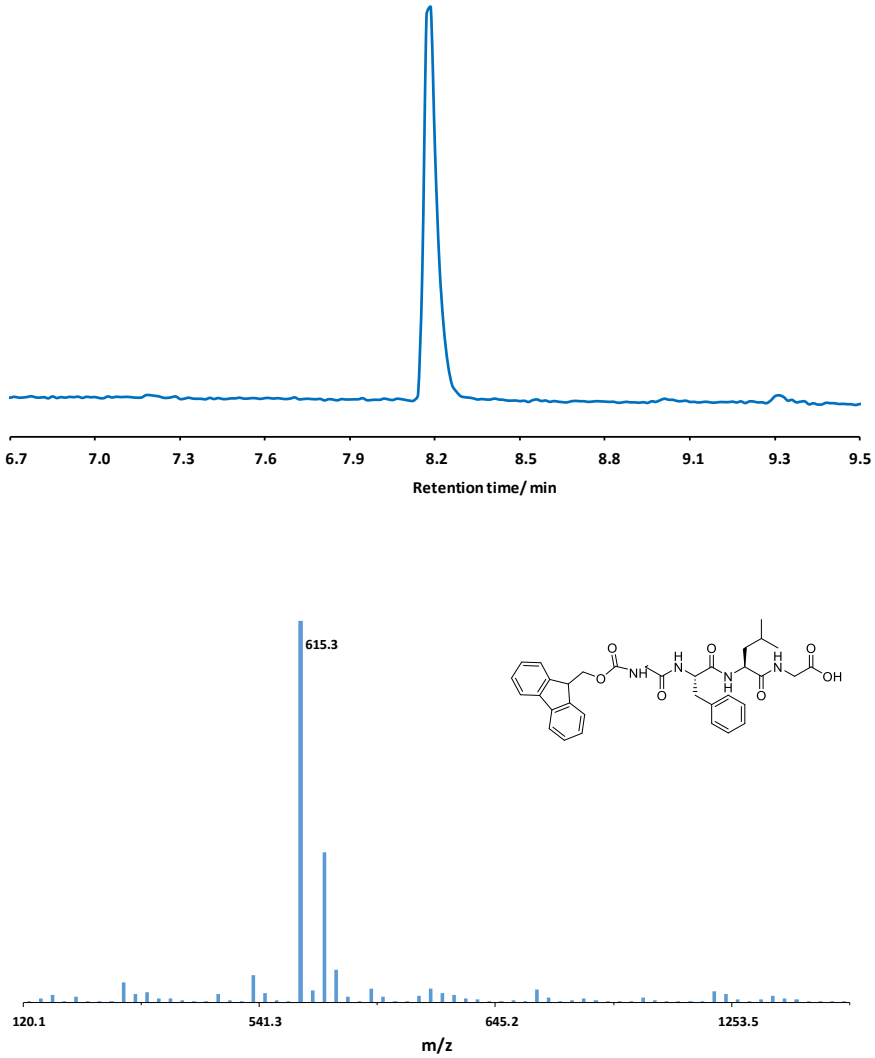

Figure. A-3. Mass spectrum of Fmoc protected tetra-peptide (Gly-Phe-Leu-Gly-Fmoc)

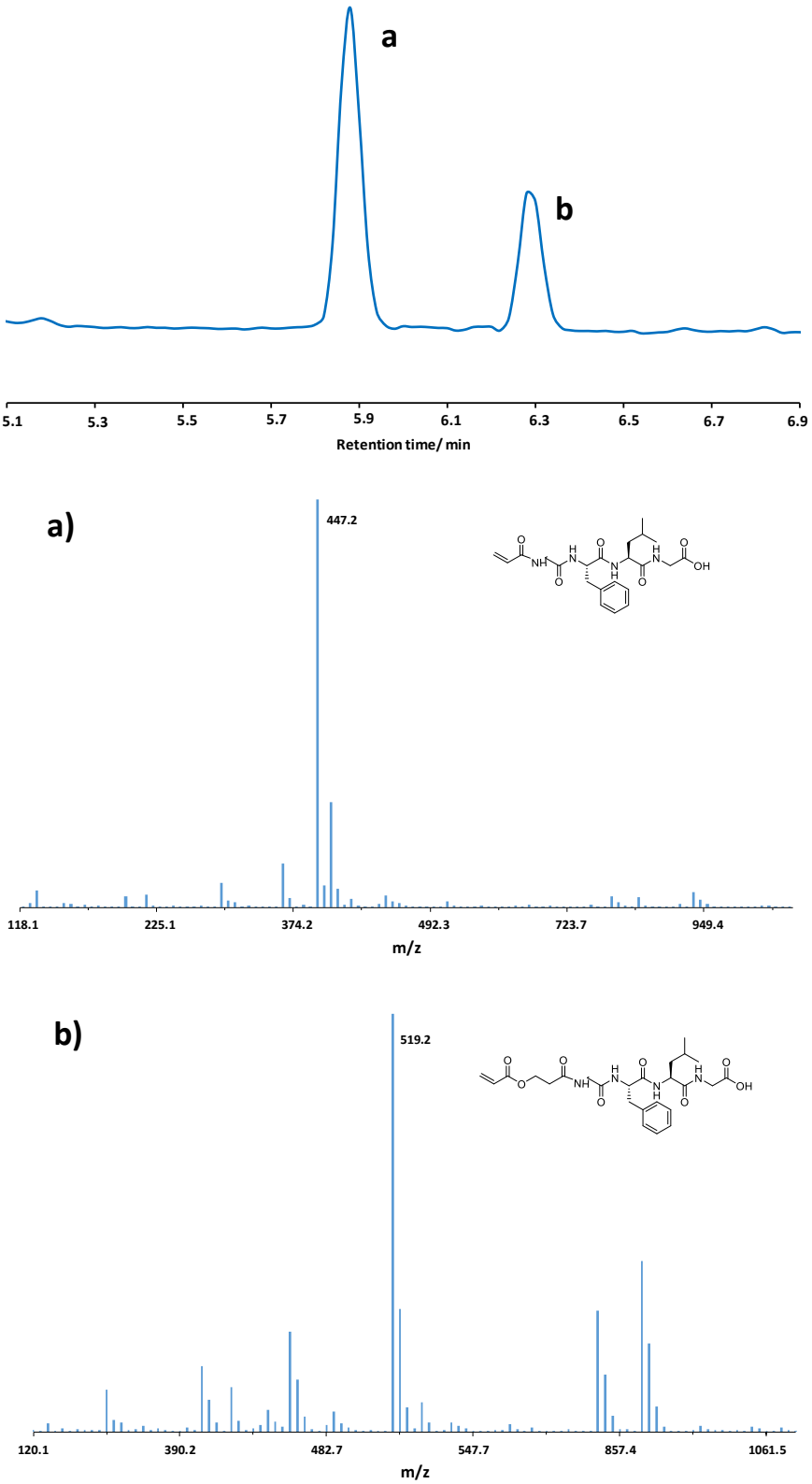

Figure. A-4. Mass spectrum of vinyl modified tetra-peptide (Gly-Phe-Leu-Gly)

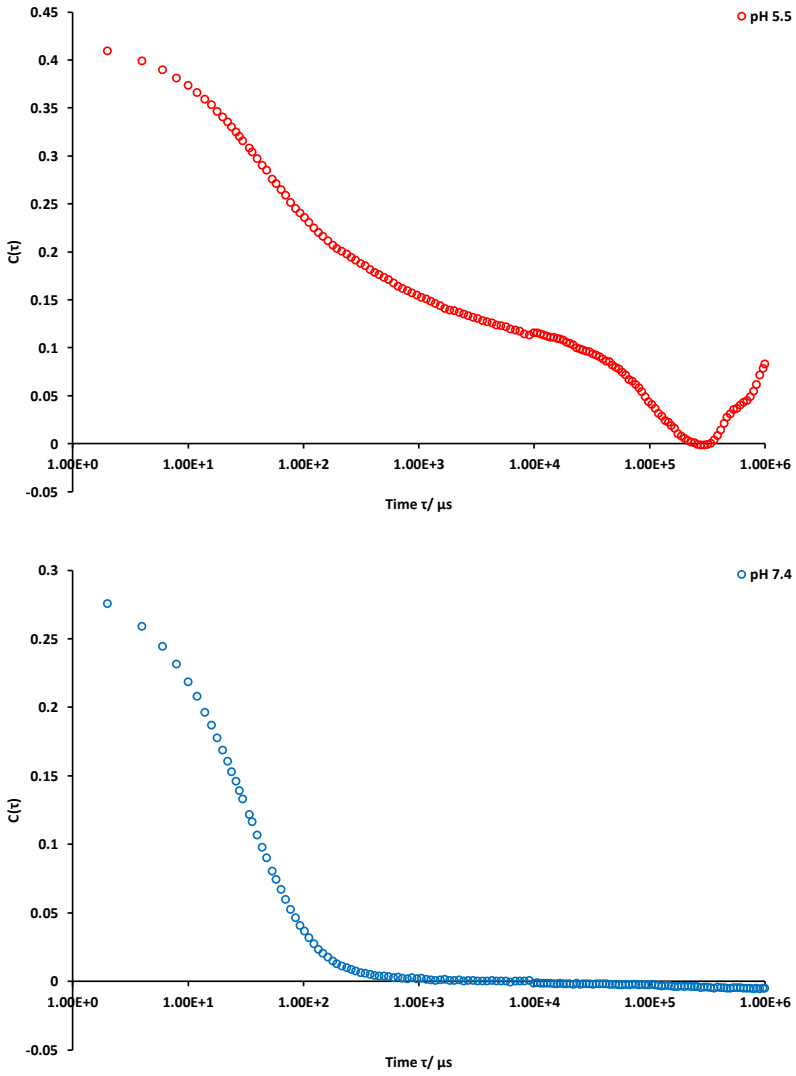

Figure. A-5. DLS autocorrelation function (ACF) curves of 5-FU polymer conjugate in PBS at pH 5.5 and 7.4.